PA 1020644

THE UNITED STATES OF AMERICA

TO ALL TO WHOM THESE PRESENTS SHALL COME:

UNITED STATES DEPARTMENT OF COMMERCE

United States Patent and Trademark Office

June 06, 2003

THIS IS TO CERTIFY THAT ANNEXED HERETO IS A TRUE COPY FROM THE RECORDS OF THE UNITED STATES PATENT AND TRADEMARK OFFICE OF THOSE PAPERS OF THE BELOW IDENTIFIED PATENT APPLICATION THAT MET THE REQUIREMENTS TO BE GRANTED A FILING DATE UNDER 35 USC 111.

APPLICATION NUMBER: ***60/448,808***
FILING DATE: ***February 20, 2003***

PRIORITY DOCUMENT
SUBMITTED OR TRANSMITTED IN
COMPLIANCE WITH
RULE 17.1(a) OR (b)

By Authority of the
COMMISSIONER OF PATENTS AND TRADEMARKS

M. K. HAWKINS
Certifying Officer

02-24-03 Attorney Docket #A/P1

Please type a plus sign (+) inside this box → [+]

PTO/SB/16 (8-00)
Approved for use through 10/31/2002. OMB 0651-0032
U.S. Patent and Trademark Office; U.S. DEPARTMENT OF COMMERCE
Under the Paperwork Reduction Act of 1995, no persons are required to respond to a collection of information unless it displays a valid OMB control number.

JC682 U.S. PTO 02/20/03

JC857 U.S. PTO 60/448808

PROVISIONAL APPLICATION FOR PATENT COVER SHEET

This is a request for filing a PROVISIONAL APPLICATION FOR PATENT under 37 CFR 1.53(c).

INVENTOR(S)

Given Name (first and middle [if any])	Family Name or Surname	Residence (City and either State or Foreign Country)
David	SPRINZAK	7 Einstein Street Rehovot Israel

[x] *Additional inventors are being named on the 1 separately numbered sheets attached hereto.*

TITLE OF THE INVENTION (280 characters max)

A SPECIMEN ENCLOSURE FOR SCANNING ELECTRON MICROSCOPE

Direct all correspondence to: **CORRESPONDENCE ADDRESS**

[ ] Customer Number [ ] → *Place Customer Number Bar Code Label here*

OR *Type Customer Number here*

[X] Firm or Individual Name	ABELMAN, FRAYNE & SCHWAB Attorneys at Law				
Address	150 East 42nd Street				
Address	New York, New York 10017				
City		State		Zip	
Country	U.S.A.	Telephone	(212) 949-9022	Fax	(212) 949-9190

ENCLOSED APPLICATION PARTS (*check all that apply*)

[X] Specification *Number of Pages* (INCLUDES DRAWINGS) 105
[ ] CD(s), Number
[X] Drawing(s) *Number of sheets* 33
[ ] Other (specify)
[ ] Application Data Sheet. See 37 CFR 1.76

METHOD OF PAYMENT OF FILING FEES FOR THIS PROVISIONAL APPLICATION FOR PATENT (check one)

[X] Applicant claims small entity status. See 37 CFR 1.27.
[X] A check or money order is enclosed to cover the filing fees
[X] The Commissioner is hereby authorized to charge filing fees or credit any overpayment to Deposit Account Number: 01-0035
[ ] Payment by credit card. Form PTO-2038 is attached.

FILING FEE AMOUNT ($): $80.00

The invention was made by an agency of the United States Government or under a contract with an agency of the United States Government.
[X] No.
[ ] Yes, the name of the U.S. Government agency and the Government contract number are: _____

Respectfully submitted,

SIGNATURE Jay S. Cinamon
TYPED or PRINTED NAME Jay S. Cinamon
TELEPHONE (212) 949-9022

Date February 20, 2003
REGISTRATION NO. (*if appropriate*) 24,156
Docket Number: 206,073

USE ONLY FOR FILING A PROVISIONAL APPLICATION FOR PATENT

This collection of information is required by 37 CFR 1.51. The information is used by the public to file (and by the PTO to process) a provisional application. Confidentiality is governed by 35 U.S.C. 122 and 37 CFR 1.14. This collection is estimated to take 8 hours to complete, including gathering, preparing, and submitting the complete provisional application to the PTO. Time will vary depending upon the individual case. Any comments on the amount of time you require to complete this form and/or suggestions for reducing this burden, should be sent to the Chief Information Officer, U.S. Patent and Trademark Office, U.S. Department of Commerce, Washington, D.C., 20231. DO NOT SEND FEES OR COMPLETED FORMS TO THIS ADDRESS. SEND TO: Box Provisional Application, Assistant Commissioner for Patents, Washington, D.C., 20231.

PROVISIONAL APPLICATION COVER SHEET
Additional Page

PTO/SB/16 (8-00)
Approved for use through 10/31/2002. OMB 0651- 0032
Patent and Trademark Office; U.S. DEPARTMENT OF COMMERCE
Under the Paperwork Reduction Act of 1995, no persons are required to respond to a collection of information unless it displays a valid OMB control number.

Docket Number	206,073	Type a plus sign (+) inside this box →	+

INVENTOR(S) APPLICANT(S)		
Given Name (first and middle (if any)	Family or Surname	Residence (City and either State or Foreign Country)
Amotz	NECHUSHTAN	32 Ha'alon Street Aseret ISRAEL

Number 2 of 2

A SPECIMEN ENCLOSURE FOR A SCANNING ELECTRON MICROSCOPE

FIELD OF THE INVENTION

The present invention relates to a specimen enclosure and a supporting liquid handling system compatible with single use and mass production, aimed for the examination of samples in a non-vacuum and wet environments using a scanning electron beam for excitation while the readout is performed using any combination of electrons and photons signal, particularly but not exclusively to the use of such an apparatus for inspection of cells, bacteria, tissues, tissue biopsies and viruses in wet environment and room or body temperature.

BACKGROUND OF THE INVENTION

Microscopic examination of biological cells and tissues is a central tool in clinical diagnosis as well as in diverse areas of research in the life sciences. Light microscopy (LM) is performed with thin sections of tissue (several micron), stained with chemicals or antibodies to reveal general tissue architecture, to identify normal or abnormal cell types, and to localize specified molecules. Transmission electron microscopy requires specially prepared ultrathin sections (0.1 micron or less), and reveals a wealth of subcellular information. Each of the aforementioned techniques has limitations: the resolution of light microscopy is limited by diffraction to 0.25 microns; the use of TEM is encumbered by extensive processing of the sample, which may alter its structure significantly. Preparation of samples for standard TEM also requires specific skills and takes at least a few days to achieve. The very thin slices present a very limited (and often arbitrary) portion of the sample, necessitating the imaging of multiple serial sections.

A recent review discusses the use of electron microscopy in clinical diagnosis (Tucker J.A., 2000. The continuing value of electron microscopy in surgical pathology. *Ultrastructural Pathology* **24**:383-389). It is found; that in a small but significant proportion of cases (3-8%), proper diagnosis can only be made based on electron microscopy; this is particularly pronounced in oncology and in selected areas such as kidney diseases (Tucker 2000). These numbers are probably an underestimate, since the

use of electron microscopy is not primarily limited by lack of utility, but by considerations of cost, the time needed to produce results, and the low throughput. Thus, there is a significant niche for an imaging system for biological tissues and cells that achieves electron microscopic resolution with sample preparation procedures comparable with those of light microscopy.

Another important need in the field of surgical pathology is for techniques that allow rapid histopathological analysis that can be completed within the time frame of an operation. Such results are particularly critical when they determine the continuation of the surgical operation; for example, in determining whether a tumor was entirely removed or further dissection is required. Currently, frozen sections of dissected tissue are prepared and examined by light microscopy. While this can be accomplished in the space of 30 minutes, the crude freezing techniques used cause significant damage to the structure of the tissue, leading to loss of delicate details.

A co-pending International patent application by one of the present inventors, entitled "Device and method for the examination of samples in a non-vacuum environment using a scanning electron microscope" (LDST/IL10/01108), the content of which is hereby incorporated by reference, discloses a non-vacuum Scanning Electron Microscope (SEM) device that enables the imaging of wet specimen, specifically for the area of life sciences. Specific examples are mammalian cells, tissues and tissue biopsies, bacteria and viruses to be examined in a wet environment, atmospheric pressure and body, room or other temperatures with a scanning electron microscope, thus combining the known advantages of electron microscopy (high resolution and high contrast or spatial signal to noise ratio) with the advantages of light microscopy (ease and speed of sample preparation as well as fluorescence readout and possible automation). This is accomplished by the use of a thin membrane, also termed hereinafter a partition membrane (PM), that is sufficiently transparent to electrons but is strong enough to withstand the pressure difference between the inside of the specimen enclosure, which is typically one atmosphere, and the vacuum required for the passage of an electron beam.

The aforementioned features of non-vacuum SEM are applied to the observation of biological tissues in the following manner.

1. Separation of the sample from the vacuum allows direct visualization of wet samples. This immediately obviates the need for all dehydration procedures, including water replacement and critical-point drying. The wet state most closely resembles the native state of the sample, preserving features that are distorted or destroyed during dehydration. This advantage is particularly important in the observation of tissues, where the true architecture involves both cells and extracellular matrix. In addition, the presence of fluid in and around the sample allows efficient dissipation of electrical charge and of excess heat. This eliminates artifacts due to sample charging, as well as thermal damage.

2. Electron microscopy of biological tissues is most frequently done in two imaging modes. Transmission electron microscopy (TEM) utilizes electrons transmitted through the sample; the entire thickness of the sample contributes to the image. Transmission techniques impose a severe constraint on the thickness of the samples: typically, 50 nm, which can be increased to 3 μm in ultrahigh voltage microscopes. Scanning electron microscopy uses a reflective mode, most frequently detecting secondary electrons that image only the surface topography of the sample. The non-vacuum SEM technique uses backscattered electron detection in a scanning electron microscope. The electron beam penetrates into the sample, and the backscattered electrons reveal features from a depth of up to a few microns. Thus, although an electron scanning/reflectance mode of imaging is employed, the image is not limited to the surface, and internal structure of the sample is revealed. Furthermore, because detection is done in a reflective mode, any material laying beyond the interaction volume has no effect on imaging. The samples can be, therefore, of a thickness far exceeding the imaged region. Typically, a tissue fragment several millimeter thick can be viewed; only the material layer of a few micrometers or less that is closest to the surface contributes to the scanned image, without interference from the bulk of the sample. The thickness of the imaged region can be modulated, by varying the acceleration voltage of the electron beam. Non-vacuum SEM thus yields "virtual sections" without the need for actual sectioning; this eliminates the need for embedding or freezing of the sample, which are otherwise required to enable thin sectioning. Finally, the dependence of electron backscattering efficiency on the material composition of the sample (through the atomic number Z) creates contrast even in the absence of heavy metal staining that is characteristic of TEM imaging. Subcellular organelles can be distinguished based on differences in local concentrations of lipids, phosphates, and salts within biological samples; and a wide variety of stains and labels can be used to enhance contrast.

An additional capability of the non-vacuum SEM technology is concurrent detection of light emitted from the sample while scanning with the electron beam. The scanning electron beam excites molecules in the sample, which may then emit light at characteristic wavelengths (cathodoluminescence). The light intensity is then used to derive an image of the distribution of scintillating molecules, either endogenous to the biological sample or labels that can be introduced extraneously. This image is obtained simultaneously with the imaging by BSE, at a resolution limited by electron-matter interactions and not by light diffraction.

The current invention describes improvements to previous inventions the contents of which is incorporated as reference (Zik, Thiberge, Moses, device and method for the examination of samples in a non-vacuum environment using a scanning electron microscope, LDST/IL01/01108; Sprinzak, Kliger, Karni, Nechushtan, Zik; automation compatible devices for scanning electron microscopy imaging of samples in a wet environment, Israeli application 150055, June 5, 2002; Thiberge and Moses, low-pressure chamber for scanning electron microscopy in a wet environment, Israeli application; Sprinzak, Karni, Nechushtan, Zik, device for fluorescent imaging of biological samples using a scanning electron microscope and fluorescence or scintillation markers, Israeli application 150054, June 5, 2002), designed to render the specimen enclosure for single use, affordable and compatible with mass production and wide spread commercial use. The goal of the current invention is thus to disclose a single use, mass-produced specimen enclosure made in an industrial process with low cost materials that are compatible with the requirements of life science and medical laboratories. For example, sterility, visibility with light microscopy as well as automation. Thus enabling the study of fully wet samples with a Scanning Electron Microscope in an efficient and low cost manner.

Further embodiments are disclosed in order to:

1. Provide a solution for the handling of liquids in a way that is compatible with the above-mentioned specimen enclosures.
2. Enable parallel readout of photons and electrons to allow parallel imaging of backscattered electrons via several detection means, multicolor analysis via fluorescence and cathodoluminescence and quantitative material composition via X-ray analysis.

3. Enable the insertion and imaging of thick samples and samples which do not adhere to the PM, such as tissue biopsies. Such a device can used by pathologists to reach rapid and precise diagnoses and clinical decisions based on ultrastructure of patient samples. Examples include classification of tumors, identification of inflammatory processes in transplant rejection, and intra-operative evaluation of the completeness of tumor removal.

DETAILED DESCRIPTION OF THE INVENTION

Prior art documents, the contents of which is incorporated as reference discuss the partition membrane (PM) LDST/IL10/01108 (Zik, Thiberge, Moses, device and method for the examination of samples in a non-vacuum environment using a scanning electron microscope); Ways to make the specimen enclosure automation compatible (Sprinzak, Kliger, Karni, Nechushtan, Zik; automation compatible devices for scanning electron microscopy imaging of samples in a wet environment, Israeli application), ways to reduce the inner pressure in the specimen enclosure to enable thinner PM's (Thiberge and Moses, low-pressure chamber for scanning electron microscopy in a wet environment, Israeli application) and ways to image fluorescence and cathodoluminescence using the electron beam excitation (Sprinzak, Karni, Nechushtan, Zik, device for fluorescent imaging of biological samples using a scanning electron microscope and fluorescence or scintillation markers). The details of the use of the PM and the considerations of resolution and contrast is discussed in the above mentioned applications and is further detailed in: Electron microscopy of wet samples, S. Thiberge, O. Zik, E. Moses (manuscript submitted to Reviews of Scientific Instruments in Jan 2003); The biological results obtainable with the PM is described in: Scanning Electron Microscopy of Wet Cells and Tissues, Stephan Thiberge, Amotz Nechushtan, David Sprinzak, Opher Gileadi, Vered Behar, Ory Zik, Yehuda Chowers, Joseph Schlessinger and Elisha Moses (manuscript in preparation). All these documents are incorporated as reference.

The current invention discloses the characterization of the specimen enclosures designed for single use (disposable / consumable) and mass production. We further disclose supporting liquid handling devices that enable the addition and extraction of fluids to and from the specimen enclosure. Practical examples for the use of the specimen enclosures for a variety of different samples are given by way of non-limiting examples.

The single use specimen enclosures may be adapted to numerous applications in diverse fields in addition to cell biology, such as material analysis, monitoring food, bacteria, printing inks, drugs and other pharmaceuticals in production, oils and so forth. A specific embodiment that enables the imaging of samples, which does not adhere to the membrane, such as tissue biopsies, is also disclosed.

Description of the Preferred Embodiments.

Reference is now made to FIG. 1. According to the current invention the specimen enclosure is composed of two major parts: the Liquid Dish (LD) and Liquid Dish Seal (LDS), both are designed for single use:

1. Liquids Dish (LD) – The LD is the lower part of the specimen enclosure (upper inside an upright SEM). It is composed of a cavity disk [30] and a cavity disk holder [4], which form together a single unit. Each LD functions as a stand-alone unit that holds fluids. According to a preferred embodiment, the LD is a "mini Petri dish" that contains the Cell medium (serum etc.) and the liquids during stages such as: cell incubation, imaging by light microscopy, fill-in and draining of the liquids. Different embodiments in which non-adherent cells, tissues and other substances are imaged are discussed below.

2. Liquid Dish Seal (LDS) – The LDS is the upper part of the specimen enclosure (lower inside the SEM) that includes a closing cup [1] and a sealing diaphragm [2]. This part when assembled with the LD creates around the Cell medium a specimen enclosure with controlled sealed atmosphere separated from the vacuum of the SEM. The sealing diaphragm is opaque to electrons. It serves to release the internal pressure while in the SEM as well as to prevent rupture of the PM from transient pressure increase. For example, while closing the LD and LDS.

The two parts (LD and LDS) combined together form the single use specimen enclosure suitable for mass production. The following contains a detailed description of these two parts including the production considerations, which allow mass production of the specimen enclosure and additional tools for liquid handling with the LD as a 'mini petri dish'.

Reference is now made to FIG. 2. A cavity disk [31] is fabricated from a disk, preferably made of plastic, with a hole in the middle, to which the PM [32], preferably made of polyimide and a grid [33] are attached. According to a preferred embodiment the grid is

metallic. According to another embodiment the grid is produced from polyimide..

When the cavity disk [30] is assembled, it forms a 'mini petri dish' where the bottom of this petri dish is actually the PM and grid. The cavity disk is inserted into the cavity disk holder [4] to form the LD. Preferably the cavity disk holder includes means for convenient closing. According to one embodiment these means consist of tapping (surface roughening) for the LDS to screw in and "holding wings" which allow holding of the LD inside a socket in the liquid handling plate and anchors for the LD while screwing the LDS. Many other configurations to improve handling are possible and can be designed by one who is skilled in the art.

The closing cup [1] in the LDS is designed to be easily tightened onto the LD by means of a thread. The sealing elastic diaphragm [2] has two roles: The first is to allow sealing between the two parts of the specimen enclosure, which is performed by the outer ring pressing against the two parts. The second is to reduce the pressure on the partition membrane, which is performed by the elastic diaphragm. Pressure reduction is achieved by allowing the volume inside the specimen enclosure to increase through the stretching of the elastic diaphragm. Evacuation of the air at the bottom side of the LDS is done through the hole in the holding leg [1], which allows expansion of the elastic diaphragm. The elastic diaphragm also prevents rupture of the PM due to transient pressure bursts when closing the specimen enclosure. One advantage of this construction over prior art is that the sealing and pressure reduction mechanisms are combined in one unit, hence, simplifying considerably the production.

Reference is now made to FIG 3, which shows a picture of a single – use specimen enclosure. Both the cavity disk holder [4] and the closing cup [1] are made of plastic. According to a preferred embodiment, the plastic is ABS coated by a thin layer of Ni-Cr. This layer provides grounding from the metallic grid attached to the partition membrane to the microscope stage. The coating serves for elimination of sample charging. This choice of material and the device, which is planned to fit conventional plastic molding, allows mass production through plastic molding and coating. This reduces production costs to levels, which are affordable to an ordinary user and allows the whole specimen enclosure to be used for single use. The plastic disc [4] of the cavity disk can also be manufactured by plastic molding. The electron-opaque sealing diaphragm has to withstand the following criteria:

1. Elasticity – sufficiently high to enable it to function as absorber of extra pressure and prevent potential rupturing of the partition membrane
2. Permeability – sufficiently low to enable the preservation of samples in the wet environment under external vacuum

Any material with these properties that can be shaped to the desired shape to seal the LD and LDS, with an o-ring shape in the perimeter and impermeable layer in the interior, can serve as diaphragm.

According to a preferred embodiment, the sealing diaphragm [2] is made from butyl or silicone rubber using a rubber-pressing mold – a manufacturing technique also suitable for mass production at low costs.

Reference is now made to FIG. 4. In order to conveniently work with multiple specimen enclosures in the environment of a cell biology lab, a set of liquid handling tools is disclosed. The parts comprising the liquid handling system include a multiple LD holding plate [11-13] and a multi drain [10].

The base plate of the multiple LD holding plate [13] has a number of positions for a plurality of liquid dishes. For example, 4 positions x 12 rows as shown in FIG. 4. Typically, the number, dimensions and locations of the LDs are designed to fit the standard automation in a life sciences lab. For example, 96 'multi' well plate as shown in Fig. 4.

Reference is now made to FIG. 5. According to a preferred embodiment, the insertion of liquids into the LDs is done using standard pipettes. In order to prevent rupturing of the PM by a pipette tip [59], a mechanical stopper shaped as a two wings structure [60] positioned on a pipette tip with attachment means such as glue. This prevents direct contact between a pipette tip and the PM.

Reference is now made to FIG. 6. Draining liquids from the LDs is performed for a whole row in the base [13] aligned to the multi drain [10] connected to a standard pumping unit via a needle valve (not shown). The liquids are drained through the needles in the multi drain, which are aligned to the right position through sliding of the two legs along grooves on the holding cover [12] sides. The flow level is controlled using a needle valve placed in the pumping line of the multi drain. This draining mechanism protects the partition membranes from accidental rupture by the user and accelerates the liquid handling process. The distances between two adjacent LD in the plate fit the standard automation in a life sciences lab. According to one embodiment, the distance between two adjacent LDs is

twice that of the distance between two wells in a 96 well plate, hence parallel insertion of liquids and automation can be easily applied.

According to the one embodiment, the LD has 'wings' for holding. Said wings are fitted into two slits in the base as shown in FIGs. 6, 7 marked as 14 in FIG. 8. Throughout the liquid handling process, the LDs are kept in place using the holding cover [12], which is mounted on top of the base plate. A sterilization cover [11] can be mounted on top of the holding cover (see FIG. 6). The top part of the sterilization cover [11] and the bottom of the base plate [13] are transparent in order to allow monitoring of the samples using a light microscope, preferably an inverted light microscope. In order to make sure that the liquids in the LDs did not evaporate during the liquid handling process, additional cavities in the base plate are added. These cavities are filled with liquid (water in most cases) to make sure that the environment under the sterilization cover is kept fully hydrated at all times.

Once the samples are ready for imaging in the scanning EM, the user removes the holding cover [12] and screw LDSs to the LDs, thus creating a closed specimen enclosures out of the base plate, turn them upside down and introduce them into the SEM.

The multiple LD holders are designed to be manufactured using a plastic mold suited for mass production.

Reference is now made to FIG. 9. which discloses a way to image a plurality of liquid dishes using SEM. According to this embodiment, a similar design to the liquid dish holder is used for parallel-automated inspection of samples. The bottom [53] is made of cavities so that the PM can is exposed directly to the electron beam, while the plurality of LDs are in place and without having to seal with a LDS. The cover [51] has embedded tightening means [511], such as screws and sealing means to seal each liquid dish in a vacuum tight manner. When the liquid handling and insertion phase is completed, the parallel plate is inverted and inserted into an upright SEM.

According to one embodiment of the current invention, the samples are not inverted. This can be achieved using an inverted SEM (available at Schlumberger, 5599 San Felipe, Houston, TX 77056, USA). It is clear that all the specimen enclosure devices disclosed in the current invention can be utilized to work in an inverted SEM, whereby the LD is lower also in the SEM.

Reference is now made to FIG. 10. It demonstrated one use of the current invention by way of a non-limiting example. The image shows a plurality EGF receptors immunolabeled

with 20-nm gold colloids on A431 cells, counterstained with uranyl acetate. Imaged at 30 kV. The low magnification image [71] shows the distribution of the label over the entire cell surfaces. Image [72], a higher magnification of the region marked by the rectangle in [71], shows individual labeled receptors at molecular resolution. The image demonstrates how the current invention can be used to analyze the distribution of receptors on the surface of cells. This can be used for life science, cell biology, receptor signaling research as well as drug screening in various disease areas such as HIV, cancer and many others.

Reference is now made to FIG. 11. It discloses a way by which a universal labeling technique can be employed for both intercellular and extracellular labeling It utilizes an enzymatic reaction of peroxidase. The antigen is labeled with secondary antibody conjugated to peroxidase, which in the presence of hydrogen peroxide, catalyzes polymerization of its substrate diaminobenzidine (DAB) to a brown precipitate. The electron density of the precipitate is enhanced with gold chloride in the presence of chelator (for example EDTA), which lowers the non-specific background. The image shows external labeling of EGFR on A431 cells with the DAB/gold chloride method at two magnifications, [81] and [82]. Most prominent signal, seen as bright precipitate, is obtained on lateral border of the cells, and is not seen on negative control cells [83]. It is appreciated that internal labeling can be achieved in a similar manner. For extracellular labeling, cells are labeled directly after fixation, whereas for intracellular labeling, an additional permeabilization step (for example incubation with mild detergent such as Triton X-100 0.2%) is added.

Reference is now made to FIG. 12, which further demonstrates that the current invention is not limited to cell surface receptors and can be utilized for internal labeling of cells. The image shows internal labeling of actin fibers in Chinese hamster ovary (CHO) cells with silver enhanced 0.8 nm gold colloids.. The silver enhancement was done with a commercially available kit -Aurion, R-Gent SE-Em, cat no. 25521 – for 60 minutes.. In the lower magnification [91], cellular pattern of actin staining can be seen, and in the higher magnification [92], single fibers in the cytoplasm are visualized.

Reference is now made to Fig. 13. It demonstrates a use of the current invention for the analysis of a variety of adherent cells, labeled in a non-specific manner. CHO cells were grown on the membrane, fixed first with 4% paraformaldehyde for 10 minutes, then with 1% tannic acid for 5 minutes. The cells were then stained with 1% uranyl acetate for 20 minutes. The lower magnification [101], shows the over-all cellular staining pattern with

uranyl acetate. In the higher magnification (x3200), [102], detailed subcellular structures, lamellipodia, and intercellular contacts are visible.

Reference is now made to FIG. 14, which demonstrates that the current invention can be used to obtain a three dimensional reconstitution of samples. This is based on the result, that images can be obtained from different planes of the sample by changing the voltage. CHO cells were fixed and stained with uranyl acetate (as described above). When imaging is done with low voltage, 10 kV [111] , the plane closest to the partition membrane, the growth surface of the cells, is visualized. Raising the voltage to 15 kV [112] and25 kV [113], , adds additional information from the more apical planes of the cells. With development of appropriate algorithms, the results obtained with different voltages can be combined to obtain a 3 dimensional reconstitution. Another source of information which can be incorporated in the three-dimensional reconstruction is images obtained at different tilt angles of the sample relative to the electron beam.

Reference is now made to Fig. 15. It demonstrates that with the current invention, live, non fixed, and non stained cells are also visualized. The image shows a CHO chinese hamster ovary cell in its native condition (without fixation and without staining treatment). Electron dense material, nuclei [121] and some cytoplasmic structures [122] are seen in bright, while less dense material, lipid droplets [123], are seen in dark due to their lower average electron density (atomic number). The result demonstrates that the current invention can be used for the analysis of lipids in unstained cells and tissues, as well as for the analysis of cells which are viable up to the point of inspection in an electron microscope.

Reference is now made to FIG. 16. This is a non-limiting example that demonstrates the use of the current invention for the imaging of microorganisms, such as the parasite Trypanosoma brucei shown in the image. Non-adherent samples such as Trypanosoma are attached to the membrane with use of attachment molecules, of which poly-L-lysine used in this sample is a non-limiting example. The microorganisms can be examined unstained, stained non-specifically or immunolabeled for specific molecules. [131] shows fixed, un-stained Trypanosoma, where electron dense nuclei is observe in bright and lipid rich structures in black. [132] and [133] show non-specific staining with uranyl acetate and osmium tetroxide, respectively. Many intracellular organelles become visible with uranyl acetate staining. Osmium stains most prominently lipid structures, and thus in contrast to un-stained samples, here lipid-rich structures are visible in white. Image [134] shows immunolabeling of Trypanosoma for an extracellular antigen. Labeling was done with 30

nm colloidal gold and attachment onto poly-L-lysine coated PM was done after the labeling procedure.

Reference is now made to FIG. 17, which demonstrates that the use of current invention is not limited to cellular samples, but is applicable also to analysis of any liquid fluidic samples. Images obtained from cosmetic and food industry samples are shown here as non-limiting examples. Image [141] shows the texture of cosmetic cream. The parallel X-ray spectrum [1410] is also shown. It demonstrate that the not only lipids create contrast but a variety of other materials. It further exemplifies the use of the current invention for material composition analysis. Images [142] and [143] are two magnifications of a sample of commercial skimmed cow milk (3% fat) and images [144] and [145] of milk from a breast-feeding woman. Vesicles rich in fat are visible in dark. Comparison of the milk samples shows the much higher homogeneity of the non-processed human milk compared to the processed cow milk.

Reference is now made to FIG. 18, which demonstrates that the current invention can be used for diagnostic applications in the field of infertility, for example, in the field of in vitro fertilization. The image shows two magnifications of bovine sperm cells fixed and stained with phosphotungstic acid. In the larger magnification (x6400) in image [152], cellular details, including acrosome, which is not visible with light microscope techniques, can be observed.

Reference is now made to FIG. 19. It demonstrates the use of the current invention in the analysis of biomaterials. A non-limiting example shown in the image is quality control of collagen disc used in medical applications. The disc was stained with uranyl acetate. Lower magnification (x100) [161] shows the general appearance of the disc, while in higher magnification (x1600) [162], detailed organization of the collagen fibers is visible.

Reference is now made to FIG. 20, which shows that the current invention can be used for analysis and identification of pathogens, such as bacteria shown in this example. Image [171] shows fixed, unstained E. Coli bacteria, and image [172] fixed Bacillus subtillis stained with uranyl acetate.

Reference is now made to FIG. 21. It demonstrates that the current invention is also applicable to examination of blood samples. This can be useful in diagnosis of various medical conditions, where alterations are seen in blood cell size, morphology or composition, such as sickle cell anemia, thalassemias, leukemia and other immunological abnormalities. The image shows two magnifications of whole blood from rat, fixed and stained with 1% uranyl acetate. The blood cells were attached to the PM coated with poly-

L-lysine. FIG. 21 also illustrates that the current invention can be applied to cytological analysis of other body fluids, of which non-limiting examples are: diagnostics of malignancy and likelihood of malignant progression of thyroid nodules (e.g., fine-needle aspiration diagnostics), analysis of pathogens in fluids from the alveolar cavity in lungs (specifically, in immune-suppressed patients), cytological analysis and diagnostics of urine, spinal cord fluid, saliva, and alike.

Reference is now made to FIG 22 which shows a modification of the specimen enclosure that enable the imaging of photons excited by the electron beam (fluorescence or cathodoluminescence). The LDS is designed in such a way that a light guide 62 is situated in the bottom of the LDS . The light guide [62], preferably made of clear plastic or glass, guides the light from said specimen enclosure to the photo multiplier tube via an additional light pipe (not shown).

Reference is now made to FIG. 23, which shows that with the current invention electron beam fluorescence can be detected from live cells. A sample irradiated with electron beam emits electrons as well as photons. Dual detection system allows simultaneous monitoring of both the signals, photons and back scattered (BS) electrons. In BS electron image of live, unstained CHO cells, nucleoli is seen in white and lipid droplets in black. In electron beam fluorescence of same cells, brightest fluorescence is obtained from lipid droplets and nuclei. Fluorescent labels are widely used in cell biology research, in diagnostics and in drug discovery platforms. Hence this ability can be used in wide range of applications, where in addition to BS electron image, detection of fluorescent signal is desirable, for example for identifying subtypes of cells and organelles which are labeled with fluorescent markers.

Reference is now made to FIG. 24, which demonstrates that the electron beam fluorescence obtained with the current invention can be used in application where high resolution of fluorescent image is required. The image shows dual image of 200 nm polystyrene beads, FluoSpheres, with embedded blue fluorophore (350/440). In electron beam fluorescence image, signal is clear due to strong fluorescence excitation, whereas in the backscattered electron image signal is weak due to minimal material contrast. The resolution reached with electron beam fluorescence is significantly higher than with conventional fluorescence microscopy.

Reference is now made to FIGs. 25 and 26.. The invention there is a need to image

specimen which does not readily attach to the PM. Examples range from tissue biopsies to samples from the area of forensics, material and earth sciences and various industries and fields of research (petroleum, sediments, pathology). The figures show how such specimen can be put in communication with the PM by means of a spring and a plunger.

This embodiment is of particular importance for the fields of histopahology. It offers advantages over currently available methods in terms of higher resolution, and faster and easier specimen preparation with minimal manipulations. Non-limiting examples of applications are given below with reference to appropriate images obtained from various tissue specimens:

Reference is now made to FIG.27. It, together with additional examples given below, demonstrates the use of the current invention for analysis of biopsies; the image shown here demonstrates, that the current invention is applicable to be used for diagnosis of cardiac pathologies from heart biopsies. The image shows a fresh sample from mouse heart - unfixed and unstained – which was placed directly into a specimen enclosure and viewed. Image [182] shows zooming into cells from image [181] (frame in black), and image [183] shows zooming into a single cell marked in image [182]. Overall structure and alignment of muscle cells can be seen in lower magnifications [181,182]. In the higher magnification (x6400) [183], detailed cellular structures are visible. The bright organelles are assumed to be either mitochondria, which are found in large numbers in heart muscle cells, or storage granules.

Reference is now made to FIG. 28, which shows that the current invention can be used for diagnosis of kidney diseases and analysis of cytotoxic effects on kidney. The image shows three magnifications of rat kidney stained with 0.1% uranyl acetate. In the high magnification image [193], morphology of single cells can be observed. Toxicological effects can be observed with current invention also in other specimens, for example from liver and blood.

The current invention is applicable also for cases, where differentiation between necrosis and apoptosis is required.

Reference is now made to FIG. 29, which demonstrates the use of current invention for analysis of specimens, where detection of lipids or fat is important. Non-limiting examples: diagnostics of atherosclerosis, where lipid structures (originated from cholesterol accumulation) are found; and analysis of female breast tissues, for example in breast

cancer. The image shows three magnifications of a sample from fixed, unstained adipose tissue. Adipocytes store lipids, which are clearly darker relative to the hydrated environment of the cell.

Reference is now made to FIG. 30. The image shows a sample of striated muscle stained with 0.2% uranyl acetate at two magnifications. Organized structure of muscle fibers is clearly visible. The results implicate that the current invention is applicable to study and diagnosis of muscular abnormalities which are manifested by structural changes in muscle, for example muscular dystrophies.

Reference is now made to FIG. 31, which shows pigmented epithelium from rabbit eye retina, stained with 0.2% osmium tetroxide, at two magnifications. Changes in the organized structure, caused for example by eye cancer or other eye pathologies, can be readily detected with the current invention.

Reference is now made to FIG. 32, which demonstrates that the current invention can be used for applications where the analysis of extracellular matrix is important. The image shows two planes of focus in a specimen from mouse pancreas stained with uranyl acetate. Image [231] is focused on cells, and shows the cellular organization of acini, whereas image [232] is focused on plane that shows the organization of the extracellular matrix . Analysis and study of extracellular matrix is important for example in dermatological conditions, where changes are seen in collagen, elastic fibers and other dermal matrix components, for examples in aging, atrophies, alopecia, and congenital skin abnormalities.

Reference is now made to FIG. 33, which shows that the current invention is applicable to analysis of neural tissues. The image shows three magnification of fixed, unstained cross section from rat spinal cord. The lowest magnification [241] shows the overall appearance of the cross section. In image [242] organization of myelinated nerves is seen, and the highest magnification [243] shows the individual nerves, seen in bright, surrounded by the lipid-rich myelin, seen in dark. The current invention is applicable to the field of pathoneurobiology, where currently available methods are insufficient in diagnosis of brain tumors in terms of ability to determine type of tumor, metastatic stage, etc..

The current invention can be used for additional applications that are not limited to specific organs, of which non-limiting examples are: early detection of immune responses (e.g., transplantation rejection and atherosclerosis), analysis of pathogens in tissues, immunolabeling of specific markers in tissues where high resolution is desired, (for example, if can distinguish between different types of samples), bacteriology

(morphological changes from antibiotics; Antibiotic resistance on the basis of morphology).

Appendix A.

An Apparatus for Imaging Liquids, Cells and Other Wet Samples in the Scanning Electron Microscope

S. Thiberge, O. Zik, E. Moses

5

Submitted to Reviews of Scientific Instruments in Jan 2003.

Appendix B.

Scanning Electron Microscopy of Wet Cells and Tissues

5 Stephan Thiberge, Amotz Nechushtan, David Sprinzak, Opher Gileadi, Vered Behar, Ory Zik, Yehuda Chowers, Joseph Schlessinger and Elisha Moses.

An Apparatus for Imaging Liquids, Cells and Other Wet Samples in the Scanning Electron Microscope

S. Thiberge[1], O. Zik[2,3], E. Moses[1*]

[1]Department of Physics Complex Systems, The Weizmann Institute of Science, 76100 Rehovot, Israel

[2] Quantomix Ltd., 12 Hamada St., Park Tamar, 76000 Rehovot, Israel

[3] El-Mul Technologies, Yavne, Israel

(January 26, 2003)

PACS:68.37.Hk, 87.64.Ee, 87.17.-d, 82.70.-y

Abstract

We present a new technique of scanning electron microscopy that is adapted to the study of wet samples. The wet environment is protected in a small chamber enclosed by a membrane, that is thin enough for energetic electrons to go through and interact with the sample studied. We detail both the technique and the general mechanisms of signal formation in the imaging of samples in a scanning electron microscope through a membrane. We first describe our setup and the properties required for the membrane, the main element in this method. Some simple measurements for its characterization are given, guiding the choice of material and thickness. We then go on to describe the capabilities of the technique in imaging a variety of different samples. We evaluate the accessible contrast and resolution, and the current needed to obtain them. Low contrast samples can be imaged with an im-

*Corresponding author

provement in resolution over optical microscopy. High contrast samples like gold markers labeling a biological cell can be imaged with a resolution of the order of $10nm$. We believe such a result opens up potential applications for routine experiments in biology, and expect this new technique to find numerous applications in domains where liquid samples are investigated such as soft materials science.

I. INTRODUCTION

Scanning microscopy techniques have seen an enormous advance in recent decades [1–6], driven by the ever increasing demand for the imaging of smaller and smaller scales, far below the resolution of light. In this paper we present the development of a new capability for the imaging of wet samples in the Scanning Electron Microscope (SEM), a need that arises in the material, medical and biological sciences. Such measurements have until now been limited by the need of sustaining the samples in a relative vacuum. Our system is based on the isolation of the fluid sample from the vacuum by the introduction of a membranous partition. Recent developments in polymer technology enable the production of thin membranes that are practically transparent to energetic electrons, yet are tough enough to withstand atmospheric pressures on one side and high vacuum on the other side. The imaged volume is the close proximity of the membrane, typically a few μm into the fluid. This is ideal for the inspection of objects that are stuck to the surface such as adherent biological cells. Our technique is furthermore easily adaptable to all existing Scanning Electron Microscopes, enabling measurements of wet samples at room temperature and at atmospheric pressure.

The approach we use was proposed and tried already at the advent of the SEM [7], but was subsequently rejected, mostly due to the unavailability of adequate materials. The material of choice at the time was colloidion, which was both unwieldy and resulted in unacceptably low resolution. The technique was left behind while users turned to the promise

of alternative approaches, such as fixation of cells followed by gold evaporation. The idea of using a membrane made of appropriate polymers as a separator between sample and vacuum resurfaced a few years ago, in the context of the Transmission Electron Microscopy (TEM) [8–11], met with limited success and was never applied to the SEM. The physics behind the image forming mechanism in these two modes of electron microscopy are in any case very different.

We show in a separate publication [12] that images can be obtained of cells in a wet environment. Cell structures that can also be immuno-gold labeled or stained are easily imaged. The method can be applied to a variety of different kinds of wet samples, not only cells but other tissue samples and complex fluids such as polymeric or micellar solutions as well.

The membrane is the central part of this method. Beyond several mechanical properties such as sturdiness and flexibility, one of the most important requirements of a membrane is that the electron beam interacts as little as possible with it. In this publication we characterize in detail the interaction of the beam with the membrane, giving some insight for the choice of a membrane for the purpose of wet SEM. We review in detail the signal formation mechanism and give a method to measure the beam - membrane interaction and to characterize the membrane. We also make a full evaluation of the minimum contrast observable with the membrane we use, and look at the resolution that can be obtained in different situations. We show that this method can be used to measure the backscattering coefficients of liquid. This is, to our knowledge, the first time such a measurement can be performed.

II. THE MICROSCOPE INSERTS

Sketches of the set-ups used are shown in Fig. 1. Chamber I addresses the various liquid samples and maintains them at atmospheric pressure. Chamber II is specifically designed to maintain samples with water at low pressure. All parts of the sample chambers are described

in the figures and captions and are straightforward, except for the membrane whose electron-transparent characteristics are a main concern of this paper. For Chamber I, sealing of the sample against the external pressure difference is done with a series of o-rings. Closing the sample presents a hazard to the membrane, since considerable deformation would be caused if we were to compress the fluid inside. To avoid this a small release channel is kept open through the stem of the insert, equilibrating the pressure inside by a slight release of fluid. The opening to this channel is subsequently sealed off with another o-ring that is screwed in place.

Decreasing the forces on the membrane is the main goal of Chamber II. This design reduces the risk of rupture, and in this way very thin membranes can be used. The idea is to keep an open channel between the sample and the microscope chamber. When the microscope is evacuated, the pressure at the sample is close to the water vapor pressure. The aperture is chosen so that the evaporation occurs at a very slow rate, and we measured about $50\mu l/hour$. The sample volume is usually between 80 and $100\mu l$. To diminish the evaporation from the sample itself, the chamber can contain a reservoir of pure water. In practice, working for several hours with the same sample presents no difficulty.

We used a JEOL 6400 SEM and a Philips XL30 ESEM-FEG microscopes. Chamber I can obviously be used with any SEM, while Chamber II was used in the ESEM microscope. Because of the vapor release, it seems more natural to work in the mode called 'low vacuum' one of three functioning modes of this microscope. In this mode a small amount of water vapor is present in the microscope chamber, and we usually worked at a pressure equal or below 0.1 Torr. However, the amount of vapor exiting our chamber is easily handled by the microscope's pump, and we discovered that we can work just as well in the 'high-vacuum' mode. This has no particular advantage with the ESEM, but demonstrates that Chamber II, like Chamber I, can be used in any SEM.

The membrane is the main element in this method and must have several important properties. First, it needs to be as transparent to electrons as possible. This implicates a low average atomic number (low Z) and a low density. Polymer films are therefore the most

adequate choice. Very good mechanical properties are also required. The membrane must resist high pressure differences, be flexible enough to handle in preparation of the sample and should have no porosity to ensure proper sealing of the chamber.

A priori, we expected that the electrical conductivity of the membrane should be high enough to prevent the local charging of the external surface of the membrane, which may blur the image. A thin conductive carbon film can be evaporated for this purpose on the external side of the membrane. However, we found that at high beam energy, this carbon layer is not necessary and that the liquid medium is sufficient to prevent charging effects. Still, at low energy a conductive layer has interesting features; it not only helps preventing charging effects, but also facilitates imaging through secondary electrons (SE) detection.

Finally, since the sample being observed has to be in very close contact with the membrane, the affinity of the membrane to biological samples may be an important factor.

We have tested, Formvar, Butvar and conducting polymers, commonly used in TEM to build supporting films [13,14], and polyimide, to build the membrane. Only the latter fulfills all the properties required. We used commercially available polyimide membranes of 1450Å thickness, that show no measurable porosity to water and resist the forces produced by atmospheric pressure over a large area, which we controlled by the use of a grid attached to the external side of the membrane (TEM Ni 125 to 330μm mesh were used). A carbon deposition of 50Å on the external surface was sometimes performed. Affinity properties were adjusted by chemical surface treatment of the membrane. For example, biological cells were grown on the membranes treated first with the extracellular matrix proteins fibronectin or laminin. Formvar membranes coated with carbon (total thickness between 50 and 70nm) have been used with the 'low pressure' Chamber II and are described in section VI.

III. MECHANISM OF CONTRAST FORMATION

There are two different contributions to the formation of a signal on the detector. The first is a source of uniform noise, while the second includes the signal:

1. When the beam hits the membrane, backscattered electrons (BSE) and secondary electrons (SE) are produced by the membrane itself. Only the SE produced in the first few nanometers (the mean free path of secondaries), can escape from the membrane [15, p.113]. This contribution is homogeneous since both the composition and the thickness of the membranes we use are the same everywhere. In the following, the suffix m (*membrane*) will refer to this contribution.

2. The portion of electrons from the beam which is not backscattered when crossing the membrane impinges upon the sample. Again, secondary electrons and backscattered electrons are produced. The SEs produced here have no chance to escape. In contrast, BSE created in the sample have the possibility to exit back out through the membrane. As they cross the membrane, they may generate secondary electrons which, if created at a distance from the surface which is below their mean free path, can escape to the detector. This second contribution to the signal is due to backscattering events in the zone of interest, which reach both the SE and BSE detectors. In the following, the suffix s (*sample*) will refer to this contribution.

The second contribution (s) is obviously the contribution of interest. It carries the information we seek while the first is related to the membrane only (m). A contrast between two neighboring points will be observable if the difference in the sample signal between them is higher than the fluctuations in the whole signal.

Given two different materials for which the backscattering coefficients are known and for a specific membrane, we would like to determine the conditions needed to form an image.

The total signal collected S is composed of both secondary electrons and backscattered electrons:

$$S \sim \epsilon_{BS}\eta + \epsilon_{SE}\delta \tag{1}$$

η and δ represent respectively the ratios of BSE and SE currents to the beam current. The coefficient ϵ represents the collection efficiency for the two kinds of electrons that are

detected. The backscattering coefficient η is on its own made of two contributions: BSE from inside the membrane (m) and BSE from inside the sample (s),

$$\eta = \eta_m + \eta_s.$$

Similarly, the SE scattering coefficient δ has two contributions,

$$\delta = \delta_m + \eta_s \Delta_m.$$

While δ_m represents the secondary electrons generated by electrons of the beam entering the membrane, Δ_m represents the secondaries generated in the membrane by electrons on their way out, after a relevant backscattering event inside the sample. The backscattering coefficient η_s thus multiplies Δ_m, because the flux of energetic beam electrons travelling back through the membrane is reduced from unity by η_s.

The SE emission coefficient Δ_m may contain a slow material dependence. Depending on the material located below the membrane, the energy spectra of the BSE can vary, and different energies of BSE may in turn have different efficiency to generate SE emissions.

Note that the definitions of backscattering and secondary coefficients we use and the coefficients usually described in the literature differ slightly. The latter are defined for a semi-infinite medium and are characteristic of the material (Gold, Carbon, Nylon, etc.). Here, the coefficients describe the charge emission for a membrane with its particular thickness and its carbon shield. They do not describe the charge emission of a semi-infinite sample of polyimide material. In the same way, the sample coefficients describe the signal coming from the material inside the sample but covered by the membrane. One of our objectives in the following will be to compare experimentally the measured coefficient to the classical theoretical coefficients characteristic of the material itself (e.g. water, gold, etc.).

Let us consider two adjacent points that give signals S_A and S_B. The material contrast between them is defined as:

$$C_{AB} = (S_A - S_B)/S_A \tag{2}$$

(assuming $S_A > S_B$). There are two basic ways to modify the signal S. One is to multiply it by a constant (amplification). The other is to add a positive or negative constant to the signal (this is the "black level"). The contribution of the membrane to the signal is the same everywhere. Its thickness and its composition are very well defined. So that neither composition contrast nor topographic contrast appear between points A and B because of the membrane. Contribution m is thus a constant that can be removed by an appropriate choice of the black level. Note that noise on the order of $\sqrt{n}$ where n is the number of electrons scattered from the membrane, may interfere with the measurement, but we ignore it here, returning to it in the next section. With this choice, the contrast between points A and B is greatly simplified:

$$C_{AB} = (\eta_{S_A} - \eta_{S_B})/\eta_{S_A} \tag{3}$$

The material contrast is related to the difference in the number of backscattering events occurring in the materials located below the membrane on points A and B.

IV. PASSAGE OF ELECTRONS THROUGH THE MEMBRANE

We proceed now to study experimentally the membrane characteristics and quantify that portion of the signal that is related to the membrane only and was suppressed in the expression of the contrast (Eq. 3) by an appropriate choice of the black level. We do this in terms of BSE and SE emitted from its surface as a function of the energy.

For this purpose we used four different samples and an assembly that allows the different samples to be inserted simultaneously inside the microscope (in practice, only three could be inserted together in the SEM chamber, so we repeated the experiment with overlapping trios and identical conditions). For different energies, the beam was positioned successively on each sample and the current between the ground and the sample was measured.

Sample A is just a Faraday Cup [16], used to measure the beam current I_b by collecting all the beam. Sample B is identical in design except that the aperture is covered with

a membrane. We call this measurement I_m. Sample C consists of a pure gold sample connected to ground and covered by a membrane. The gold was first melted so that its surface was smooth enough to obtain large areas where a direct contact with the membrane was achieved. Finally, Sample D is our experimental chamber, containing water and sealed by a membrane. Samples C and D define two values for I_s, where s refers here to gold or water.

The difference of currents measured on Samples A and B, normalized by that of Sample A, gives the percentage of electrons emitted by interaction with the membrane. This measures the sum of the secondary and backscattering coefficients of the membrane:

$$1 - I_m/I_b = \eta_m + \delta_m.$$

Similarly, the percentage of electrons emitted by interaction with the membrane plus the material located below is the difference of A and C or D:

$$1 - I_s/I_b = (\eta_m + \delta_m) + \eta_s(1 + \Delta_m).$$

The three measurements are shown in Fig. 3(a). For energies below $5keV$, the gold and water curves are seen to superpose on the membrane curve. This means that the beam is not energetic enough to reach the sample and send BSE back to the detector. Above $5keV$, the three curves differ; a growing portion of the signal detected is due to interaction with the material below the membrane. For the water sample and incident electrons energy of 10keV, beam-membrane interactions contribute 50% of the charge emission. Their contribution decreases to 35% at 15 keV. In the case of gold, because of its high atomic number, the membrane contribution falls already to 2% at $15keV$.

The next step is to subtract the membrane component and obtain the material contribution to the signal (Fig. 3(b)). This includes only electrons that are scattered by their interaction with the material of interest. At low energies the electrons of the beam do not reach the samples and the curves should be zero. At very high energy, the curves should follow the behavior of the backscattering coefficients of the materials, since the membrane

becomes practically transparent. This is indeed what we observe on the two curves. The decreasing slope of the water curve follows the theoretical behavior of the backscattering coefficient, as calculated from Hunger and Kuchler's derivation [17] (see also [15, p.95]). The increasing slope of the gold curve also follows directly the calculated backscattering coefficient evolution with energy (as derived from the same expression).

Normalizing these curves by the backscattering coefficient of the respective materials (with their appropriate energy dependence), we get curves where only a low material dependence remains (Fig. 3(c)). We attribute the observed small difference between the water and gold curves to different effects. One of them could be a slight overestimation of the backscattering coefficient of water with the Hunger and Kuchler expression. We must stress that, to our knowledge, no experimental data on the backscattering coefficient of liquid water exist, and that our method is the first that can be used for such a measurement, using high energies when the membrane effect is negligible. The second reason could be a filtering property of the membrane, since it is known that the energy spectra of BSE emitted depends on the material considered [18,15]. The energies range from 0 to E_0, where E_0 is the energy of the incident electrons. A light material (e.g. carbon) has a distribution that is approximately centered on the value $E_0/2$ and is symmetric. A heavy material (e.g. gold) has a distribution of BSE that is strongly asymmetric, with a peak closer to E_0. This difference has several consequences. First, the ratio of BSE that are able to cross back through the membrane to the total BSE produced is higher for heavy materials than for light ones. Thus, the membrane enhances artificially the contrast between light and heavy elements. Second, the difference in energy spectra of BSE can also influence the SE emission Δ_m since low energy BSE have a higher probability to generate SE on their way out. At 30keV, we observe a discrepancy of 25%, which we believe is due both to membrane related effects and to an overestimation of the backscattering coefficient.

The secondary emission Δ_m, is high at intermediate energies. The peak on the gold curve which reaches a value higher than 1, demonstrates this. At high energies, it decreases because energetic BSE generate less SE on their way out.

The two curves of Fig. 3(c) represent two extreme possible cases of low and high atomic numbers. For other materials of atomic number between that of water and gold, the corresponding curve will lie between the two extremes shown.

We summarize our conclusions from the results up to now as follows. For energies below $4 - 5keV$, no signal from the sample can be detected. This threshold can be decreased by using thinner membranes. In the intermediate region of energy Δ_m, the coefficient of emission of SE is high, and it is possible to image with the SE detector. This is illustrated by Fig.4(a) which shows milk imaged with SE. In the same intermediate region of energies, the membrane cuts a part of the BSE emitted by light materials, enhancing the contrast between heavy and light materials. For high energies, the charges emitted approach the theoretically predicted BSE coefficients (Δ_m diminishes and η_s approaches η) and it is easier to image using the BSE detector (Fig.4(b-e)).

V. DEDUCING A MINIMUM PROBE CURRENT

As soon as a small difference in the mean atomic number exist between two points, it is theoretically possible to observe it. The question is how many electrons are needed to make an observation. Such an estimate is useful since it indicates the ease and the feasibility of an observation. When high doses are required, charging and radiation damage are more of a problem. Also, high currents cause a lower resolution because the beam is less focused, and too long integration times may be damaging and are inconvenient.

We calculated the minimum current required to image specimens of specific contrast using the *threshold equation* [19], described in detail in Goldstein *et al.* [15]. Adapted to our case this equation is written as

$$I_B > 16/\eta_s T C^2 \quad (pA) \tag{4}$$

where η is the backscattering coefficient of the specimen and T the image scan time in seconds.

Results concerning biological specimens such as a cell, an oil/water emulsion and a gold particle in water are shown in Table I. A scan time of 100s was assumed. The results are strictly valid for high energies, for which the contrast C is simply related by equation 3 to the backscattering coefficients of the materials below the membranes.

A cell surrounded by an aqueous medium presents a low contrast, and furthermore the backscattering coefficients are low [21]. The minimal current required is then in the range of nano-Amperes. An oil/water emulsion presents a contrast ten times higher. The minimal current falls in that case to a few tens of pico-Amperes. Finally, a high contrast sample like gold particles requires only a fraction of a pico-Ampere.

These results match our experimental observations. Emulsions of oil/water, like milk, can be observed directly in standard conditions of current and integration time (Fig.4(a)). A biological sample such as a cell needs a high current to be imaged in a reasonable integration time (Fig.4(c)). Even under these conditions, the observable details are often close to the detection limit. One can advantageously use labeling with heavy markers such as colloidal gold particles (Fig.4(b)) to decorate the cell or stains like Uranyl Acetate or OsO4. Fig.4(d) shows the same cell as in Fig.4(c) after treatment with OsO4, with an evident increase in contrast. Fig.4(e) shows an assembly of lipid droplets in a cell treated with the same stain. Mitochondria are also visible.

VI. RESOLVING SMALL DETAILS AT DIFFERENT DEPTHS

Perhaps our strongest and most surprising result, and one that we need to understand, is that the experimental resolution is orders of magnitude better than what could be predicted theoretically. It turns out that the resolution obtained with the wet SEM depends on the size as well as the composition of the object observed. By large objects we mean those that are bigger or comparable to the interaction volume, or the volume sampled by the BSE. For them, the resolution is at this scale, i.e. the micron scale. For objects below this range like colloids, gold particles in water or small fat droplets in milk, it is possible to isolate in the

BSE signal a contribution of high spatial resolution. As we explain below, the mechanism for resolving small inclusions relies on the existence of a small, high resolution signal riding on a large, sometimes noisy, background. The resolution is ultimately limited by the size of the electron beam and determined by the issue of contrast and the associated detection capability.

A. Large objects

The theoretical way to calculate the resolution is to evaluate the effective signal producing volume, characterized by a diameter d_{eff} [15, p.162]:

$$d_{eff} = (d_B^2 + d_m^2 + d_{BSE}^2)^{1/2}.$$

The diameter of the beam entering the membrane, d_B, depends on the microscope electron source [20]. As the beam crosses the membrane, some scattering occurs. A beam with zero initial width $d_B = 0$ will emerge from the membrane with diameter d_m. The distance d_{BSE} is the mean diameter of the volume covered by electrons in the sample before returning as BSE.

The Kanaya-Okayama range R_{KO} is the typical radius of the volume of interaction of the electrons inside the material:

$$R_{KO} = 0.0276(A/Z)Z^{0.11}E_0^{1.67}/\rho$$

R_{KO} is expressed in μm, E_0 is the incident beam energy in keV, A is the atomic weight in $g/mole$, ρ is the density in g/cm^3 and Z is the atomic number. In the case of a gold sample, 80% of the BSE originate in a volume of diameter $d_{BSE} = 0.4R_{KO}$, for carbon it is $d_{BSE} = 1.0R_{KO}$ [15].

If the sample is mainly water, a simple approximation is that the membrane and the sample have close enough atomic numbers to be estimated as identical. Then, the resolution is simply

$$d_{eff} = (d_B^2 + d_{BSE}^2)^{1/2}.$$

Considering an average density $\rho = 1$ and a beam size in the nanometer range [20], this theoretical estimation predicts a resolution of few microns at $10keV$, while at $20keV$, it goes up to ten microns!

Luckily, the resolutions obtained experimentally are few orders of magnitude better. The estimate above is the general way to calculate the resolution when the signal originates from backscattering events. However this way to calculate applies to large objects without variations in composition on a smaller scale. It does not apply to many of the samples we studied, as well as most of the samples this wet electron microscopy technique could address. In reality, it is a convolution of the size of the object with the beam size that determines the resolution. Small inclusions can be imaged with a much higher resolution and include, for example, gold particles that label specific proteins in a cell, cell organelles stained with heavy materials or fat droplets in milk.

B. High contrast inclusions

For gold particles inside water, the scale of the volume of interaction is about a micrometer, while the scale of a the resolution obtained experimentally at high energy is about ten nanometers (see Figure 4(b)). Beads of actual diameter $40nm$ appear to be around $45nm$ diameter at $30keV$. Beads of diameter $20nm$ appear to be around $23nm$. The resolution is related to the diameter of the beam when reaching the depth at which the particle is located, not to the volume of interaction of BSE.

The important point is the following. At high energies, the beam can diffuse inside the water if there is no bead to intercept it, and the volume sampled by the BSE is deep and wide (up to ten microns as we saw above). The signal that the BSE generate is the result of integrating over a very large volume and for this reason, does not vary significantly when the beam is scanned. Furthermore, at high magnification, when the image size itself is on the order of the size of the BSE sampled volume, this deep BSE signal is a constant that can be removed by an appropriate choice of the black level. On the other hand, when the

electron beam crosses a heavy material bead, a significant part of the beam is intercepted and immediately many more BSE are emitted because of the high backscattering coefficient. Thus, the resolution obtained is dependent on the spatial extension of the electron beam when reaching the particle.

A bead that is located just below the membrane is imaged with the best resolution because there, the spreading of the beam is the lowest. The deeper is the particle inside the sample, the lower is the resolution at which it can be imaged.

The spreading of the beam is a problem that is well adapted to solution by Monte-Carlo simulations. We used a code devised by D.C. Joy [22,23] to perform such a calculation. Input values for the simulation are the Polyimide stoichiometric formula $C_{22}O_5H_{10}N_2$, the mean atomic number 6.4 and the mean atomic weight $9.8 g/mol$. The density of the material is $1.4 g/cc$.

Fig.5(a) shows the evolution of the 68% beam broadening diameter with energy, as determined from simulations using an incident beam of zero diameter and normal incidence. At $20keV$, the limit of resolution just below the $1450\AA$ thick membrane is estimated at $18nm$. At 30keV, the beam diameter at the same position would be $10nm$. The choice of 68% beam width is somewhat arbitrary, and is dependent on the efficiency of the particular detection system in use. It was made according to the experimental results with the 20nm gold beads in contact with the membrane. A 90% portion would yield a resolution two times lower than what is observed. The simulation predicts that using a membrane twice thinner enables imaging with $10nm$ resolution. We verified this experimentally with the 'low vacuum' Chamber II and carbon coated Formvar membranes of 50-70nm thickness (the manufacturer does not give definite thickness for these membranes, and they may vary between these two extremes). Ten nanometers gold particles stuck to the membrane could be resolved, appearing as object of approximately 15nm at 20keV.

To calculate the resolution for inclusions located deeper inside the sample, one must also take into account the spreading of the beam due the layer of water in between. An approximation is given by $d_{eff} = (d_b^2 + d_m^2 + d_{water}^2)^{1/2}$. The beam scattering d_{water} calculated from

Monte-Carlo simulations is shown in Fig.5(b). Summing the different contributions estimated, at 30keV, a particle located at 200nm below the 1450$\AA$ membrane should be imaged with a resolution around 14nm ($d_b = 1nm, d_m = 10nm, d_{water} = 10nm$). At 500$nm$ depth, the resolution is around 100nm and at 1000nm depth, it is few hundreds of nanometers.

Resolution is not the unique factor which determines whether inclusion imaging is good quality or not. Whether an object can be resolved or not depends also on how well it is detected. A second determinant factor is the contrast these objects produce. We first discuss this for high contrast (large Z) materials, and in the next subsection discuss the issue of low contrast (low Z) materials).

As a first illustration, we note that 20nm gold beads in contact with the 1450$\AA$ Polyimide membrane were imaged with very good resolution while 10nm were not even detected. This is because the beam size is by a factor two or three times bigger than the object, the signal amplitude is very low. A heavy inclusion is detectable if its size and the beam size are close together. If the object is smaller, the contrast is lost.

Also, when considering smaller and smaller particle size, the probability to generate BSE decreases. At high energies, the cross section for scattering of electrons decreases, and the BSE sampling depth in gold reaches the hundred nanometers scale. For example, at 30keV, it is in the range of 150 to 300nm ($0.1 - 0.2R_{KO}$). When considering a particle smaller than these values, a large proportion of the beam may cross it without interaction. Thus, for the same amount of electrons hitting it, a ten nanometers particle generates less BSE than a twenty nanometers one. The first conclusion to draw is that, to image small inclusions, we need higher currents then those estimated in section III which are strictly valid for large objects. Further, when increasing the energy to get the best focused beam, we may lose some more signal. Our experiments show that the particle size this becomes a real problem is very small in the case of gold and is around 10nm.

For completeness, it is of interest to evaluate how deep an inclusion can be detected inside

the sample. Considering that a heavy particle can be detected if its size is comparable to the beam size, the values of beam spreading calculated above should indicate the particles that can be observed at the considered depth. With the membrane used and at 30keV, a $20nm$ gold particle is visible until $250nm$ below the membrane, a $40nm$ diameter one should be detectable until $340nm$ approximately, and a 100nm one until $550nm$. These values differ for other energies, raising the intriguing possibility of obtaining depth information by varying the beam energy.

C. Low contrast inclusions

The case of light material inclusions presents many similarities with the previous situation. With milk, we were able to image details down to $100nm$ (data not shown). We were surprised to get better results with emulsions than with beads of similar material composition, and attribute this to the fact that emulsion droplets may wet the membrane. They can deform as they do so, exposing more material in contact with the membrane. Here, again, the resolution obtained is by far better than the size of the volume sampled by the BSE.

The best resolution for light inclusions should be similar to those of gold particles; it is related to the diameter of the beam. In practice, this is not so, and our ability to detect small light inclusions in water is limited more by contrast than by beam size. This is illustrated by the fact that while latex beads smaller than 150nm are hard to observe in pure water even with high probe current and long integration times, $93nm$ latex beads immersed in a solution containing a heavy elements like NaI salt at high concentration (4 Molar), were easily resolved (data not shown).

The limit on the smallest light inclusion size detectable is thus related to the ability to distinguish between small variations in BSE emission. While for gold beads, this limit seemed to be below 10nm, for carbonaceous compounds in water the limit is approximately ten times higher.

VII. DISCUSSION

Using our new technique, the full power of the SEM can be brought to bear upon the imaging of liquid samples, including wet cells, emulsions and any other material of interest. That full power is in practice limited by the physics of electron-matter interactions, and these constraints must be kept in mind when designing optimal experiments with the Wet SEM. The membranous partition has little or no influence on the resolution and contrast of BSE in comparison to a regular SEM. Still, the strongest physical constraint is probably that the resolution of SEM in soft (low Z) material turns out to be about 100 nm, only slightly better than the optical resolution. This resolution is still orders of magnitude better than what might have been expected using naive theoretical considerations.

For high Z materials the resolution is on the order of 10 nm, more in line with the standard (but also high Z!) SEM usage. Imaging 20nm particles is easily achieved when these are located in proximity of the polyimide membrane, as well as 10nm particles with a twice thinner membrane. Imaging of deeper inclusions requires them to be larger: a 40nm gold particle is visible and resolved until approximately $350nm$. This also allows some three dimensional information to be gleaned.

To our knowledge no other technique allows this kind of measurements. The closest in comparison is probably Soft X-Ray microscopy, whose limitation is that it requires very heavy equipment [24]. Only the wet SEM technique would allow simple, fast routine experiments at these resolutions.

Wet SEM has many interesting features for cell biology. Some cell organelles produce enough contrast to be visualized directly. In most cell lines, these are generally the nucleus, nucleoli, the cell membrane and the lipid droplets. This constitutes an original way of imaging in the context of cell biology since contrast originate from the materials mean atomic number.

Beyond the highly visible organelles, the difficulty to image biological samples without any staining is real. However, many biological issues can be visualized by the use of high

atomic number stains and labels. Staining and specific labeling are, as a matter of fact, techniques commonly used for both electron and optical microscopies in biology.

The development of non-destructive stains for biological cells is an important direction for further improvements. We used with success ferritin, a protein rich in Iron atoms, to image cells. The development of recombinant ferritin as a marker for SEM is an obvious next step, taking care to avoid an iron imbalance in the cell.

On the technical side, several improvements can be seen. The development of stiff, thinner membranes could allow working with a larger range of energies. The secondary emission was due for the main part to the carbon layer deposited on the membrane. Enhancing this emission using other material could be of interest for the detection at low energies. Effectively, using the backscattered electron detector is possible above a detection threshold usually around 7keV (for a semiconductor detector).

Finally, we believe this technique can also find applications in numerous areas of physics, such as materials research and complex fluids.

ACKNOWLEDGMENTS

We thank N. Levit-Binnun, Y. Karni, I. Shariv and D. Zajfman for insight and advice, J. Fineberg for a critical reading of the manuscript, and E. Klein for help in use of the SEM and O. Yeger for help in staining the cells.

REFERENCES

[1] G. Binnig, C.F. Quate and C. Gerber, Phys. Rev. Lett. **56**, 930 (1986); B. Drake *et al.*, Science **243**, 1586 (1989).

[2] G. Binnig, H. Rohrer, Ch. Gerber and E. Weibel, Phys. Rev. Lett. **50**, 120 (1983).

[3] U. Durig, D.W. Pohl and F. Rohner, J. Appl. Phys. **59**, 3318 (1986).

[4] E.H.K. Stelzer, J. Microsc. **189**, 15 (1997); J.T. Frohn, H.F. Knapp and A. Stemmer, PNAS **97**, 7232 (1999).

[5] W. Denk, J.H. Strickler and W.W. Webb, Science **248**, 73 (1990).

[6] G.D. Danilatos, Microsc. Res. Tech. **25**, 354 (1993); E.R. Prack, *ibid.* **25**, 487 (1993); G.D. Danilatos, Adv. Electron. Electron Phys. **71**, 109 (1988).

[7] R.F.M. Thornley, Ph.D. thesis, Univ. of Cambridge, 1960.

[8] I.M. Abrams and J.W. McBrain, J. Appl. Phys. **15**, 607 (1944).

[9] E.F. Fullam, Rev. Sci. Instrum. **43**, 245 (1972).

[10] J.A. Swift and A.C. Brown J. Phys. E: Sci. Instrum **3**, 924 (1970).

[11] Fujiyoshi *et al.* United States Patent 5,406,087 (1995).

[12] S. Thiberge, A. Nechushtan, D. Sprinzak, O. Gileadi, V. Behar, O. Zik, Y. Chowers, J. Schlessinger and E. Moses (unpublished).

[13] E. Davison and W. Colquhoun, J. Elec. Microsc. Tech. **2**, 35 (1985).

[14] D. Handley and B. Olsen, Ultramicroscopy **4**, 479 (1979).

[15] J.I. Goldstein *et al.*, *Scanning Electron Microscopy and X-Ray Microanalysis* (Plenom Press, New York, London 1992).

[16] The Faraday cup is constructed of a bulk of carbon connected to ground, with a cavity

(2*mm* diameter, 3*mm* deep) at its top, closed by a Ni plate with an aperture of 10μm diameter in the middle. The beam enters through the aperture, hits the bottom of the carbon cavity, so that the main beam and practically all scattered electrons are collected.

[17] H.J. Hunger and L. Kuchler, Phys. Status. Solidi A **56**, K45 (1979).

[18] H. Bishop, in *Proceedings of the 4th International Conference on X-ray Optics and Microanalysis, Paris, 1966,* edited by Hermann (Paris, 1966).

[19] C.W. Oatley, *The scanning electron microscope* (Cambridge University Press, Cambridge, 1972).

[20] A Field Emission source produces a beam of 1nm size in the best conditions(low current, high energy) and 10nm in the worst. A tungsten filament source produces a beam between 10nm and 100nm [15].

[21] The four elements C,H,N and O make up nearly 99% of the weight of a biological specimen like a cell. The cell is composed of 70% water and 29% organic compounds. About 50% of the atoms in these compounds are H atoms, 24% are C, 24% are O, and 1% are N atoms (B. Alberts *et al.,Molecular Biology of The Cell* (Garland Publishing Inc, New York, 1994)). Given these values, the mean atomic number of a typical organic molecule is 6.72, that of water is 7.22, and for a living cell, it is 7.07. Calculation of the corresponding backscattering coefficient at 20*keV* give 0.075 for water, 0.073 for a cell [17].

[22] D.C. Joy, computer code Monte Carlo Simulations of Electron Beam - Solid Interactions, available at www.microanalysis.org, 1991.

[23] D.C. Joy, *Monte Carlo Modeling for Electron Microscopy and Microanalysis* (Oxford University Press, New York, London, 1995).

[24] C. Jacobsen, Trends in Cell Biology **9**, 44 (1999).

TABLES

TABLE I. Evaluation of the minimum current needed for different samples containing water. I is calculated from the Eq.4. η are calculated with Hunger and Kuchler expression at $E = 20keV$, using the mean atomic number Z indicated. A scanning time of $T = 100s$ is assumed.

material	Z	η	contrast to water	I (pA)
water	7.22	0.075	-	-
Cells	7.07	0.073	0.027	2900
Oil	5.8	0.055	0.267	30
Gold	79	0.78	0.90	0.25

FIGURES

FIG. 1. A- Chamber I: The atmospheric pressure chamber set-up (a) and details of the membrane assembly (b). The membrane (1) is mounted on a plastic ring of inner diameter $2.8mm$. A TEM Ni grid is attached to the external side of the membrane to minimizes the risk of rupture due to the difference of pressure between the vacuum outside and the fluid inside. The whole membrane assembly is sandwiched between two stainless steel pieces, thus forming part I. The second part (II) is built on the basis of a conventional specimen mount for the SEM (diameter 12.7mm, pin diameter :3.2 mm). A small cavity (3) is drilled in the middle and a thin channel (4) joins the cavity to a small hole located at the middle height of the mounting pin. When preparing the sample, part I and II are first fully filled with fluid. Then they are assembled together using o-ring (2) while excess fluid is drained from the chamber through the bottom aperture. A second o-ring (5) is then put onto the pin to seal the bottom aperture. Part III screws on to seal the chamber assembly completely, pressing the second o-ring against the aperture.

B- Chamber II: The low pressure chamber set-up. The plastic ring where the membrane and the grid are mounted is itself mounted on a perspex ring (inner diameter 6mm, thickness 3mm). The cavity thus formed is filled with the liquid sample ($90\mu l$). The bottom of the chamber (12mm inner diameter) is filled with pure water ($100-200\mu l$). The ring is assembled to the chamber using an o-ring in between. The assembly is pressed by a aluminium part positioned on the top and attached by screws. The apertures used have a $100\mu m$ inner diameter and are 10 to 50mm long.

FIG. 2. Schematic of events giving rise to the *membrane* and the *sample* components of the signal. The upper dark gray region (1) represents an optional carbon-coated shield. The middle gray region (2) is the membrane itself, while the lower hatched region (3) is the sample. The middle thick arrows represent the incoming beam of electrons. SE escaping the sample are represented by short thin arrows, while BSE are represented by thin long arrows. When the beam penetrates the membrane, SE are emitted. These are 'membrane events' such as the two events shown on the left, while the two on the right carry 'sample' information.

FIG. 3. (A) Sum of the secondary and backscattering coefficients. Triangles represent the membrane signal: $\eta_m + \delta_m$. The circles (gold) and the squares (water) represent the total emission due to the membrane and the sample: $(\eta_m + \delta_m) + \eta_s(1 + \Delta_m)$.
(B) Sample signal: $\eta_s(1 + \Delta_m)$. The lines represent the backscattering coefficients as deduced from Hunger and Kuchler expression.
(C) Material signal divided by the corresponding theoretically determined backscattering coefficient.

FIG. 4. (a)Milk. The fat droplets appear dark on the background of the water which appears bright. SE detector. Bar $5\mu m$.
(b) Gold beads (diameter $20nm$) in water, attached to the membrane. Bar $500nm$.
(c)Unstained Chinese Hamster Ovary cells grown on a fibronectin coated membrane, fixed. Bar $10\mu m$.
(d)The same cell as (c) after 5minutes treatment with OsO4. Bar $10\mu m$.
(e)Lipid droplets in a CHO cell stained with OsO4. The contrast enhanced area shows mitochondria. Bar $2\mu m$.
All images shown were acquired with the Philips microscope at $30keV$ with the BSE detector, except (a) obtained in the JEOL microscope with the SE detector at $12keV$.

FIG. 5. A- Monte Carlo results for the beam diameter d_m after crossing the Polyimide membrane (see text). The squares are for a foil thickness of 1450Å, the triangles for a membrane which is half as thick (700Å). The values correspond to the 68% beam broadening diameter with an incident beam radius of zero. Taking into account the lateral extension of the incident beam, the effective beam diameter after crossing the membrane is given by $d_{eff} = \sqrt{(d_b^2 + d_m^2)}$.

B- Monte-Carlo simulation results for the 68% beam broadening diameter d_{water} after crossing a water layer, at 15keV (circles), 20keV (squares), and 30keV (triangles). Those values were calculated assuming that the beam radius is zero when getting into water. The effective beam didius is zero when getting into water. The effective beam diameter is given by $d_{eff} = \sqrt{(d_b^2 + d_m^2 + d_{water}^2)}$.

A

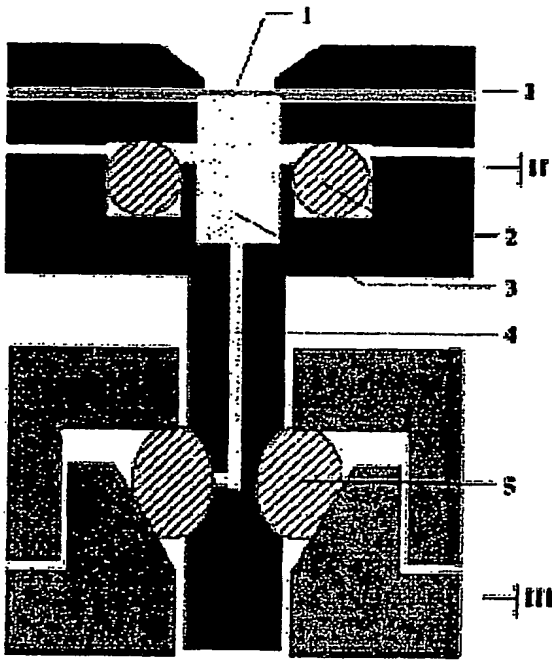

B

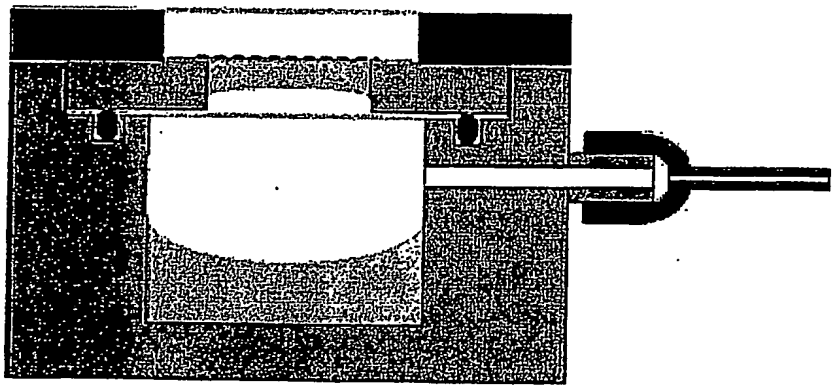

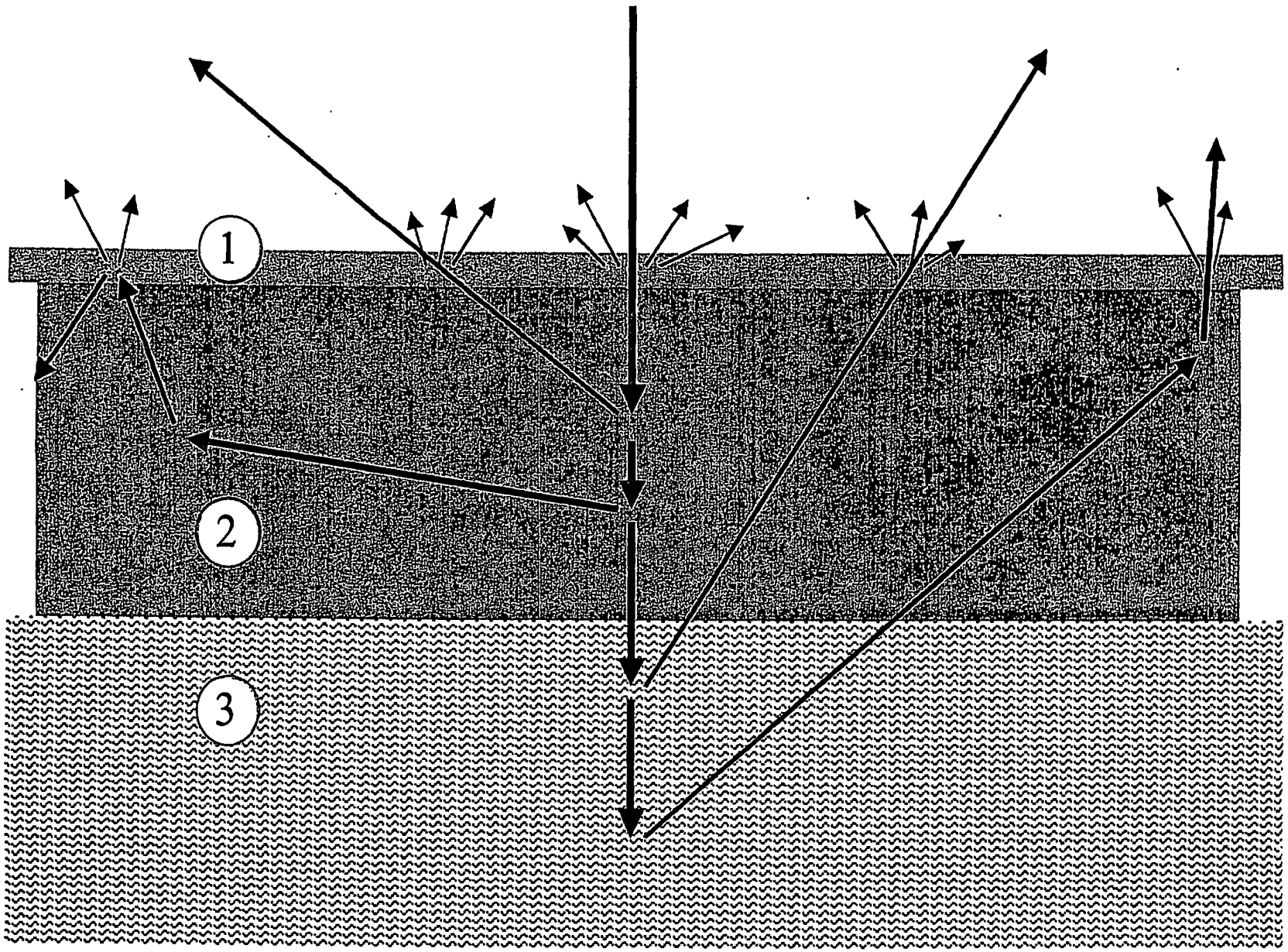

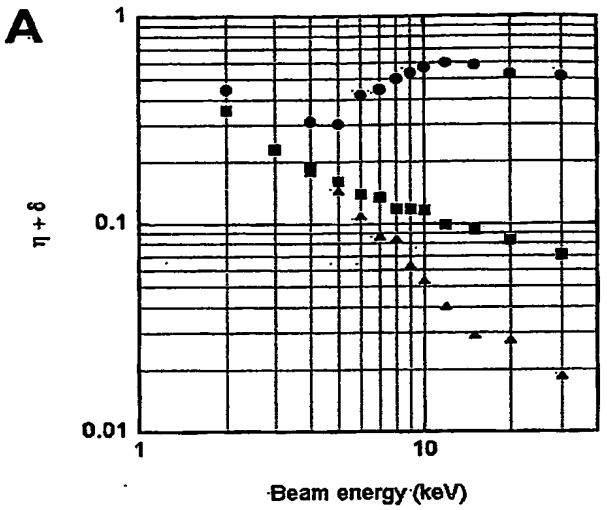
A
1
0.1
0.01
η + δ
1
10
Beam energy (keV)

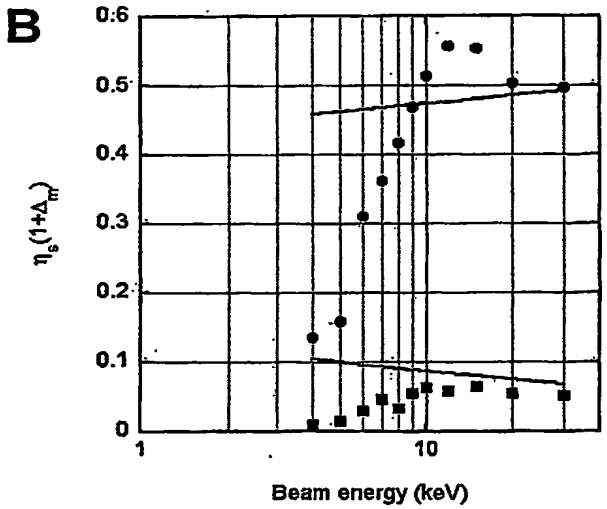
B
0.6
0.5
0.4
0.3
0.2
0.1
0
η_s(1+Δ_m)
1
10
Beam energy (keV)

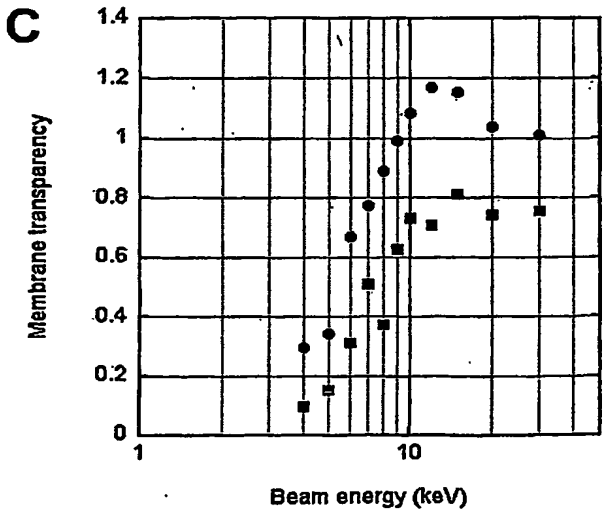
C
1.4
1.2
1
0.8
0.6
0.4
0.2
0
Membrane transparency
1
10
Beam energy (keV)

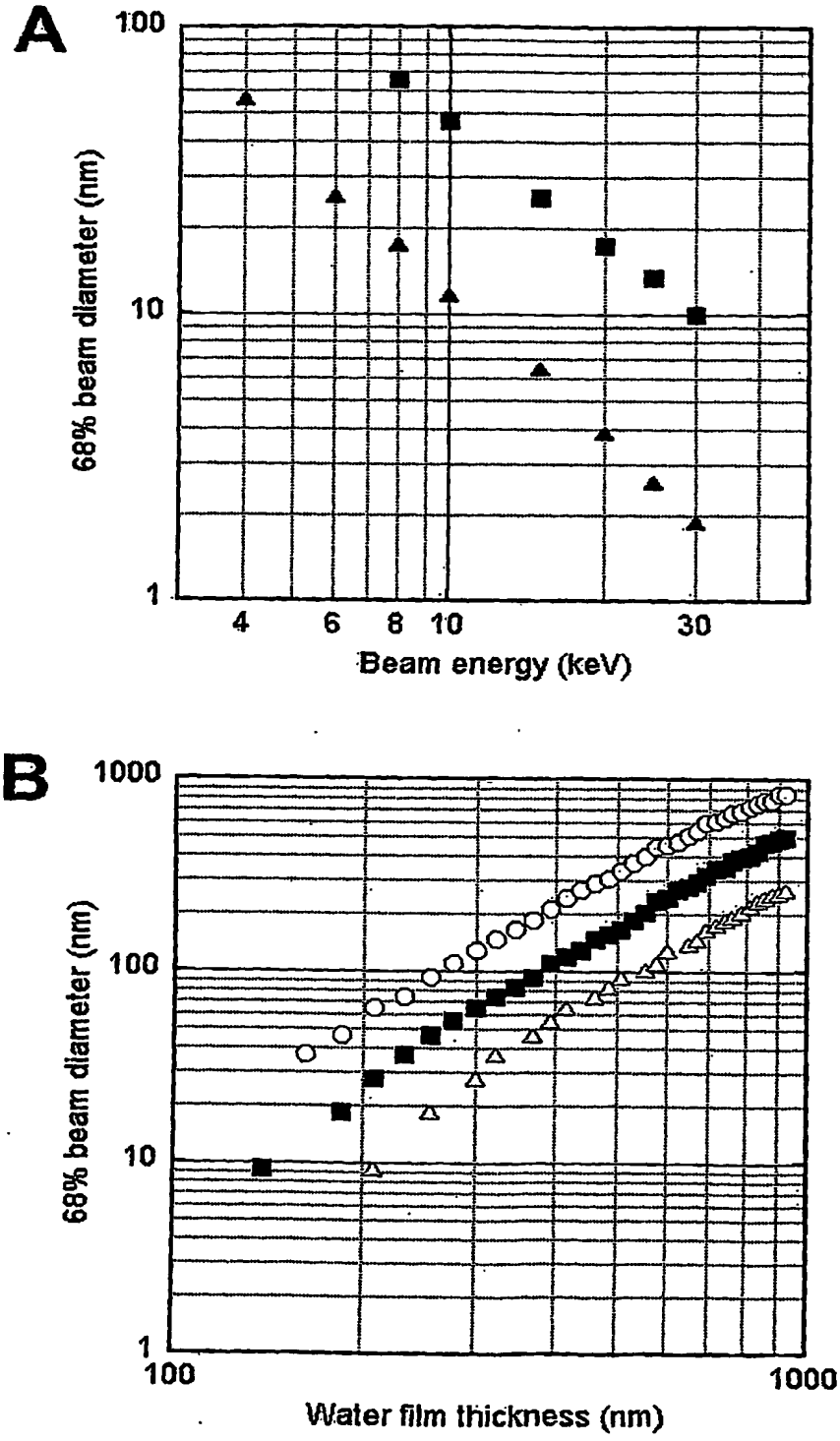

APP. 6

Scanning Electron Microscopy of Wet Cells and Tissues

Stephan Thiberge[a], Amotz Nechushtan[b], David Sprinzak[b], Opher Gileadi[b], Vered Behar[b], Ory Zik*[b], Yehuda Chowers[c], Joseph Schlessinger[d] and Elisha Moses[a]

[a]Department of Physics of Complex Systems, The Weizmann Institute of Science, Rehovot 76100, Israel

[b]Quantomix Ltd., 12 Hamada St., Weizmann Science Park, Rehovot, Israel

[c]Department of Gastroenterology, Chaim Sheba Medical Center, Tel-Hashomer 52621 Israel

[d]Department of Pharmacology, Yale University School of Medicine, New Haven, CT 06520 USA

A new capability for scanning electron microscopy (SEM) of wet biological specimens is presented. A membrane that is transparent to electrons protects the fully hydrated sample from the vacuum. The resulting images are a striking combination of morphological aspects of the whole cell with a wealth of internal details. The technique employs immuno-gold for specific molecule labeling and stains for observing intracellular structures. Thick tissue slices are directly inspected (with or without stains) at varying magnifications, while imaging only the external layer of cells. Simultaneous imaging with photons excited by the electron beam incorporates data on material distribution, with the potential for multi-labeling and specific scintillating markers.

Electron microscopy (EM) has been an indispensable tool for the life sciences since its inception more than half a century ago. Much of the substantial advances in the field have been propelled by the goal of imaging wet samples, and in particular biological cells. An ability to observe fully hydrated samples at room or body temperatures could help eliminate many artifacts of sample preparation and allow routine and reproducible imaging.

Recent progress in adaptation of Scanning EM (SEM) for observation of partially hydrated samples relies on technological improvements in differential pumping capabilities and of detectors, that together allow conditions that sustain the sample in a vapor environment (e.g. Environmental SEM, (*1-3*)). However, the goal of imaging wet, fully fluid samples has not been met by these advances till now. The question whether imaging at acceptable resolution and contrast is at all possible, and what will be seen once cells are imaged, remained open.

We present here a significant step in this direction, in which wet samples can be maintained in fully physiological conditions and imaged with little loss of resolution compared to standard SEM. Wet SEM relies on a thin membranous partition that protects the sample from the vacuum while being transparent to the beam electrons. This approach was proposed at the advent of the scanning electron microscope (*4*), but yielded an unacceptable resolution due to the unavailability of adequate materials at that time. Developments in polymer technology have yielded thin membranes that are practically transparent to energetic electrons, yet are tough enough to withstand atmospheric pressure differences. The volume imaged is in close proximity to the membrane, typically probing a few micrometers into the sample. This is ideal for the inspection of fluids or objects that are in close contact with the surface. The presence of fluid helps in preventing charging effects and eliminates the need to coat the sample.

This imaging system enables a number of observations that were previously inaccessible to SEM. First, the SEM can now be used to probe the *inside* of whole cells, giving information on organelles and internal structure. Second, staining and gold immunolabeling can be imaged with no subsequent critical point drying and coating (*5*). Third, we show that tissue sections can be viewed, giving structural information on the connectivity and organization of cells and extracellular structures *in situ*.

A further important advantage is the development of concurrent monitoring of light emitted from molecules inside the sample that are excited by the electron beam (*6*) (cathodoluminescence, or CL). This gives a complementary view of material distribution, including the ability to distinguish multiple labels.

Figure 1A is a schematic depiction of the basic sample holder used in Wet SEM, which can be used with any scanning electron microscope. The sample holder is essentially a rigid enclosure with a window that consists of a thin, electron-transparent partition membrane. Beam electrons go through the partition membrane, probe the sample and scatter back to the back-scattered electron (BSE) detector placed above the sample. Several membranes have been tested, of which polyimide membranes of 1450Å thickness were found to be the most appropriate. Variations on the basic design have been developed that allow different modes of insertion of the specimen to close contact with the membrane. For example, adherent cultured cells can be grown directly on the partition medium; bacteria or mammalian cells grown in suspension can be adsorbed or centrifuged onto the membrane prior to imaging; and tissues may be manually or mechanically brought to direct contact with the membrane. Another design incorporates a small leakage hole to the microscope chamber that is calculated to maintain the sample at low pressures while keeping it fully hydrated. This reduces the strain on the membrane, improves the endurance of the membrane and enables ultra-thin membranes (down to 500Å) to be used for increased resolution.

Theoretically, the resolution of Wet SEM depends on the volume sampled by Rutherford scattering of electrons (BSE). This volume depends mainly on the atomic number (Z) of the sample and on the acceleration voltage, or energy, of the beam electrons and is approximated by the Kanaya-Okayama radius (*5*). For biological samples the atomic number is low (e.g. carbon, Z=6 and oxygen, Z=8), and the radius of interaction is typically a few μm for acceleration voltages of 15-30 kV. Surprisingly, as Fig. 1B shows, the actual resolution is an order of magnitude better, since fat droplets in milk smaller than 100nm can be resolved. This is because the multiply scattered BSE probe such a large region (on the scale of a few μm) that their signal varies only slowly from point to point. The contrast is then obtained from electrons that scatter back after only a few interactions. These probe a much smaller region, on the scale of the width of the beam in the sample, and define a high resolution (similar to the description in chapter 4.6.2 in reference (*5*)). Images similar to Fig. 1C were used to evaluate the resolution numerically (*7*), giving values in the range of 100-120 nanometers. We found that emulsions yield a strong signal (and are easier to resolve than polymeric beads), presumably because they deform to wet the membrane and have more material close to the surface.

Figure 1D shows an untreated Chinese Hamster Ovary (CHO) cell in normal culture medium, at room temperature. The cell outline and the nucleus with its internal structure

are clearly visible, as are a series of dark spherical particles in the cytoplasm. The identification of these particles is discussed below.

Under the intense radiation of the electron microscope, the question of viability of cells naturally arises. It is well known that the amount of radiation absorbed during high magnification imaging is sufficient to cause cell death (*8*). However, no obvious structural damage was apparent and several repeated scans gave the same images. At longer times, on the scale of an hour following the imaging, some signs of deterioration such as cell shrinkage were visible.

The contrast for the main biological constituents is expected to be low. However, we observe that even in unstained samples, the differences between water and oil droplets (Fig. 1B), or between different constituents of the cell (Fig. 1C), generate sufficient contrast to distinguish some level of detail. In cells, higher Z materials such as salts, phosphor or iron concentrated in different regions may improve the contrast.

However, the limits on resolution and contrast when observing low atomic number (Z) materials suggest that substantial advantages can be achieved by staining the cells with high Z markers such as electron-dense stains or colloidal gold labels. Indeed, we have been able to detect gold beads in water down to a diameter of 10 nm (*9*).

Differential staining of organelles inside cells using electron dense materials is a standard in EM technique, though it is not usually applied for the SEM. Figures 2A-D show a rich variety of structures inside of cultured cells that were grown directly on the partition membrane, then fixed and stained with uranyl acetate (*10*). Intracellular organelles are clearly visible, including internal details of mitochondria (Fig. 2C), actin stress fibers (Fig. 2D), and complex tubular and cytoskeletal structures (Fig. 2A,B). The higher beam energy in Fig. 2C probes internal structure, while at lower energy (Fig. 2D) the surface close to the membrane is visualized. Thus, different energies can be used to obtain three-dimensional information.

The highest resolution and specificity of detection can be achieved by binding of antibodies or other ligands. As with other EM methods, labeling is most conveniently done using gold colloids. In contrast with transmission electron microscopy (TEM), which samples only very thin and often arbitrary sections, Wet SEM allows a quick switching between the local and global view of labeling all over the cell. Figures 2E-G show labeling of the epidermal growth factor (EGF) receptor on the surface of A431 cancer cells using 40-nm gold colloids. Fixation is often useful and convenient even in Wet SEM, it may facilitate the labeling, as well as the transfer to the microscope. The cells presented here are also stained with uranyl acetate, which allows alignment of the labeled receptors with the general structure of the cells. The high contrast and uniform size of the colloids enable unambiguous identification and localization. Knowing the precise localization of single receptor molecules opens the possibility of measuring events such as EGF-induced receptor dimerization. Labeling of actin filaments inside of cells has been achieved using sub-nanometer gold particles, followed by silver enhancement (data not shown).

An example of gold labeling on bacteria is given in Fig. 3G. Here, the putative gastrin receptor of *Helicobacter pylori* (*11*) is detected by incubation with complexes of biotinylated gastrin and strepavidin coated 20nm gold colloids. Administering the biotinylated gastrin prior to that of the strepavidin-gold yielded almost no attachment of

colloids to the bacterium. This result was obtained independently of the time between the two steps, suggesting that the uptake of gastrin into *H. pylori* is almost immediate. The fact that complexed gastrin did not enter the cells, points to the possibility of defining the limits of the size of particles that can be internalized by the bacteria.

Wet SEM can be used for thick specimens such as tissue fragments, by simply mounting the specimen against the membrane. The limited sampling depth of backscattered electrons allows imaging of a "virtual section", extending from the surface into a defined depth of up to a few microns, without the need for thin sectioning.

Figures 3A,B show the direct visualization of untreated tissues from mouse. Figure 3A is a small magnification image of cardiac tissue. The organization of the muscle cells is apparent. Zooming onto one cell (Fig. 3B) gives a vivid view of the nucleus and of intracellular organelles, possibly mitochondria, and their dispersion in the cell. As shown above for cultured cells, staining of tissues is advantageous but not imperative, and can enhance the visualization of many features. Figures 3C-D show a region of the renal cortex of a rat. The staining (potassium ferricyanide) accentuates the overall organization and cell contacts within the epithelia of the renal tubules. Careful adjustment of staining and imaging conditions can reveal different and complementary information such as tissue architecture, for example tissues stained with uranyl acetate yield a clear image of the extracellular matrix (*9*).

Backscattered electron detection in Wet SEM can be complemented by the simultaneous collection of photons. The scanning electron beam excites molecules in the sample, which may then emit light at characteristic wavelengths (cathodoluminescence). The light intensity is then used to derive an image of the distribution of scintillating molecules, either endogenous to the cell or labels that can be introduced extraneously. This image is obtained simultaneously with the imaging by BSE, at a resolution limited by electron-matter interactions and not by light diffraction (*6*). We have inserted a light guide into the fluid below the sample, which guides the emitted light to a photomultiplier. This setup achieves good coupling and efficient collection of the photons excited by the electron beam without compromising the efficiency of concurrent BSE detection.

Figure 4 shows untreated CHO cells, visualized simultaneously by BSE and by photons. In Fig. 4A the cell borders are clearly outlined in the electron imaging mode, and the nucleus, along with its nucleoli, are prominent as are the dark ~1μm spots around the nucleus. These appear in the cytoplasm of all mammalian cells we investigated, and while their number varies, they are usually dispersed around the nucleus. In the CL image shown in Fig. 4B the cell outline and the nucleus are clearly defined, indicative of a distribution of scintillating molecules (similar to autofluorescence) in the cell. In this mode the same spots are characterized by a high emission of photons. The combination of a high cathodoluminescent signal and high carbon content is typical of lipid droplets (*12*), which participate in the energy storage of the cell (*13*). We have confirmed this identification by using an independent test, adding 200μM oleic acid to cause a strong proliferation of lipid droplets in the cell (data not shown).

High-resolution imaging of markers is a highly desirable capability of the CL detection mode, requiring the development of labels for specific molecules in cells. We have easily imaged standard fluorescent beads of 0.2 micrometer, which emit photons

intensely under the electron beam (*9*), at a resolution of about 100nm (*7*). Imaging of smaller beads is limited by low brightness, entailing the development of specialized scintillation beads at small diameter (similar to the larger particles used in Scintillation Proximity Assays (*14*)). Since the mechanism for excitation of scintillation is strongest when the beam is directly impinging on the bead, we expect that this can extend the resolution of fluorescent imaging an order of magnitude beyond that available with optical microscopy.

Future directions of developing and applying Wet SEM are manifold. The easy processing of multiple samples suggests assays involving multiple time points or treatments. The system is easy to automate, as was previously done for the inspection of semiconductors (*15*) and this opens the possibility for drug screening based on high-resolution imaging of the treated cells. The development of specific and localized labeling in the cell, such as scintillating markers and recombinant metal binding proteins (e.g. ferritin) is promising. Finally, the direct imaging of tissues opens opportunities for investigative and medical histopathology.

In summary, Wet SEM combines several advantages: the ability to probe into cells like optical microscopy or TEM, a simplicity of sample preparation comparable to optical microscopy, and the resolution of the standard SEM along with its ease of use and ability of zooming in.

Acknowledgements:
We thank Nathan Ezov for help with tissue samples, Sini Ezer, Miri Horowitz, Yiftach Karni, Eugenia Klein, Trisha Rice, Alon Sabban, Anya Vainshtein and Orna Yeger for support and assistance, Iris Barshack, Deborah Brown, Benny Geiger, David Joy and Daniel Zajfman for helpful advice and discussions. Work partially supported by the Segre Research Grant.

References and Notes:

1. Robinson, V.N.E., "A wet stage modification to a scanning electron microscope", *J. Microscopy* **103**, 71 (1975).

2. G.D. Danilatos, "Review and outline of environmental Sem at present", *J. Microscopy*, **162**, 391 (1991).

3. Philips Corp. *Environmental scanning electron microscope*, Eindhoven the Netherlands (Robert Johnson Assoc. El dorado Hills CA) (1996).

4. Early attempts are best seen in the work of R.F.M. Thornley "New Applications of the Scanning Electron Microscope", PhD thesis, Univ. of Cambridge (September 1960).

5. J.I. Goldstein, D.E. Newbury, P. Echlin, D.C. Joy, A.D. Romig, C.E. Lyman, C. Fiori, E. Lifshin., "Scanning electron microscopy and X-ray microanalysis", 2nd edition (Plenum Press, New York 1992).

6. A. Boyde, S.A. Reid, "A new method of scanning electron microscopy for imaging biological tissues", *Nature* **302**, 522 (1983).

7. D. Joy, Y.U. Ko, J. Hwu, "Metrics of resolution and performance for CD-SEMs", can be downloaded from http://web.utk.edu/~srcutk.

8. "Health Effects of Exposure to Low Levels of Ionizing Radiation"; Biological Effects of Ionizing Radiation (BEIR) Report V; National Research Council (1990).

9. Further information is available on Science Online

10. S. Levenberg, B-Z. Katz, K.M. Yamada, B. Geiger, "Long-range and selective autoregulation of cell-cell or cell-matrix adhesions by cadherin or integrin ligands", *Journal of Cell Science* **111**, 347 (1998).

11. M.Y. Chowers, N. Keller, R. Tal, I. Barshack, R. Lang, S. Bar-Meir, Chowers Y, "Human gastrin: a Helicobacter pylori--specific growth factor" *Gastroenterology* **117**, 1113 (1999).

12. G. Ning, T. Fugimoto, H. Koike, K. Ogawa, "Cathodoluminescence-emitting droplets in rat testis: a study by analytical color fluorescence electron microscopy", *Cell Tissue Res.* **271**, 217 (1993).

13. D.A. Brown, "Lipid droplets: Proteins floating on a pool of fat", *Cur. Biol.*, 11, R446 (2001).

14. N. Bosworth, P. Towers, "Scintillation proximity assay", *Nature* **341**, 167 (1989).

15. S. Somekh, "Increasing overall equipment effectiveness (OEE) in Fab manufacturing", *Seminconductor Fabtech*, **10th ed.**, 39 (1999).

Figure legends.

Fig. 1. Imaging of unstained specimens.

(A) Wet SEM sample holder (schematic). The sample is depicted here as cultured cells grown on the thin partition membrane (a) that separates the vacuum from the fluid in the holder. Imaging is done in a SEM: the electron beam (thick arrow) penetrates into the sample, and back-scattered electrons (thin blue arrow) are detected by a BSE detector (b). A grid (dashed line) is used to support and reinforce the membrane. A light guide (c) is introduced at the bottom for cathodoluminescence applications (see text and Fig. 4). The membranes are mounted on a plastic ring and treated with extra-cellular matrix proteins. Cells in their appropriate growth medium are deposited onto the membrane and incubated. Before observation, the membrane is turned upside down and assembled onto the sample holder. Different microscopes were used: JEOL 6400 SEM, FEI XL30 ESEM and FEI XL30 ESEM-FEG in both low (0.1 Torr) and high (10^{-4} Torr) vacuum modes.

(B) Lowfat (1.5%) milk. Voltage 12kV. Scale bar: 5µm

(C) As in (B). Scale bar: 2µm

(D) Untreated CHO cell, grown on fibronectin-coated membrane in normal growth medium. Scale bar: 5µm

Fig. 2. Imaging of cells

Asterisks denote nuclei, thin arrows denote mitochondria, arrowheads in F denote gold colloids.

(A) HeLa cells, grown on the membrane in normal growth serum then fixed with paraformaldehyde and stained with uranyl acetate. Imaged at 12 kV. Bar: 10 µm.

(B) Magnification of the marked rectangle in (A). Bar: 2 µm.

(C) CHO cell, fixed with glutaraldehyde and paraformaldehyde, stained with uranyl acetate (pH 3.5) and maintained in water. The thick arrow denotes a mitochondria which engulf a lipid droplet. Imaged at 30 kV. Bar; 5 µm. Inset: higher magnification showing mitochondria (arrowheads). Bar: 1 µm.

(D) Actin fibers in stained HeLa cells, as in (A). bar: 20 µm.

(E) EGF receptors immunolabeled with 40-nm gold colloids on A431 cells, counterstained with uranyl acetate. Imaged at 30 kV. Bar: 10 µm.

(F) Magnification of the marked rectangle in (E). Bar: 2 µm

(G) *Helicobacter Pylori* gastrin after incubation with complexed biotinylated gastrin on streptavidin coated 20nm gold particles, followed by glutaraldehyde and sedimentation onto the poly-L-lysine coated membrane. Imaged at 20kV Bar: 1 µm

Fig. 3. Imaging of tissues.

(A) Mouse heart, untreated, imaged directly in the sample holder at 30kV. Bar: 20 µm.

(B) Higher magnification of the rectangle in (A). Bar: 2 µm.

(C) Rat kidney was dissected, cut and fixed in formalin for 24h. The tissue was then stained with 0.1% uranyl acetate for 10 minutes. The images in (C) and (D) show epithelial cells within the inner surface of the tubules of the medullary. Rays. The grid supporting the membrane is visible in this picture. Bar: 100 μm.
(D) Magnification of box in (C). Bar: 5 μm.

Fig. 4. Simultaneous imaging with backscattered and electron beam excited photons (cathodoluminescence).
(A) CHO cell, imaged using back-scattered electrons as in 1(C). bar: 10 μm.
(B) Emitted light image taken simultaneously with (A).

Fig. 1

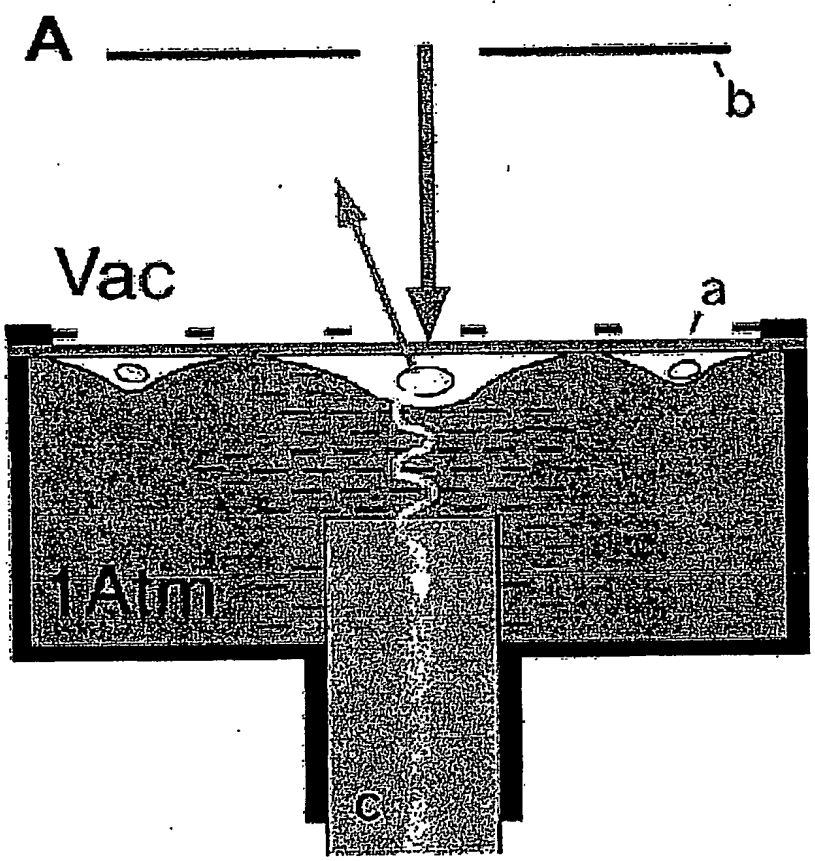

Fig. 1

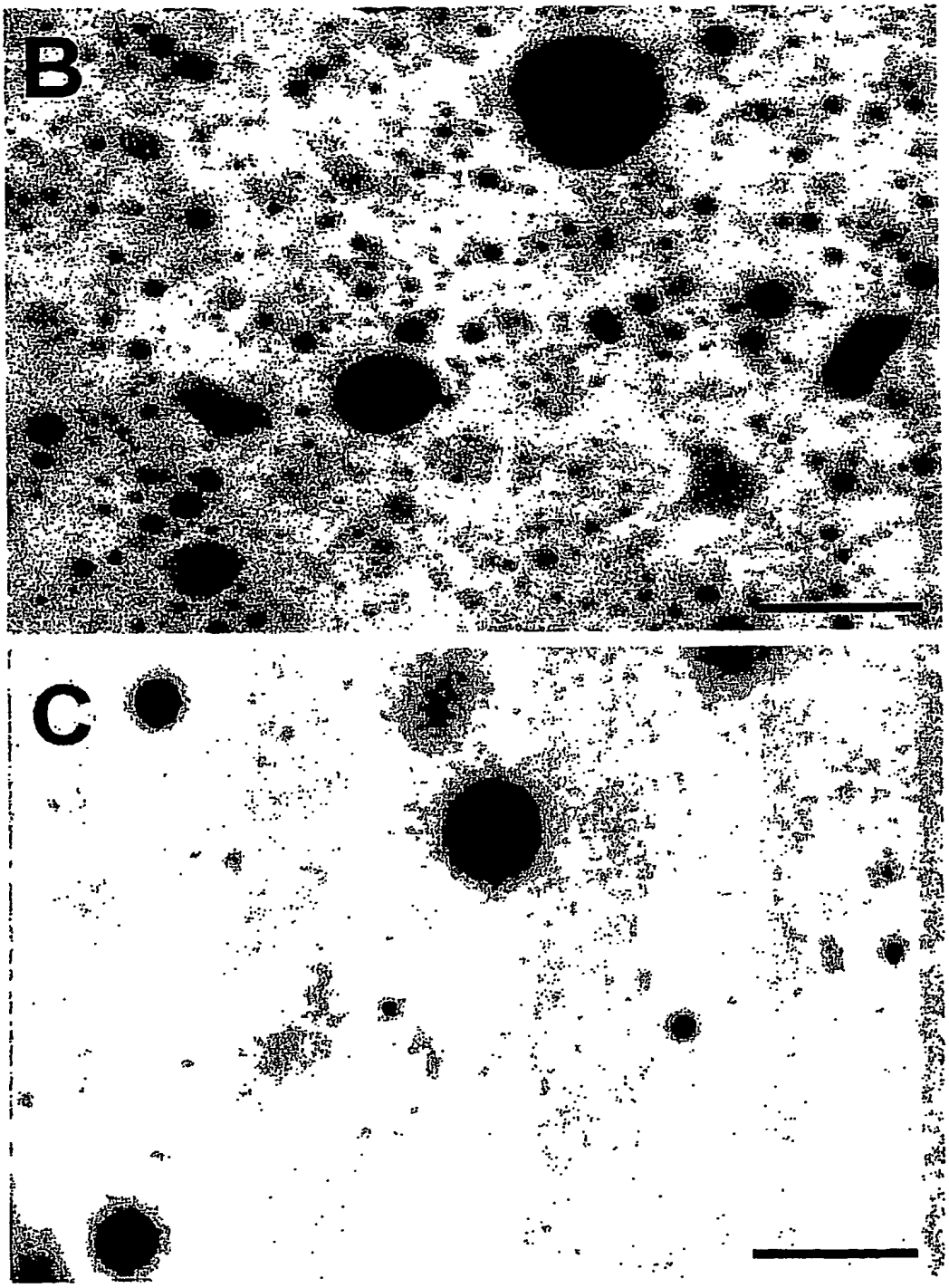

Fig. 1

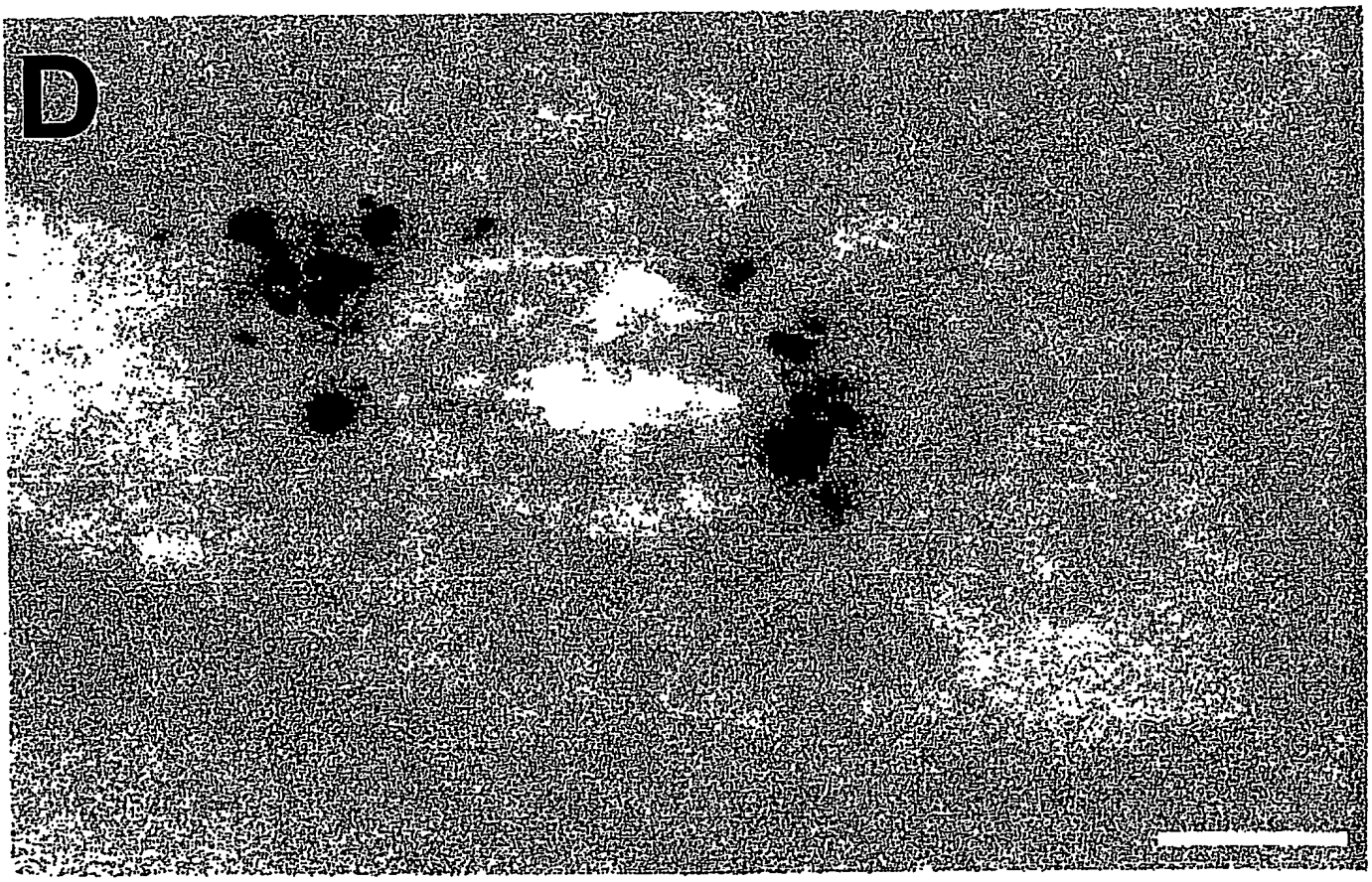

Fig. 2

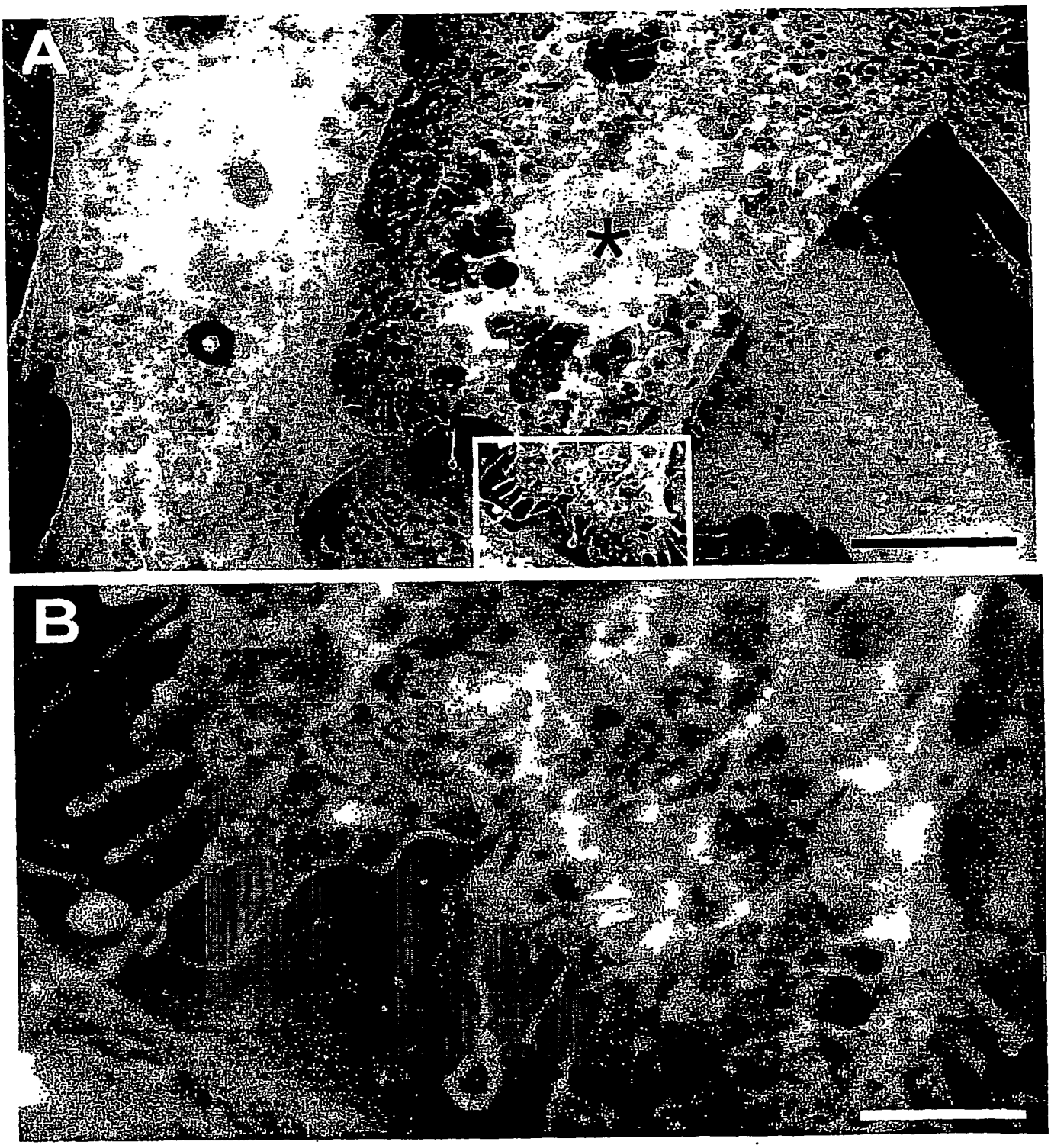

Fig. 2

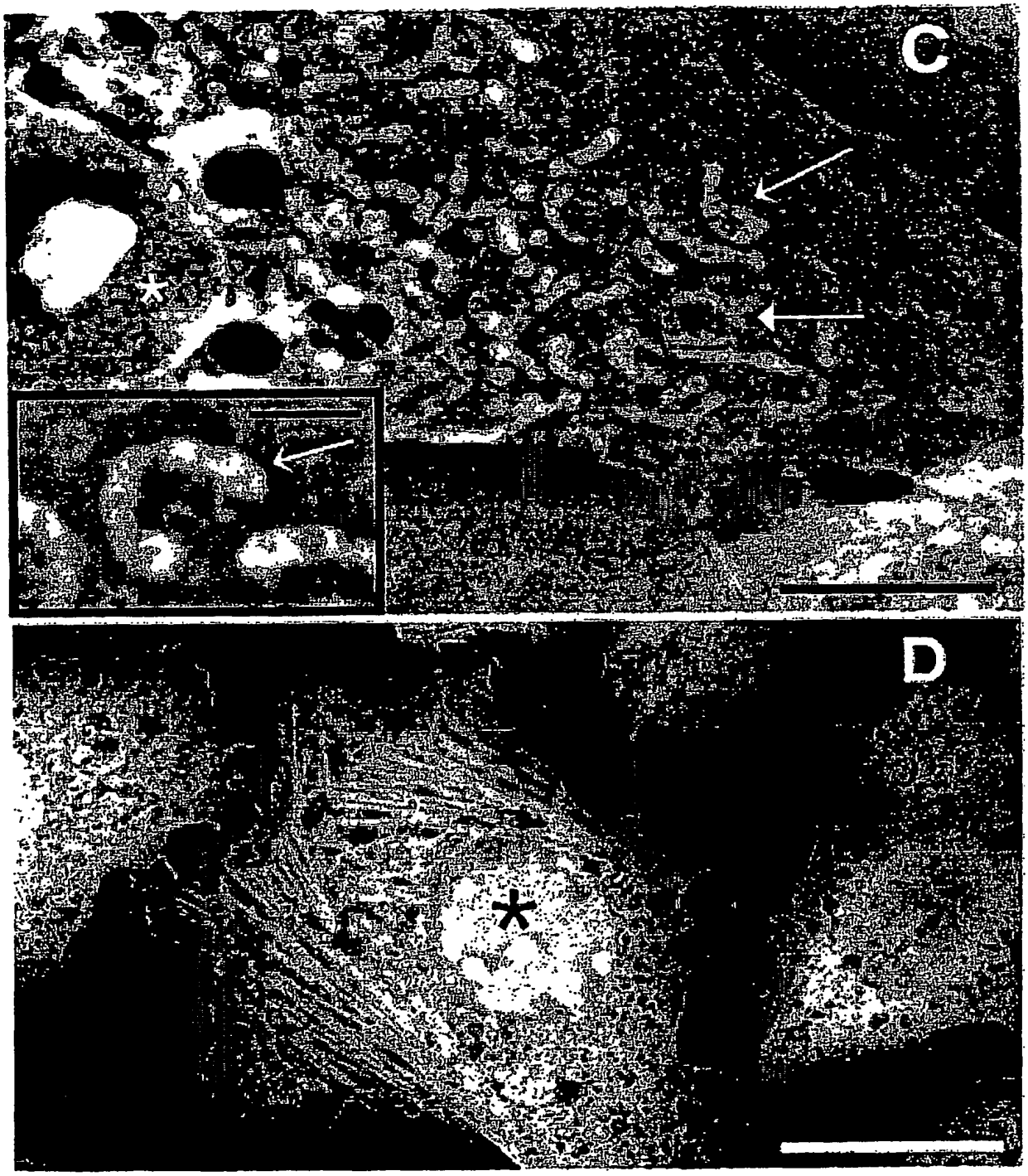

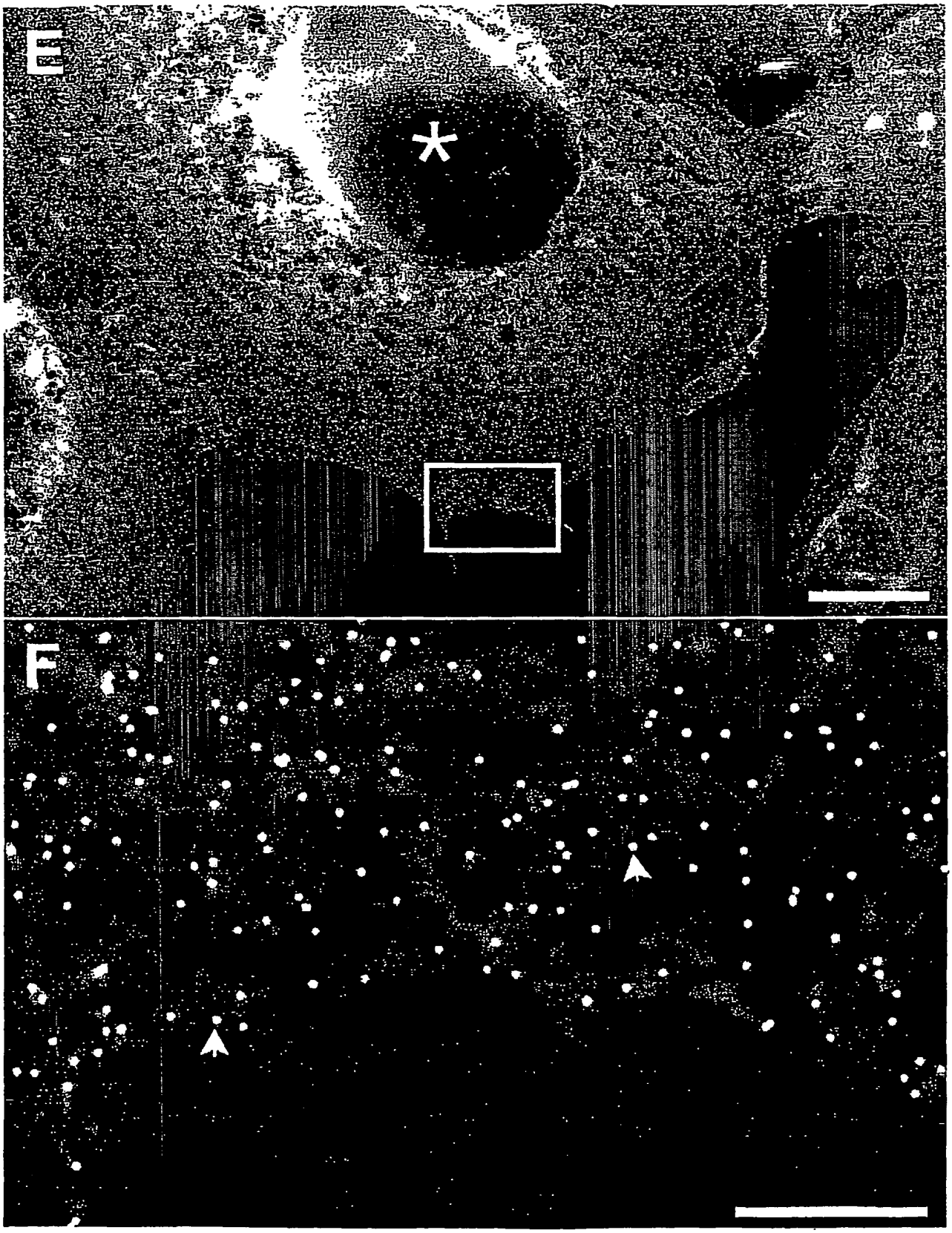

Fig. 2

Fig. 2

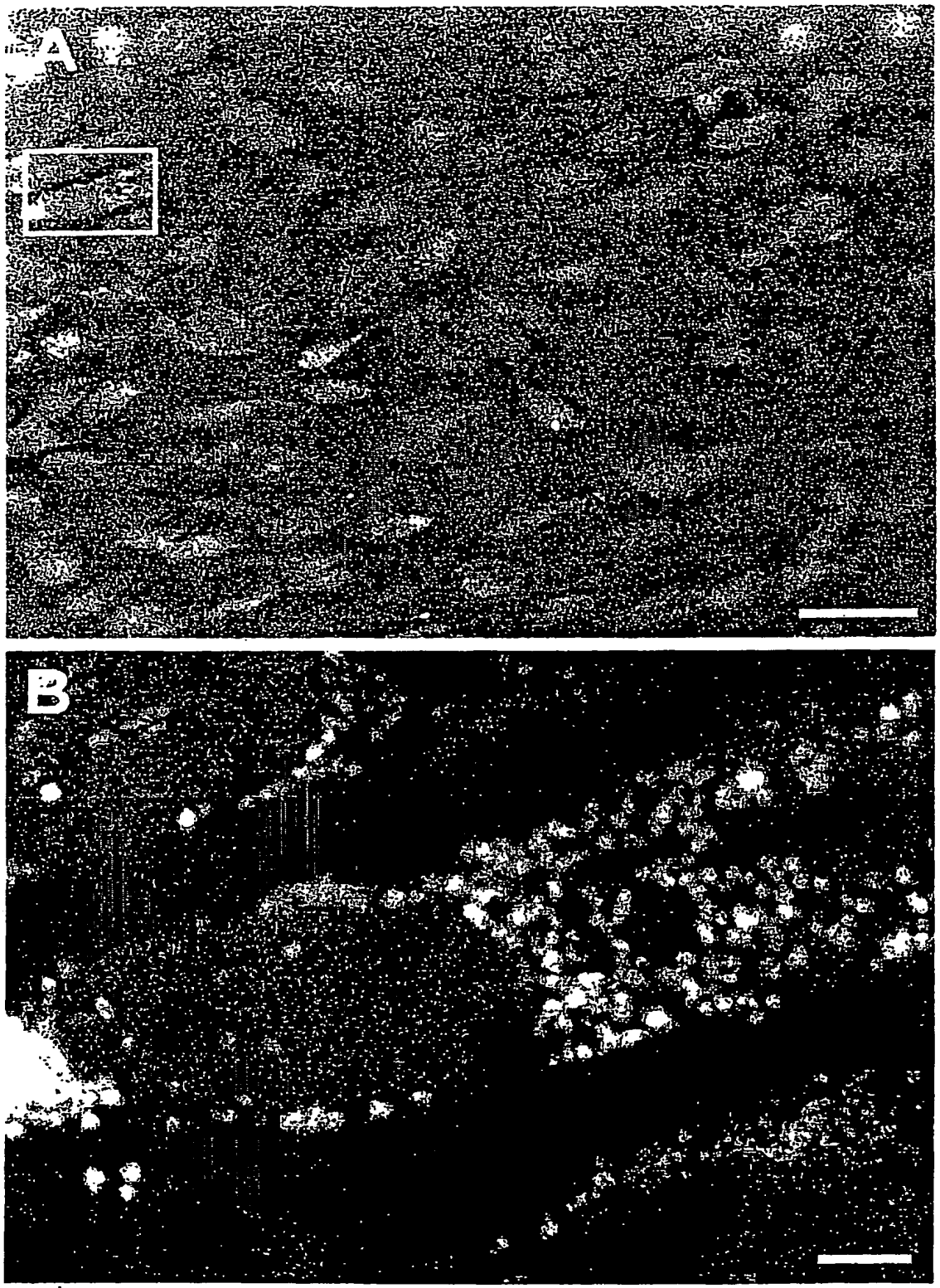

Fig. 3

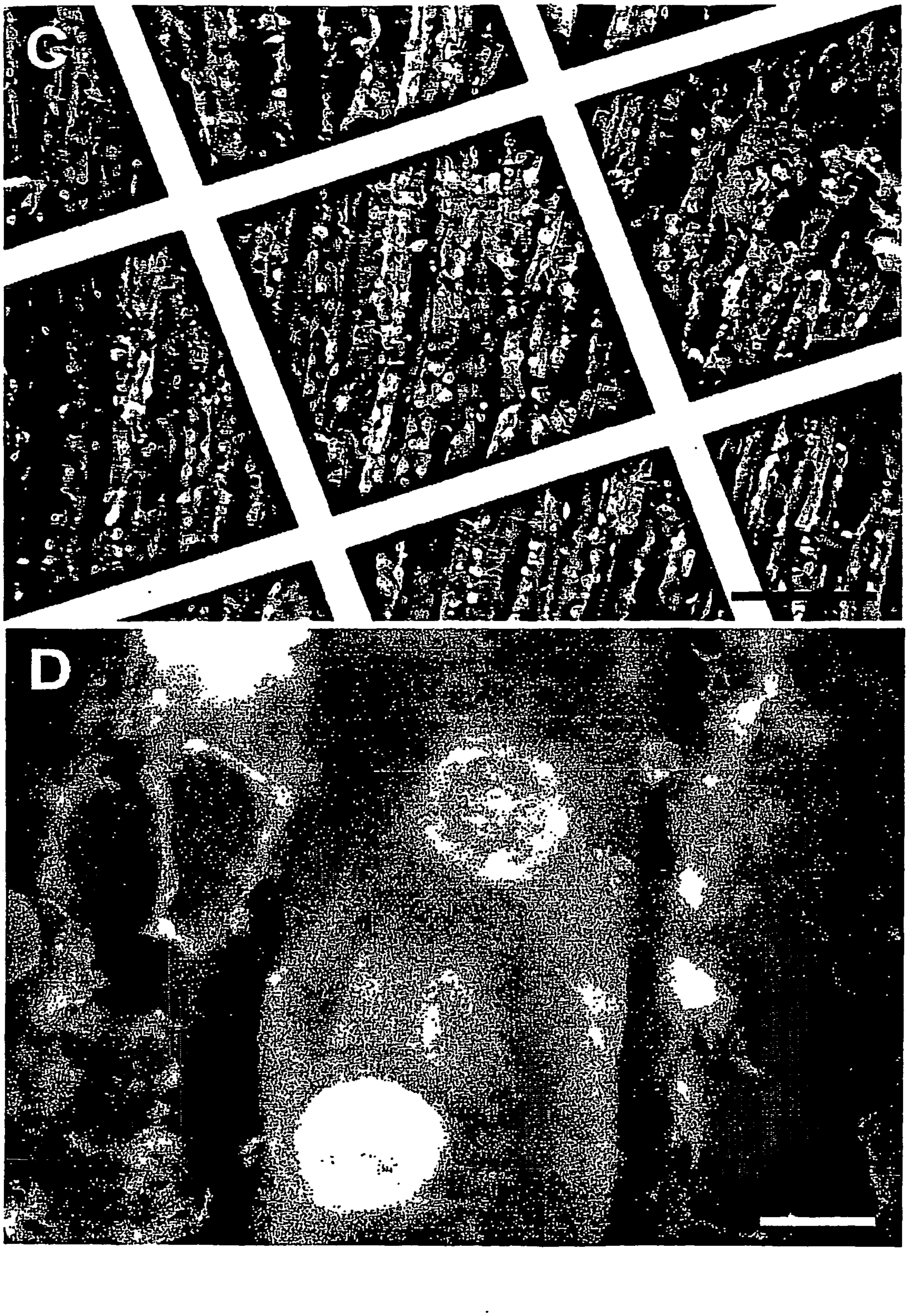

Fig. 3

Fig. 4

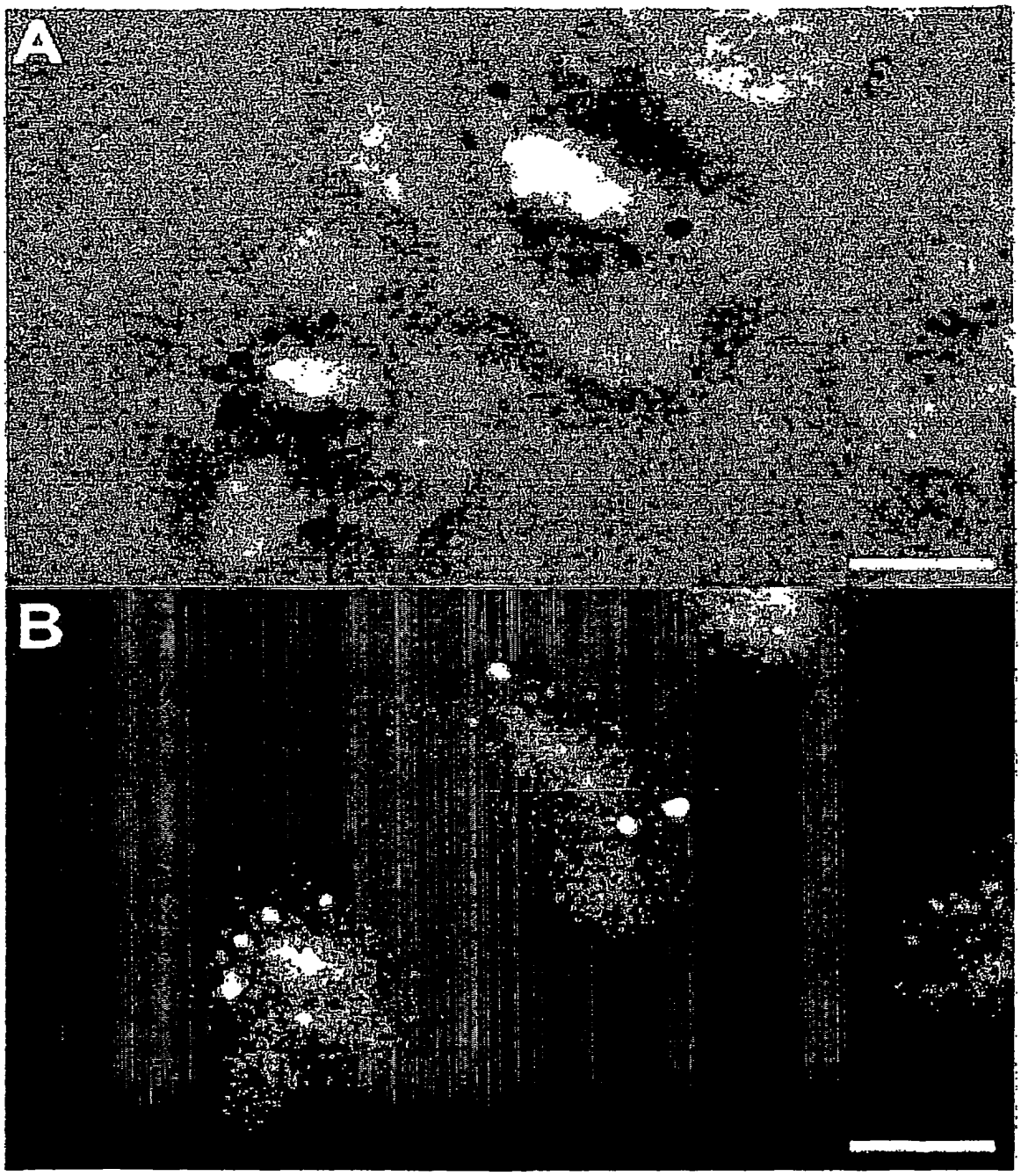

SUPPORTING MATERIALS

for the paper

Scanning Electron Microscopy of Wet Cells and Tissues

by Thiberge et al.

Fig. A. 10nm cationic gold colloids in water, imaged under a 50nm Formvar and carbon membrane mounted on a TEM grid. Voltage: 30kV, Scale bar: 100nm.

Fig. B. Polystyrene beads with Surf-Green fluorescent dye, 200nm diameter (BLI, Indiana, USA) imaged by cathodoluminescence. Voltage: 15 kV, Scale bar: 2 µm.

Fig. C. Extracellular matrix of mouse pancreas stained with uranyl acetate. Voltage: 15 kV, Bar: 20 µm

Supporting materials

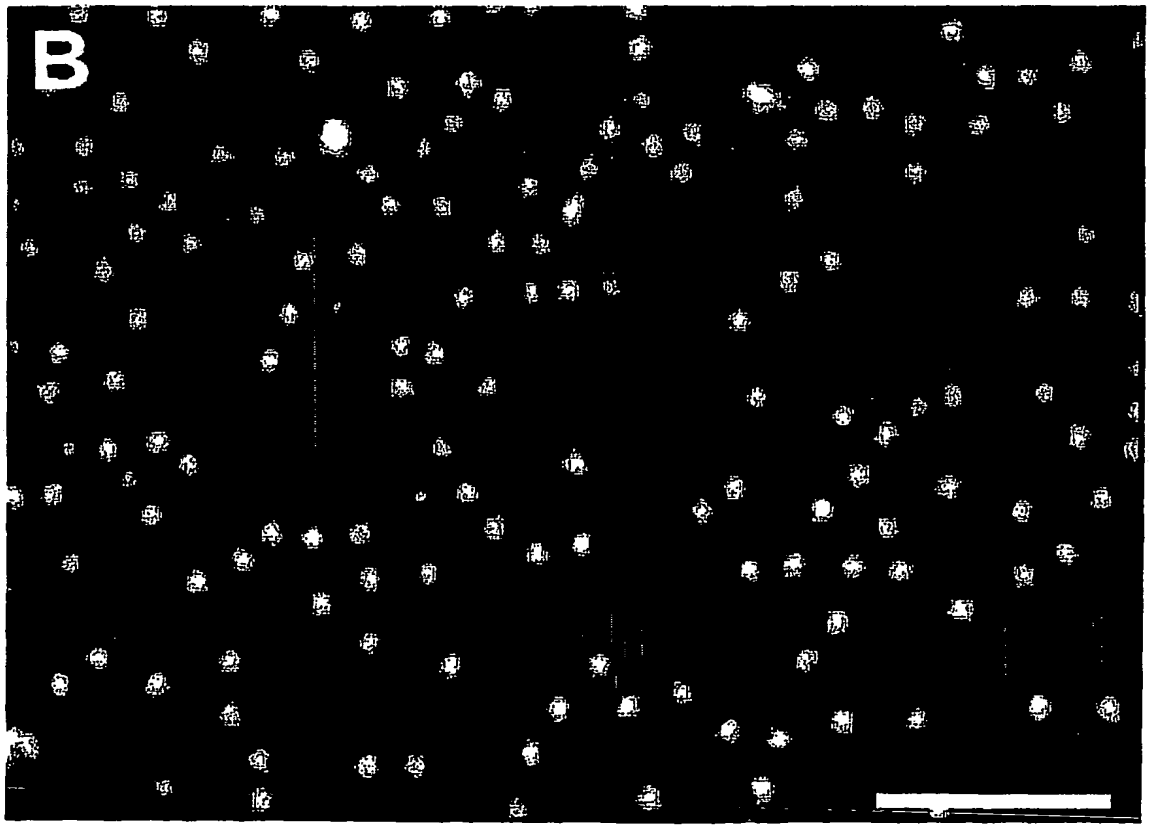

Supporting Materials

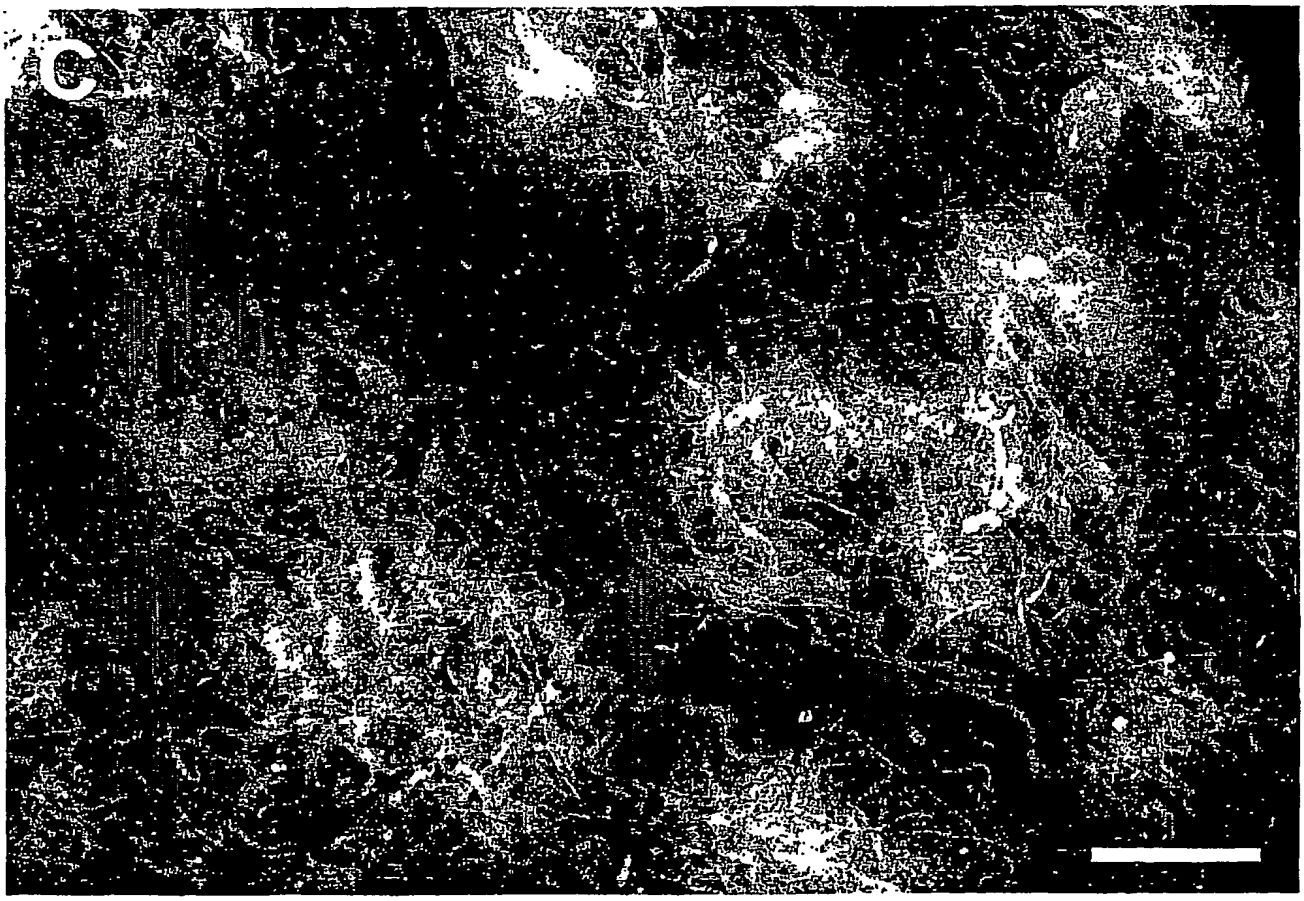

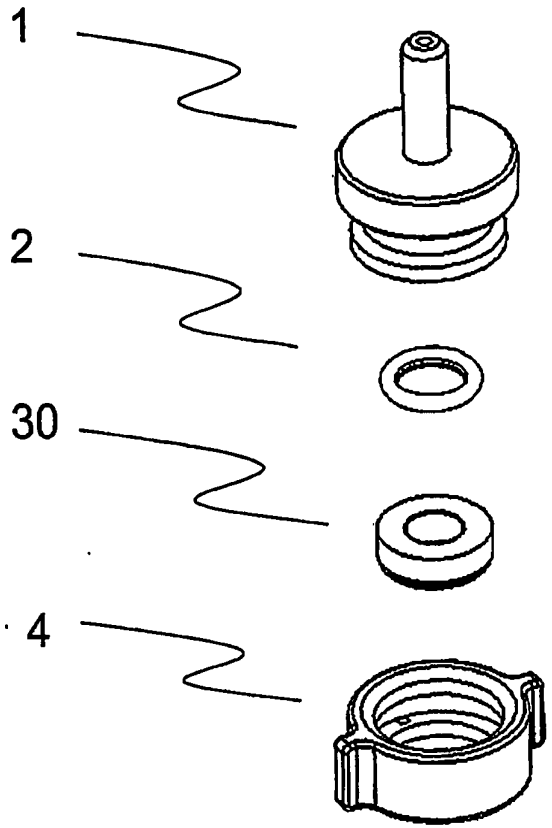

FIG. 1

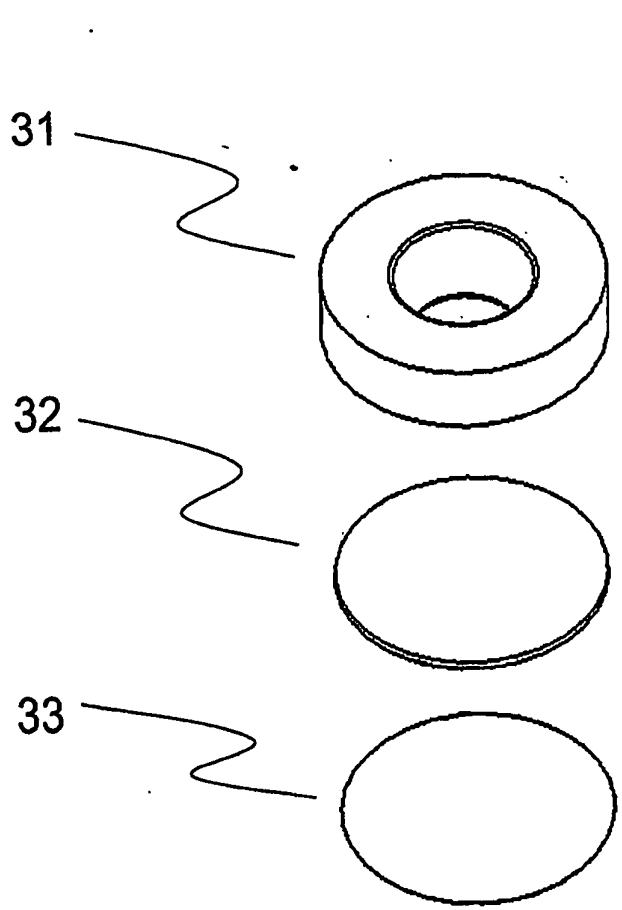

FIG. 2

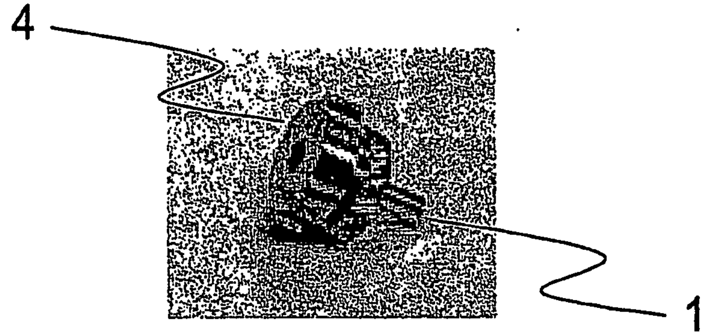

FIG. 3

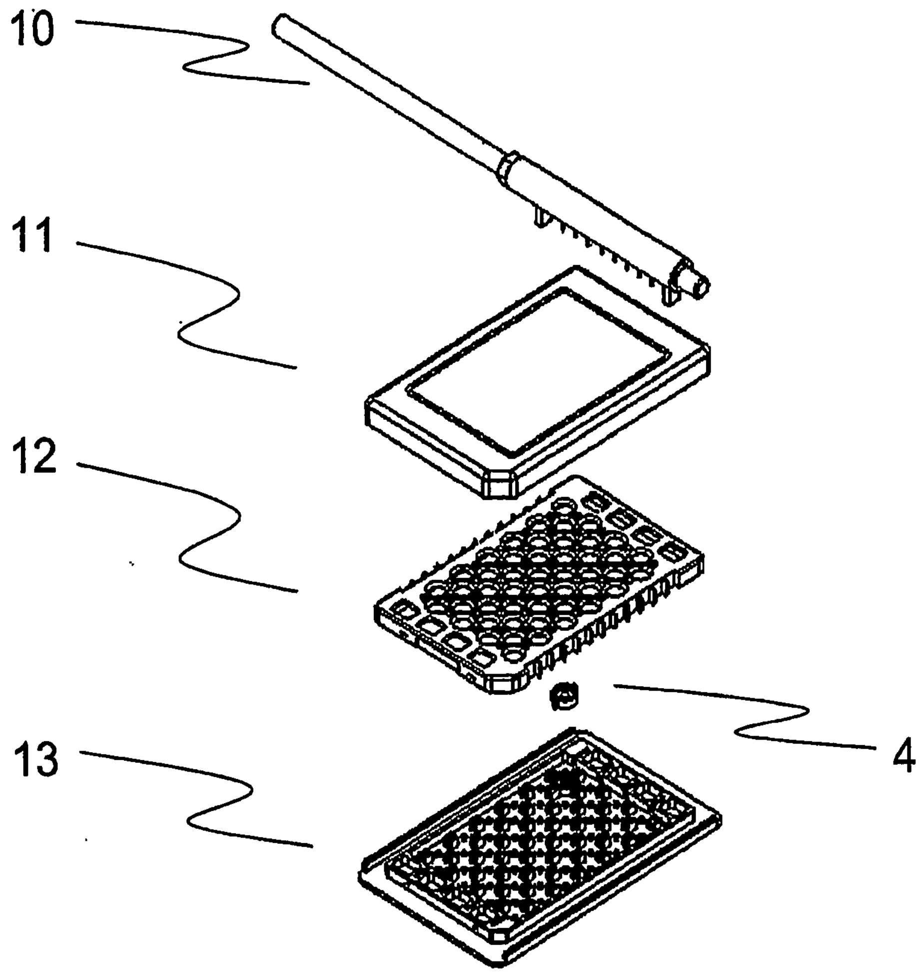

FIG. 4

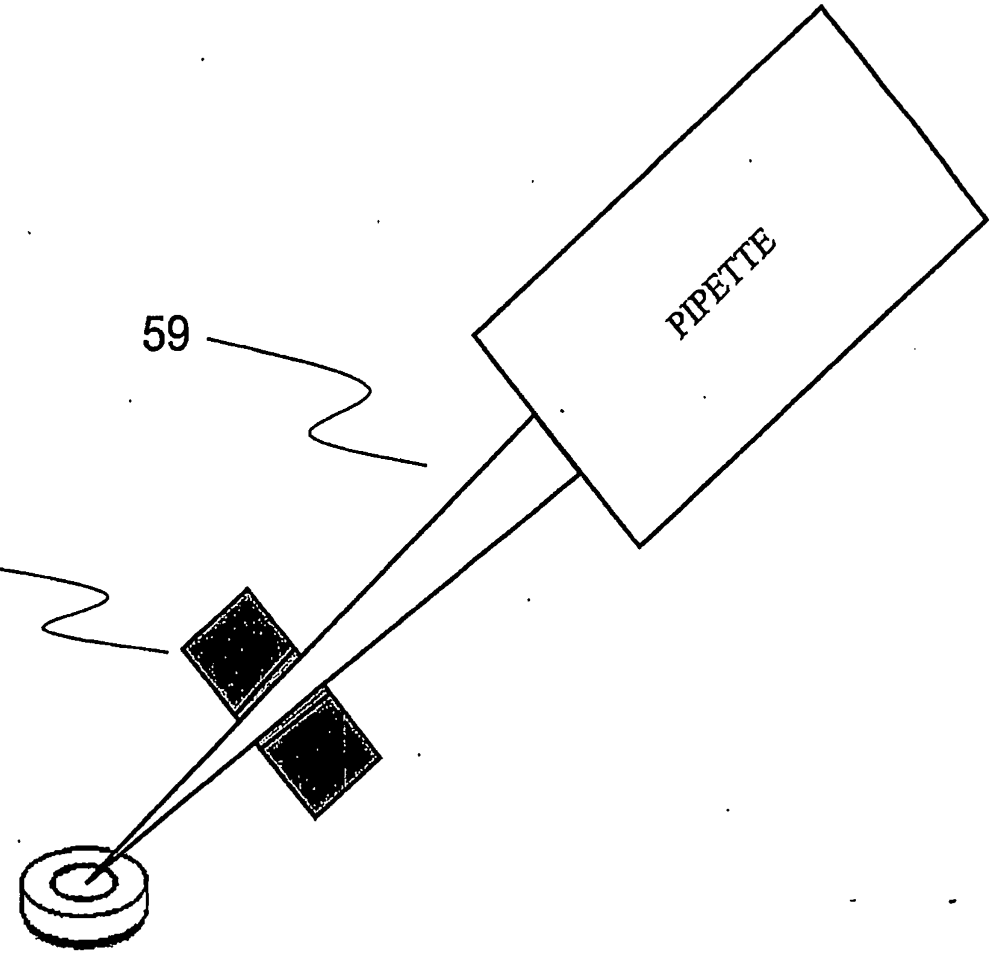

FIG. 5

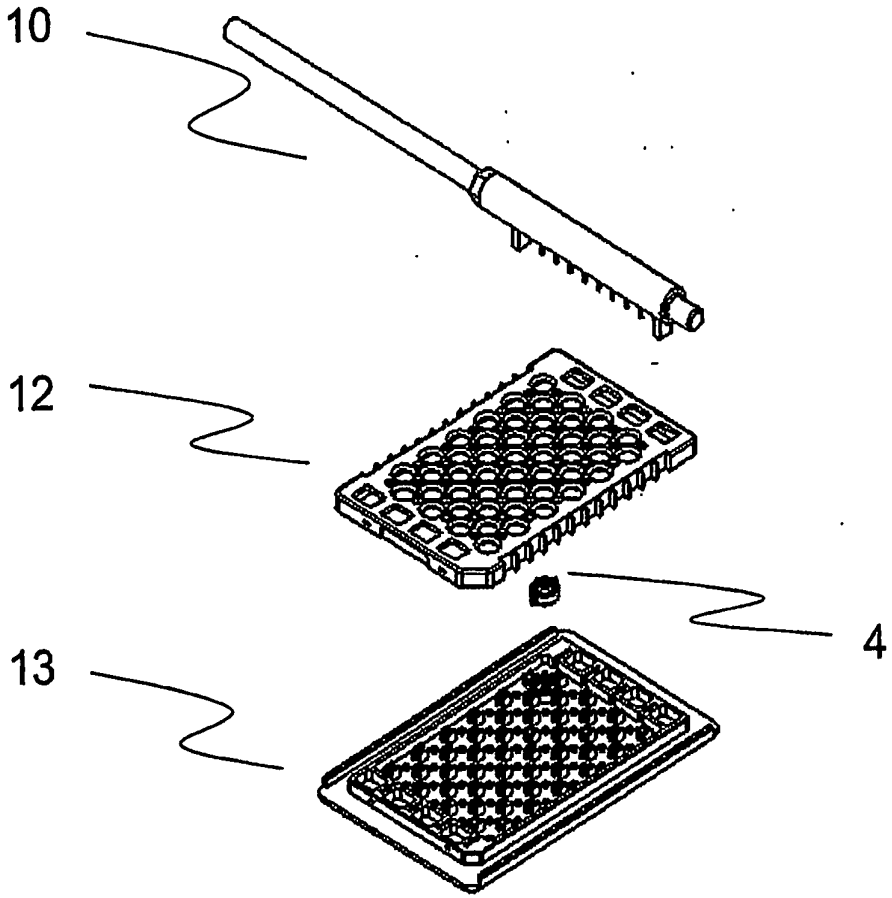

FIG. 6

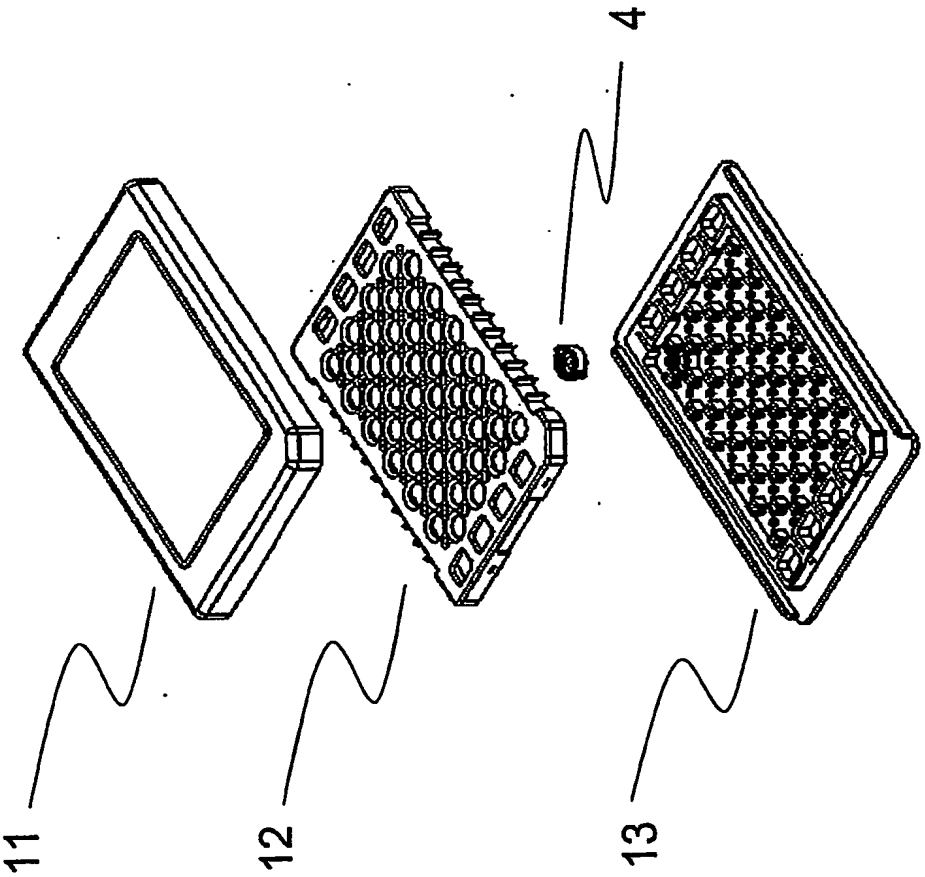

FIG. 7

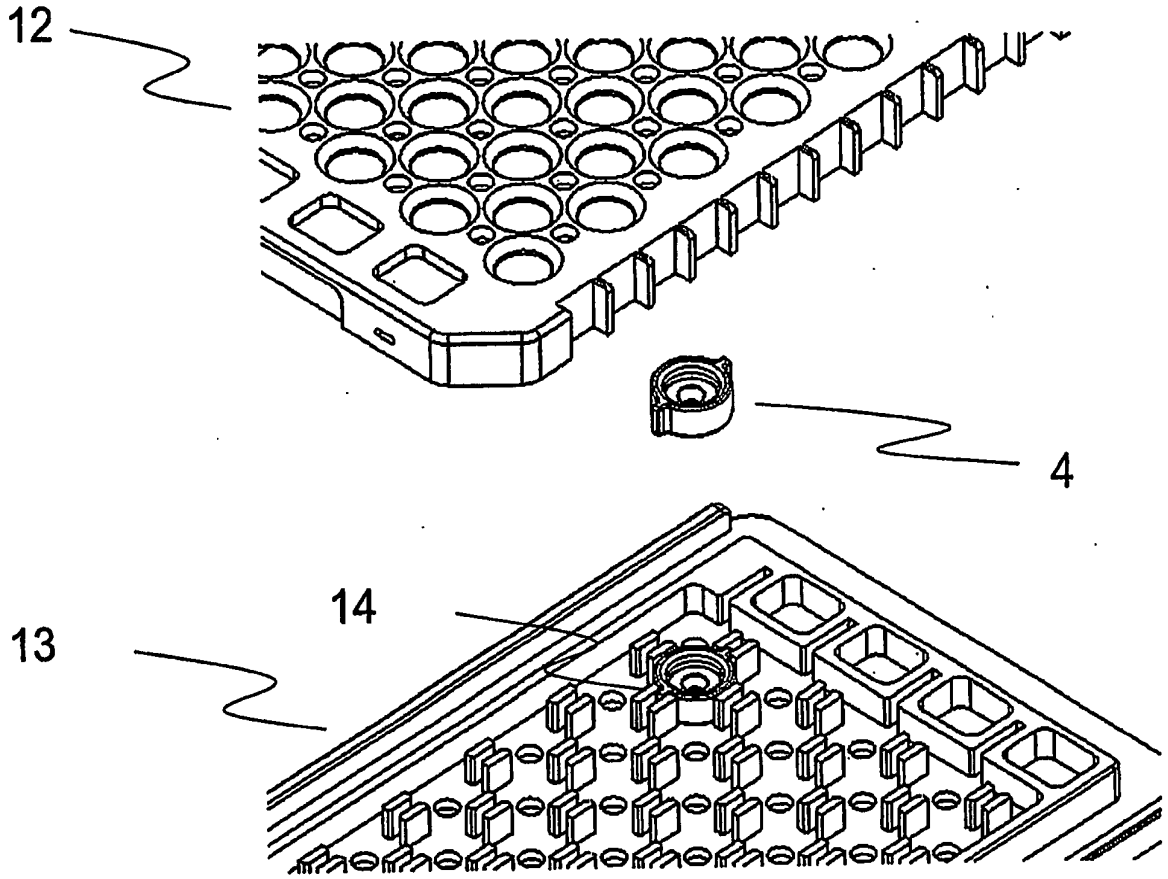

FIG. 8

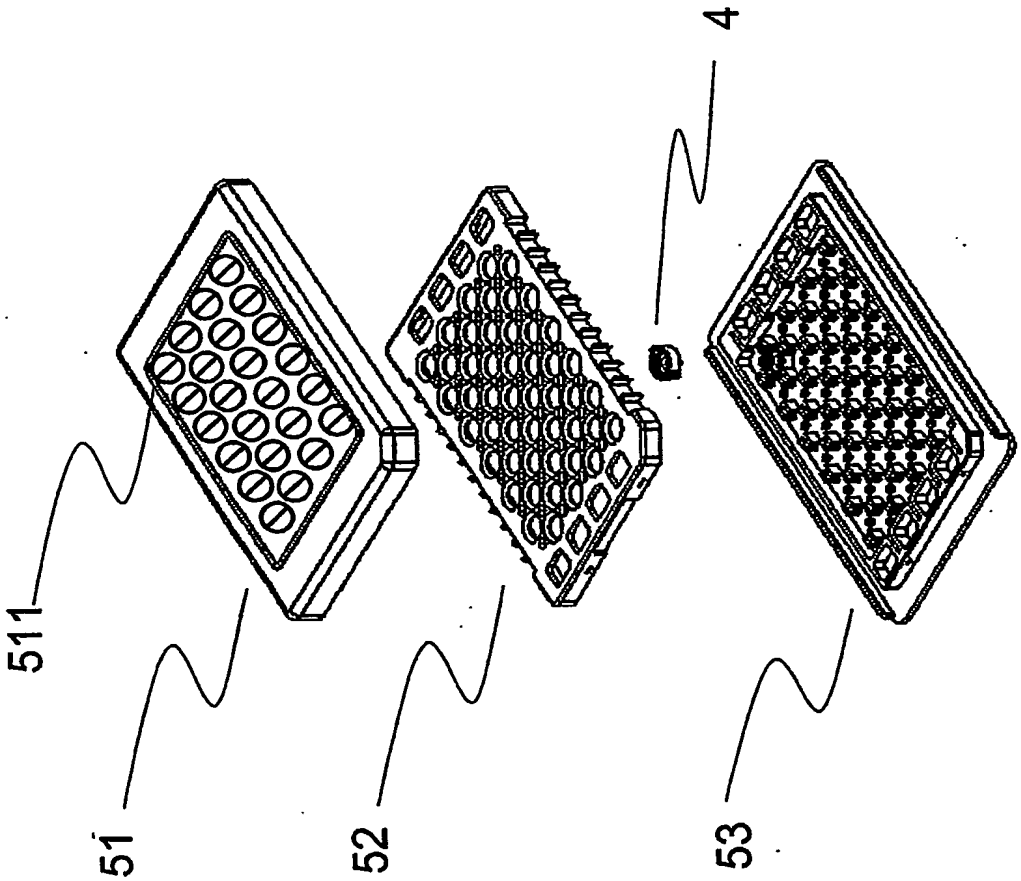

FIG. 9

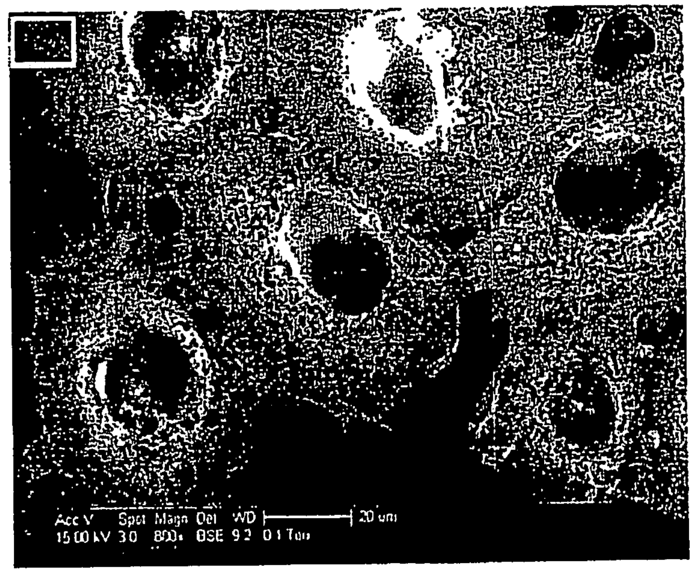

71

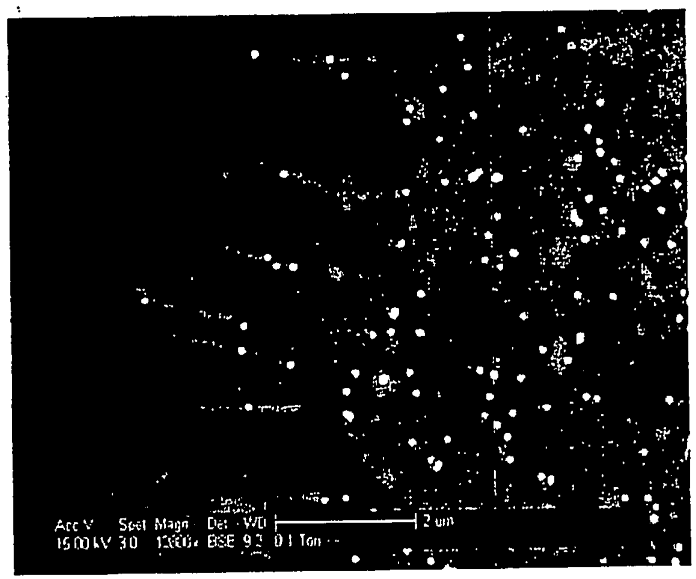

72

FIG. 10

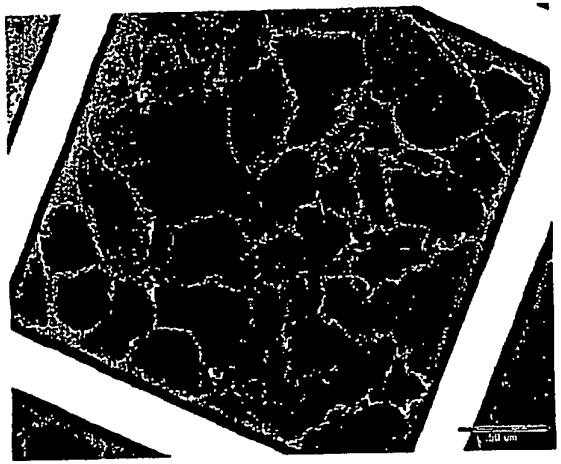

81

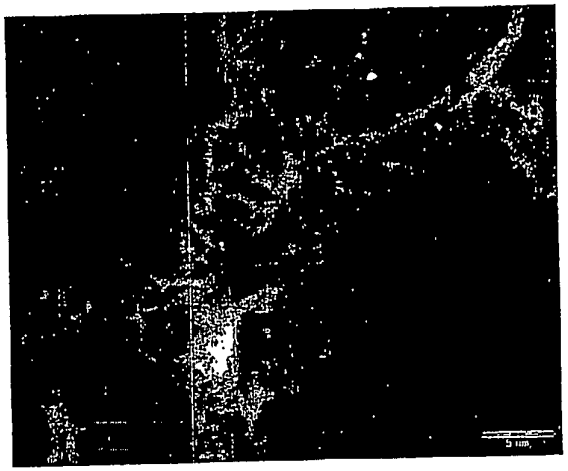

82

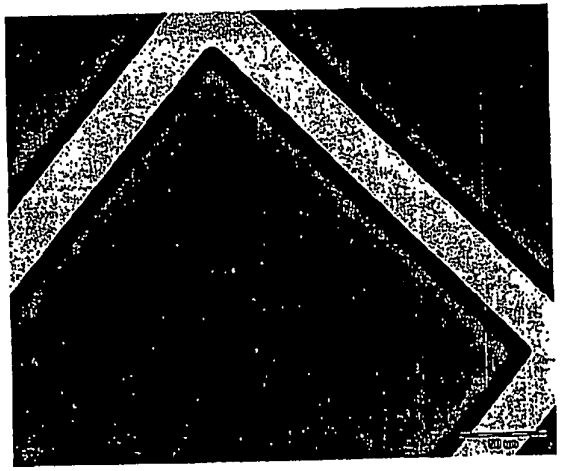

83

FIG. 11

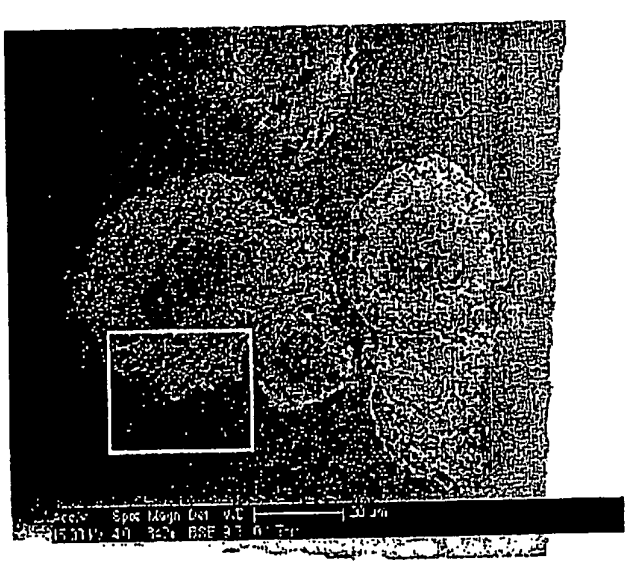

91

92

FIG. 12

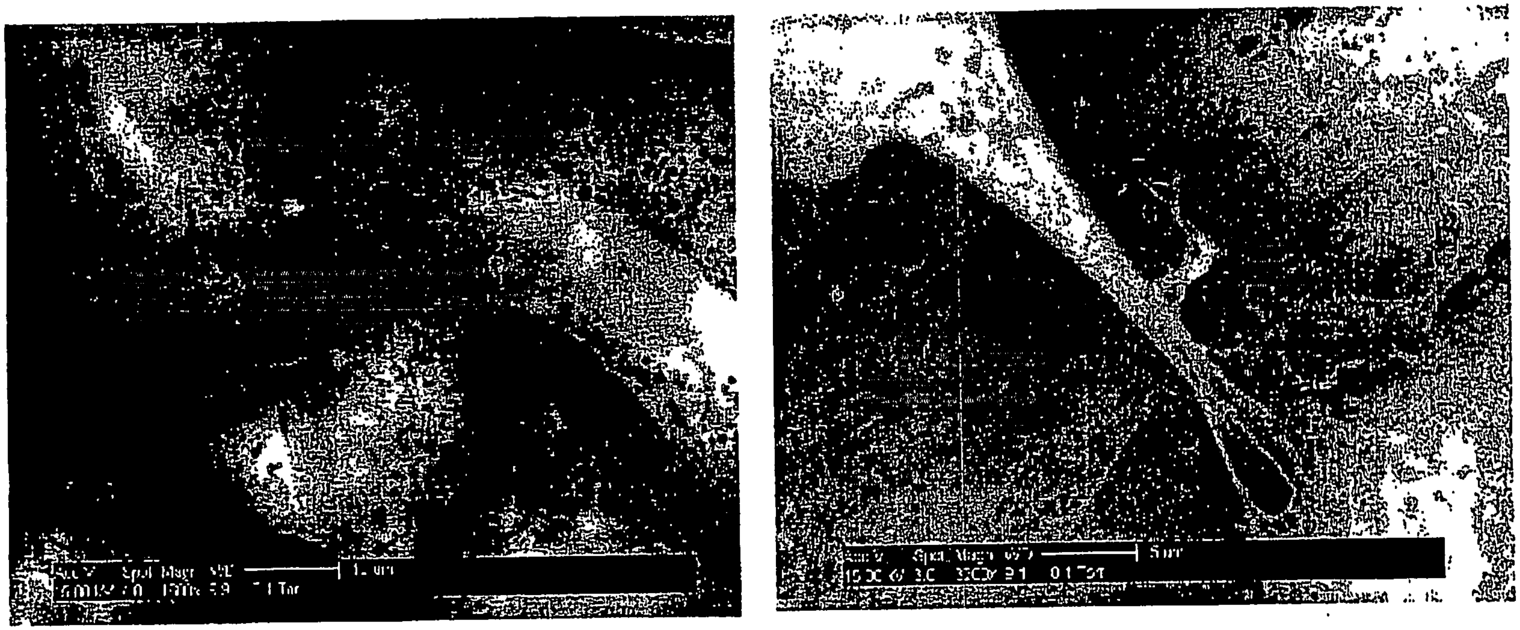

101

102

FIG. 13

111

112

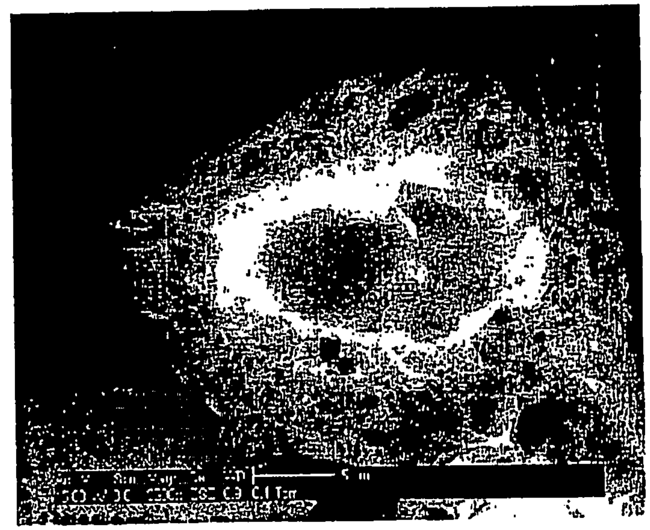

113

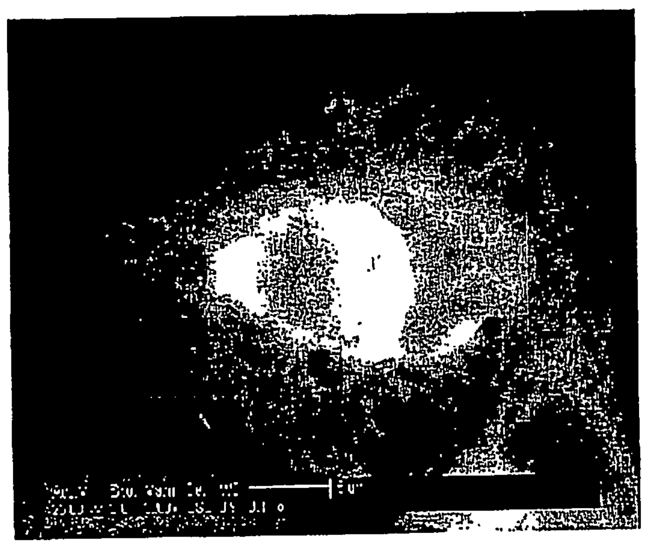

FIG. 14

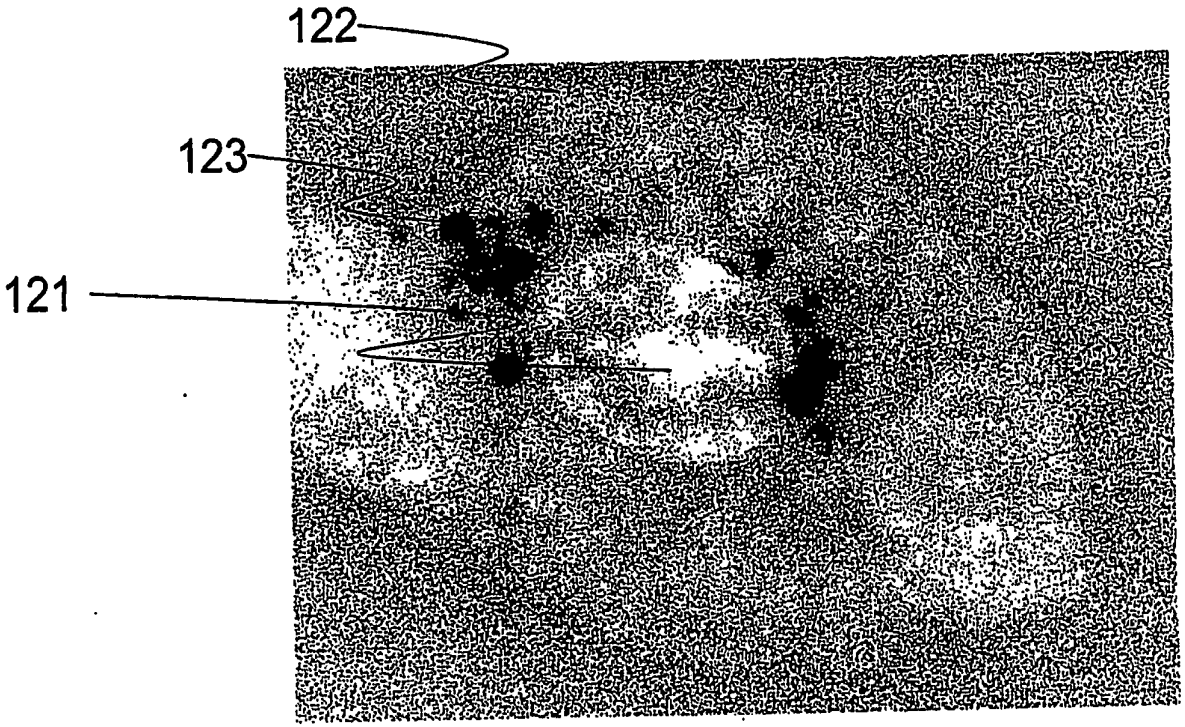

FIG. 15

131

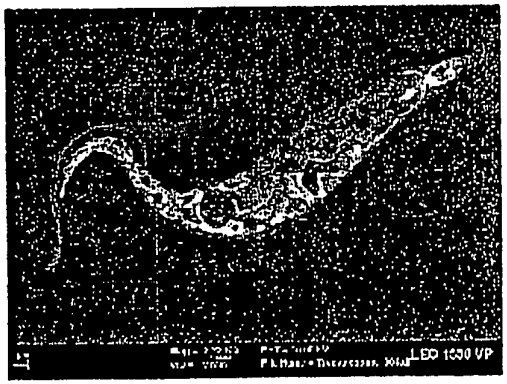

132

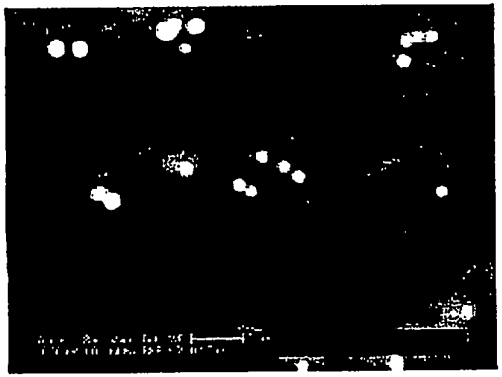

133

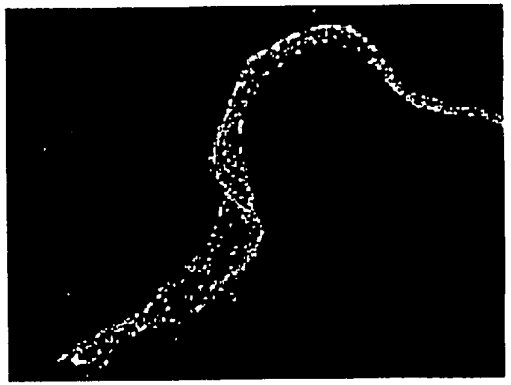

134

FIG. 16

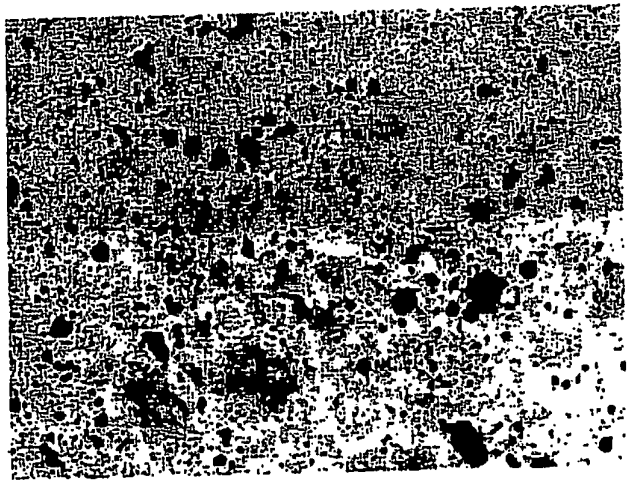

141

140

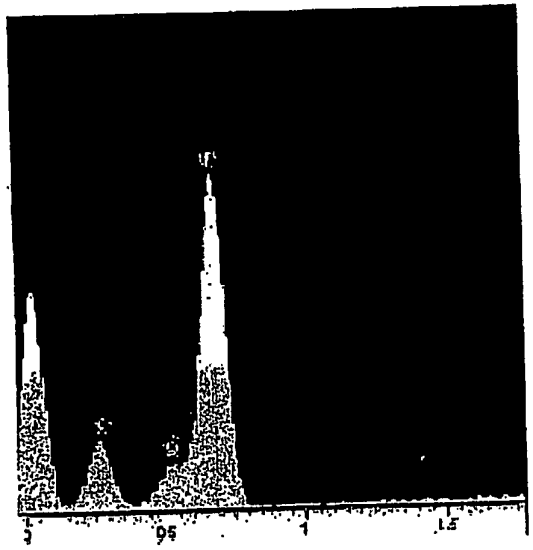

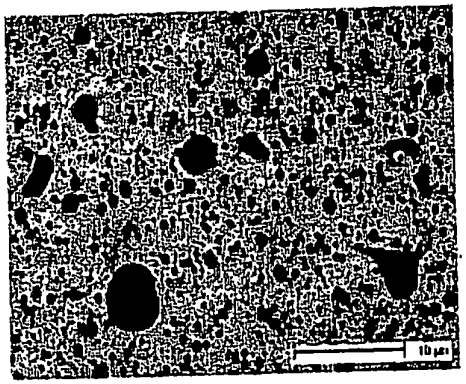

142

143

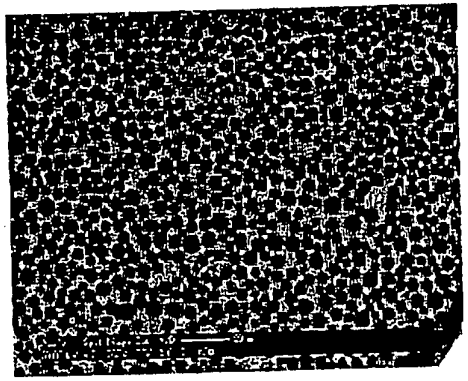

144

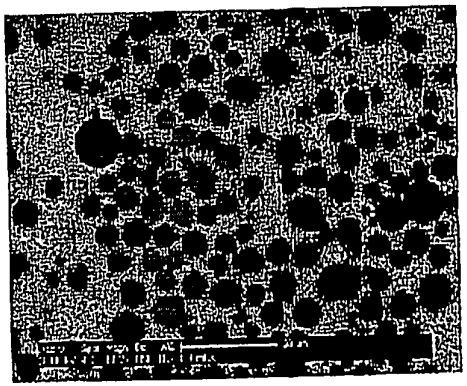

145

FIG. 17

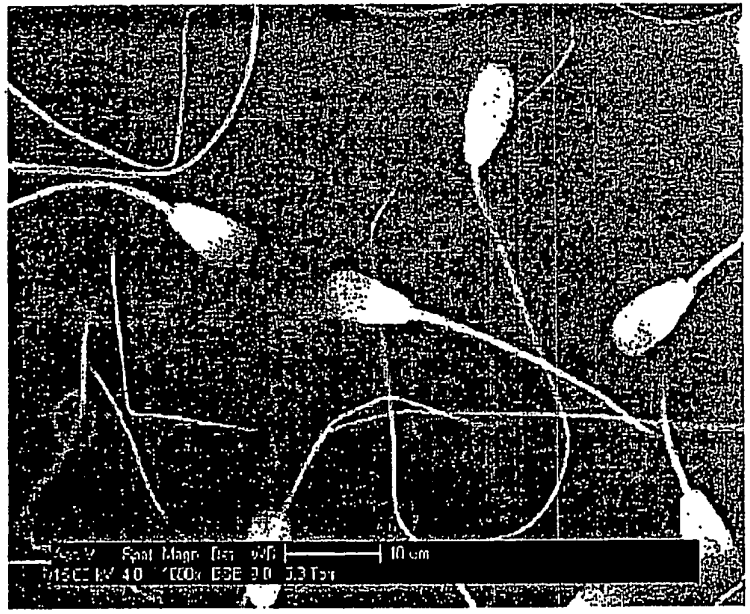

151

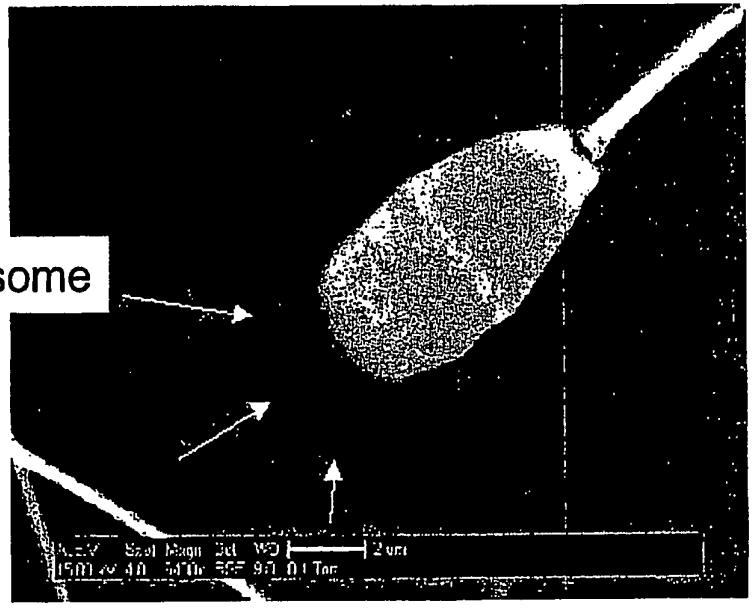

152

FIG. 18

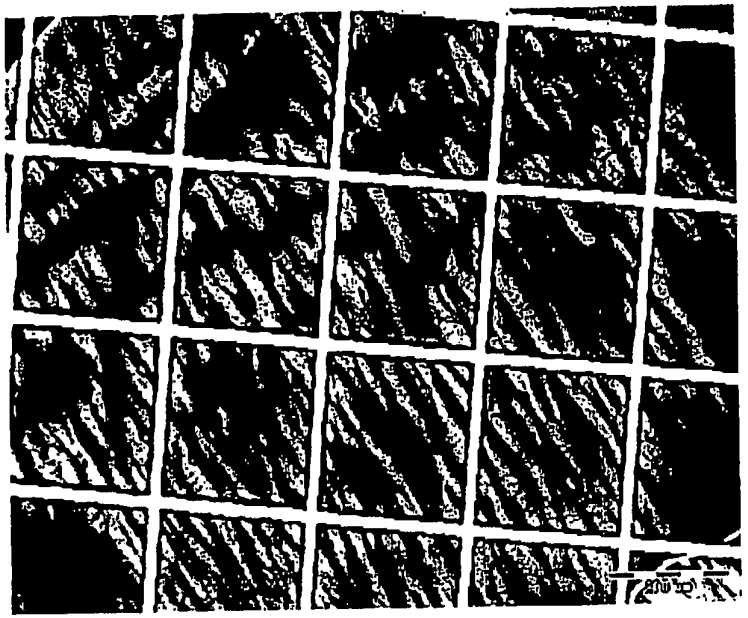

161

162

FIG. 19

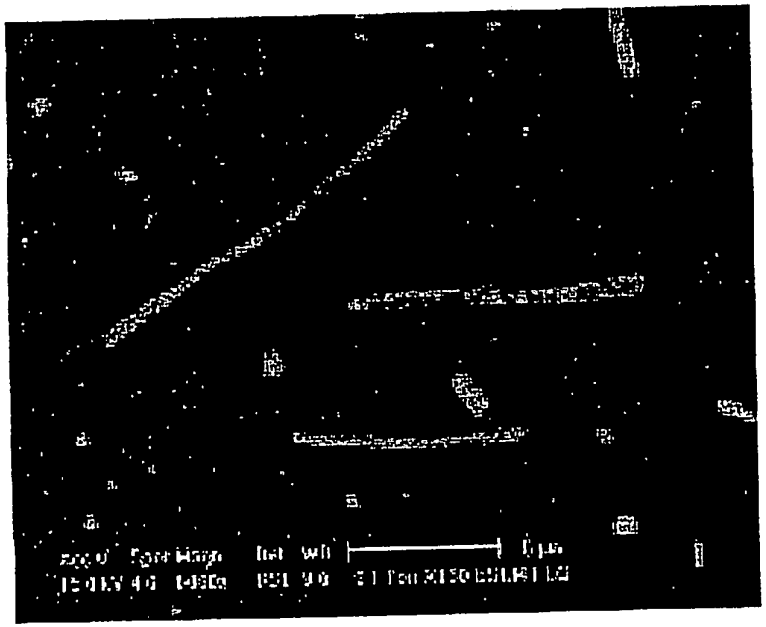

171

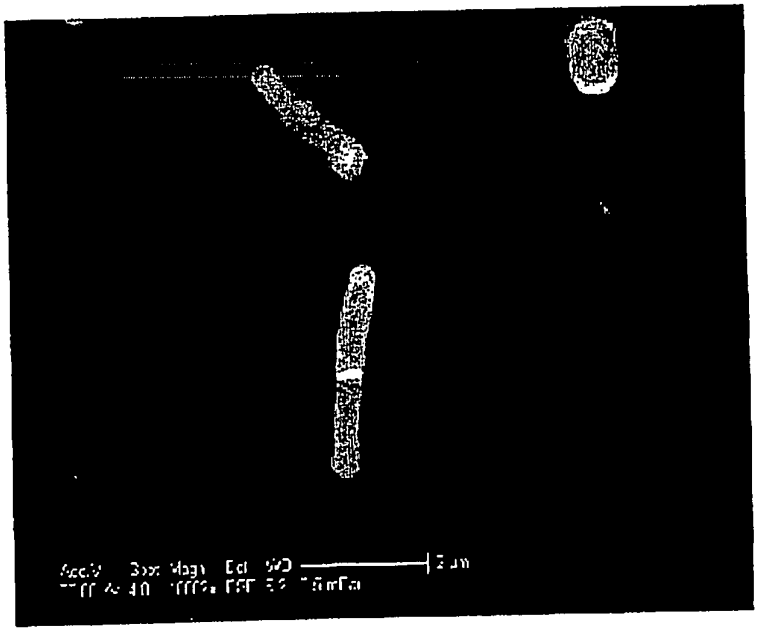

172

FIG. 20

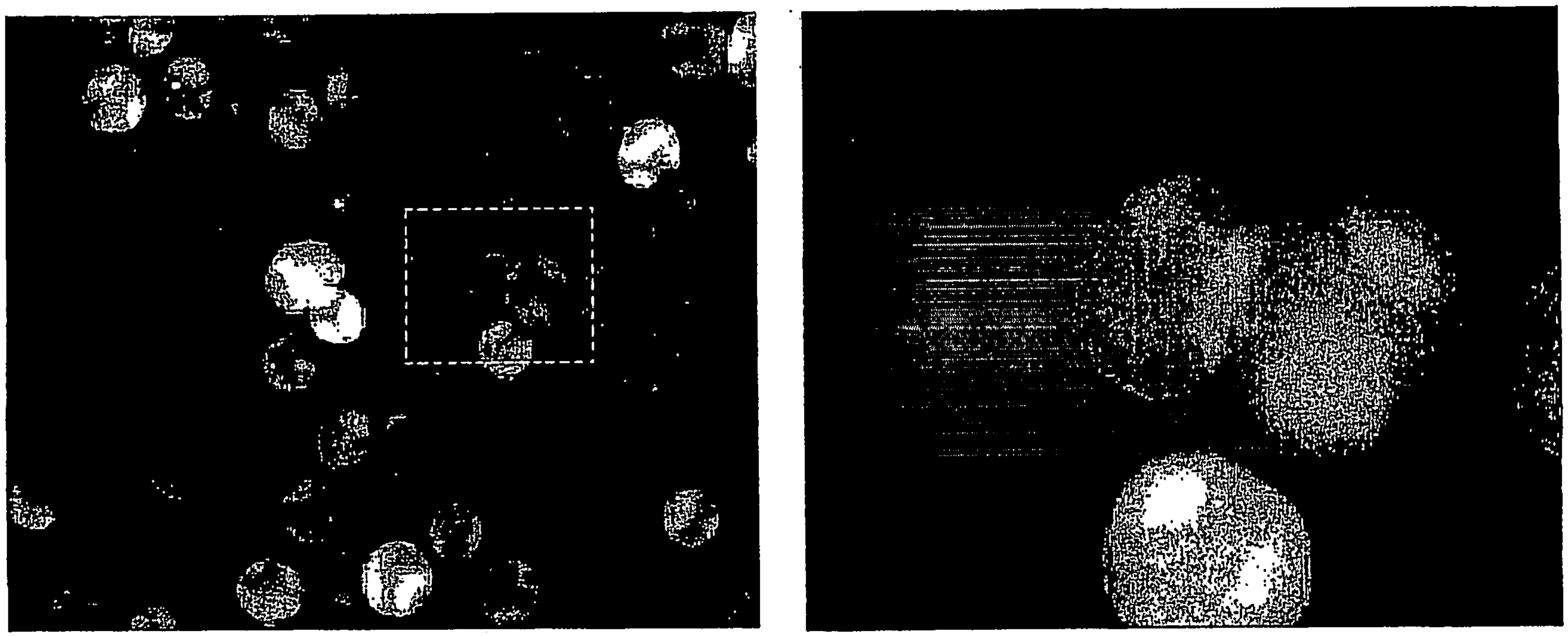

FIG. 21

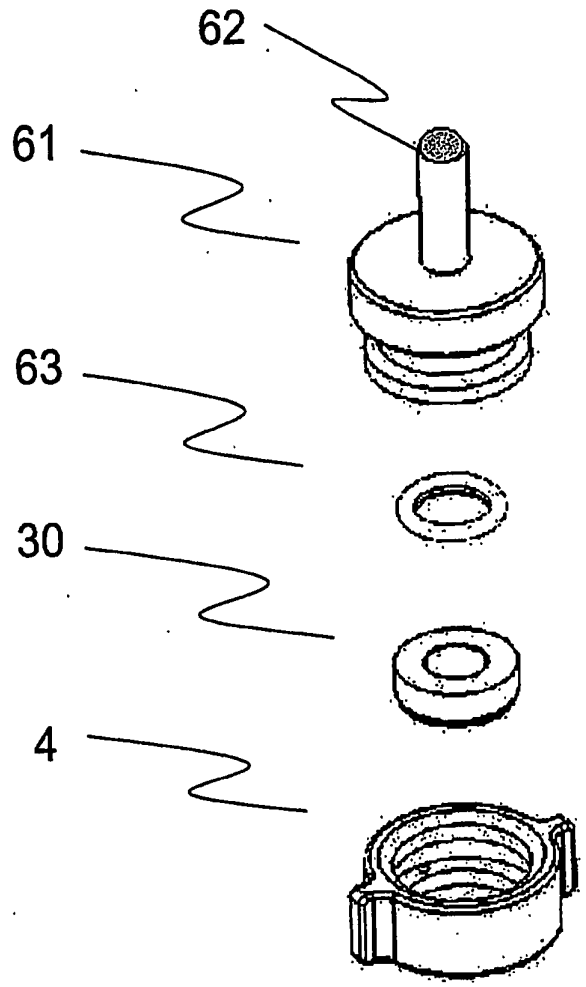

FIG. 22

Electron Beam Fluorescence (photons)

BS electrons

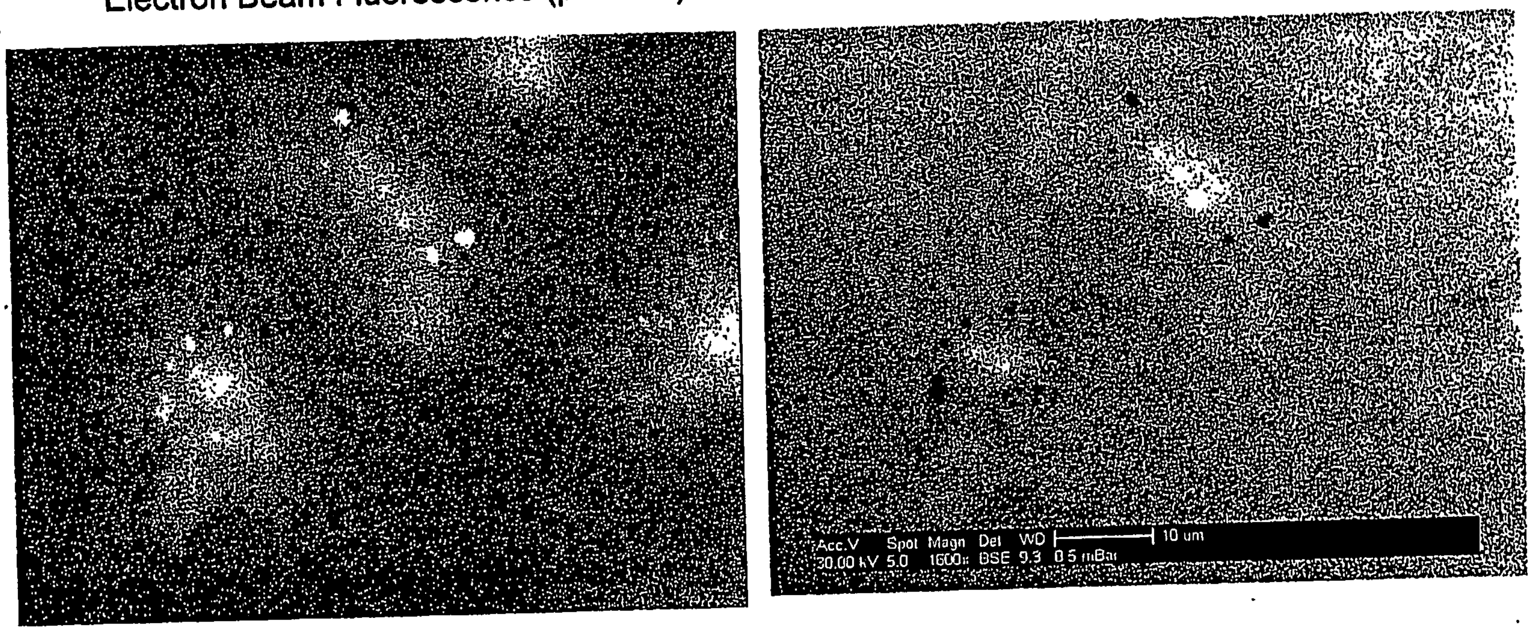

FIG. 23

Electron Beam Fluorescence (photons)

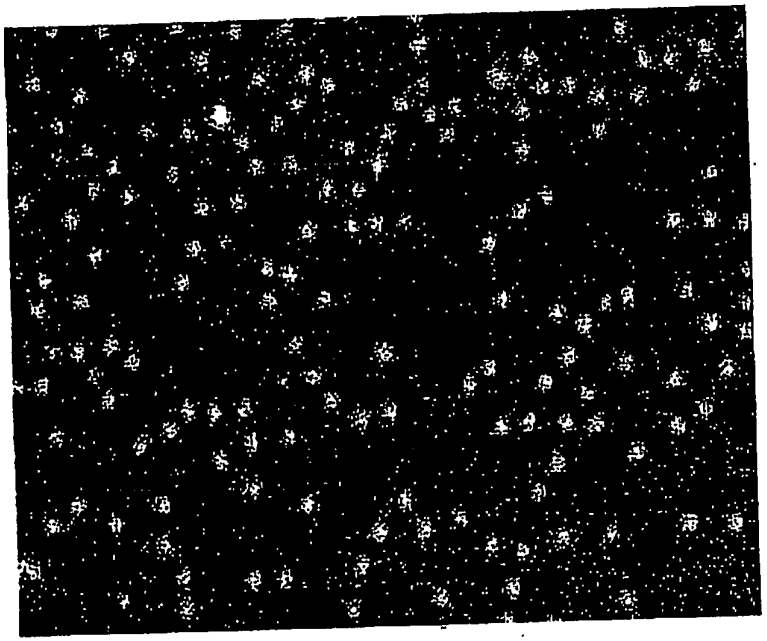

Back Scattered Electrons

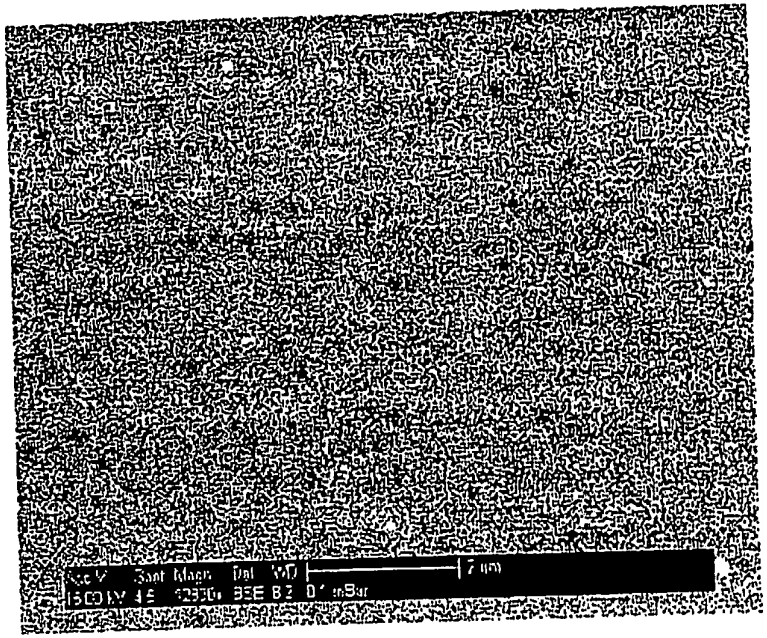

FIG. 24

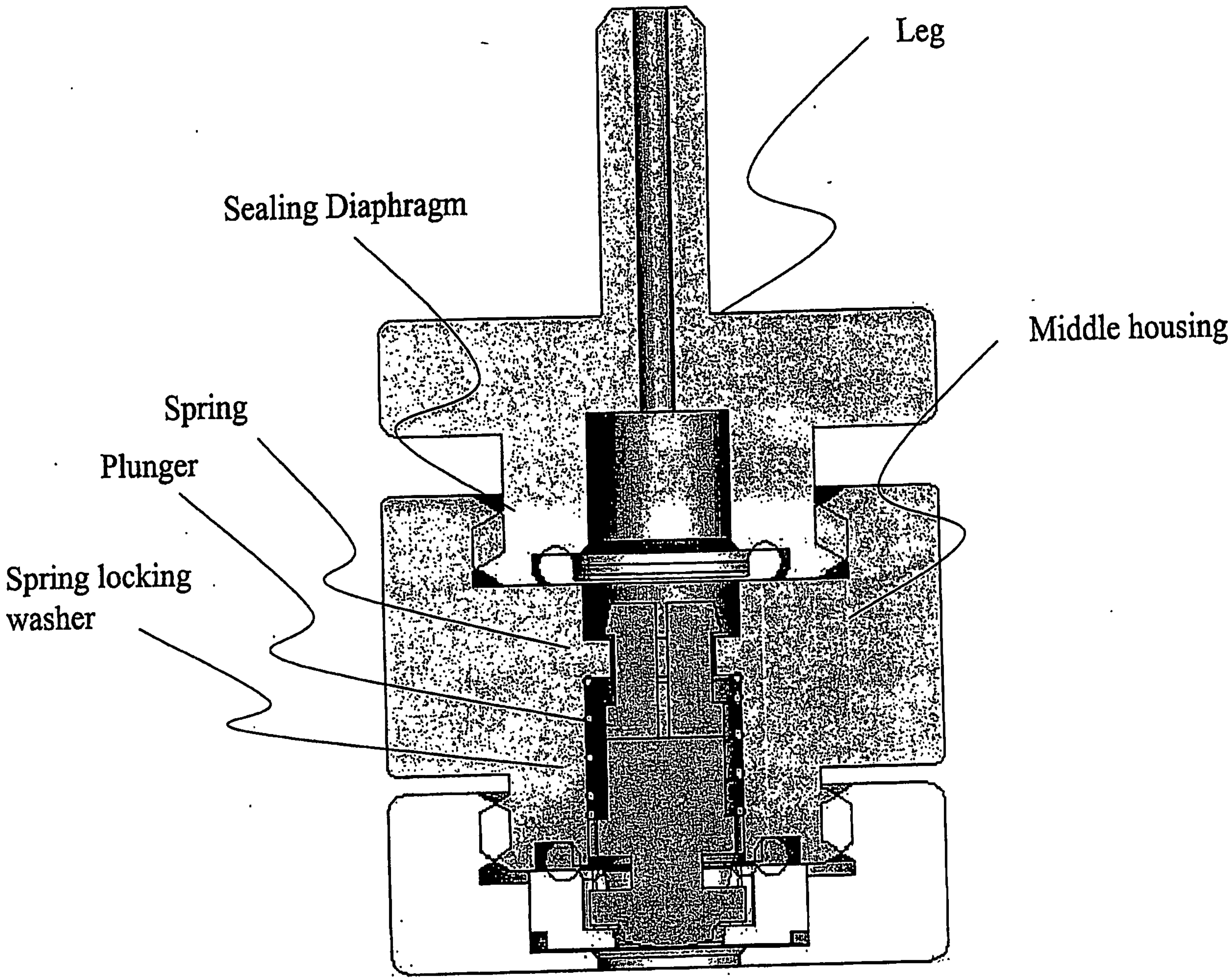

FIG. 25

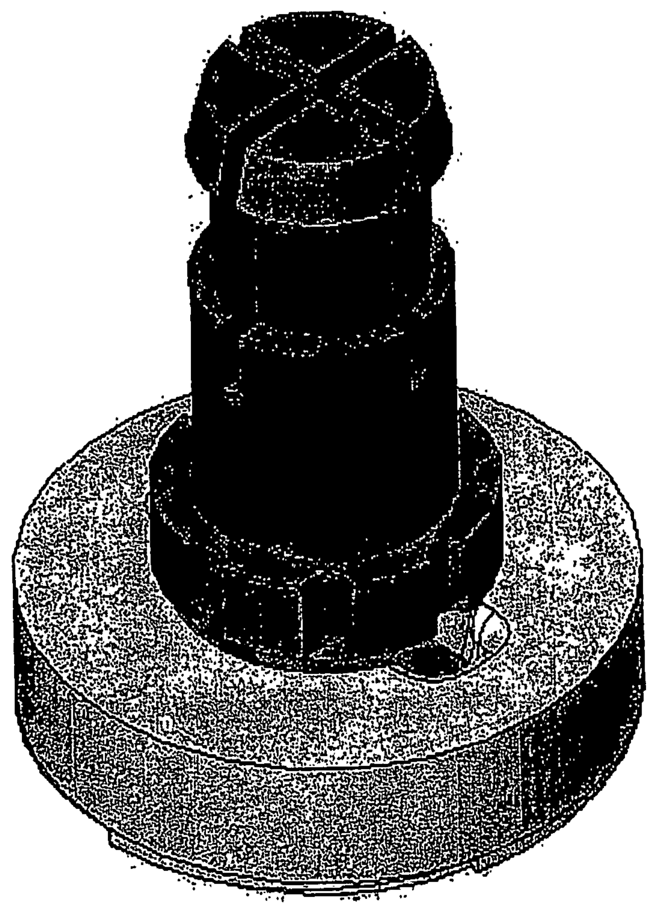

FIG. 26

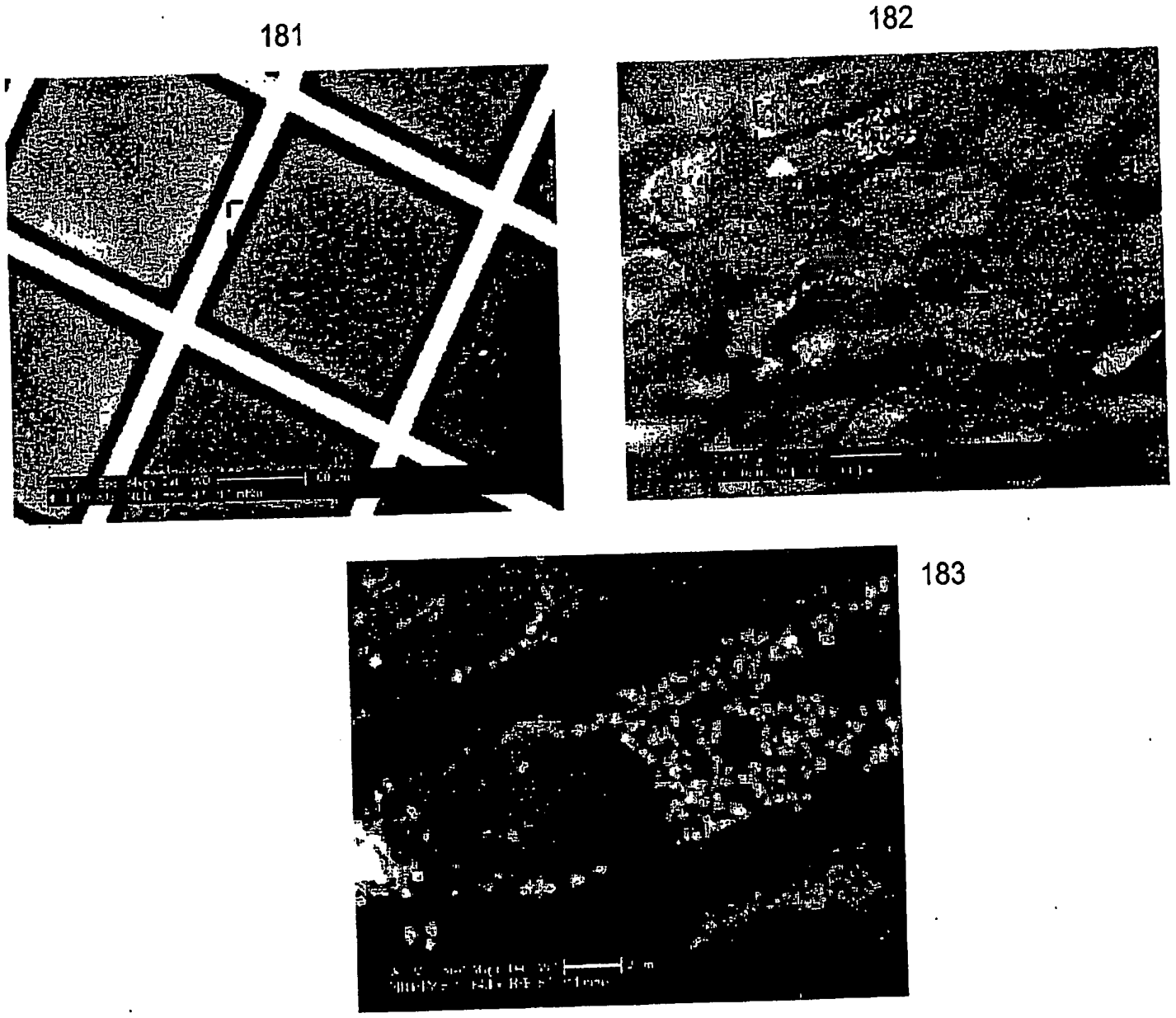

FIG. 27

191

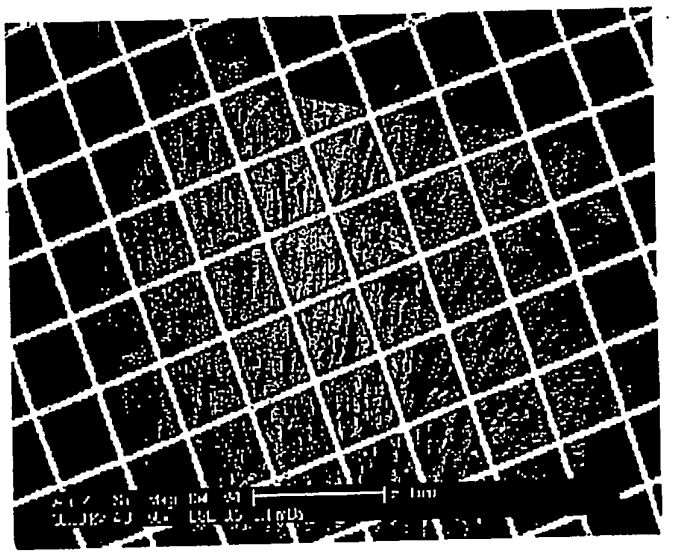

192

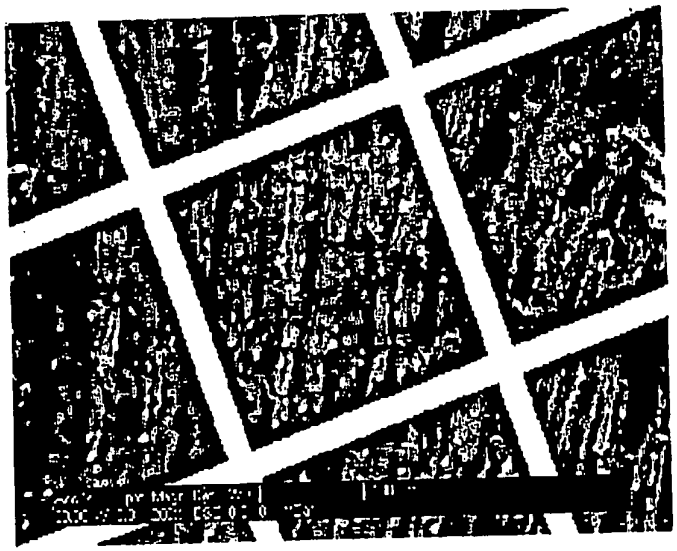

193

FIG. 28

201

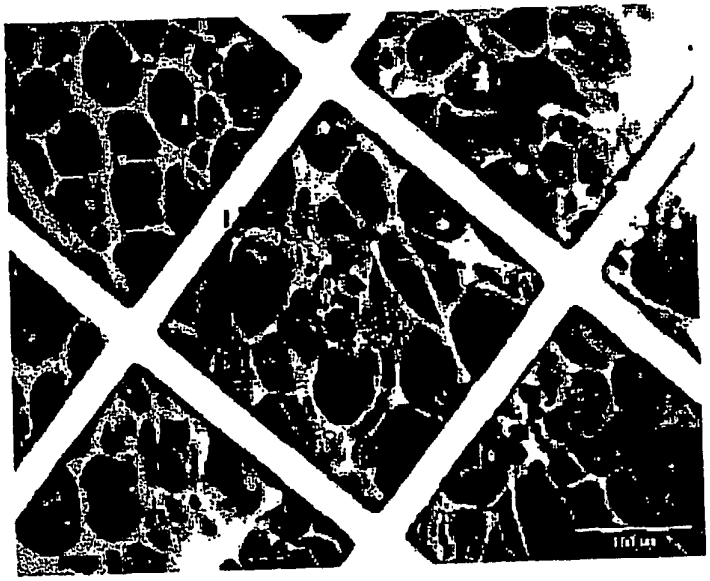

202

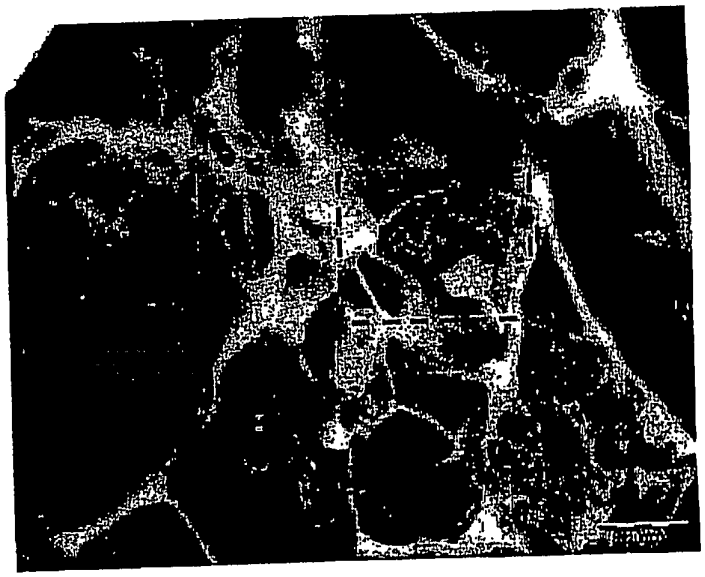

203

FIG. 29

211

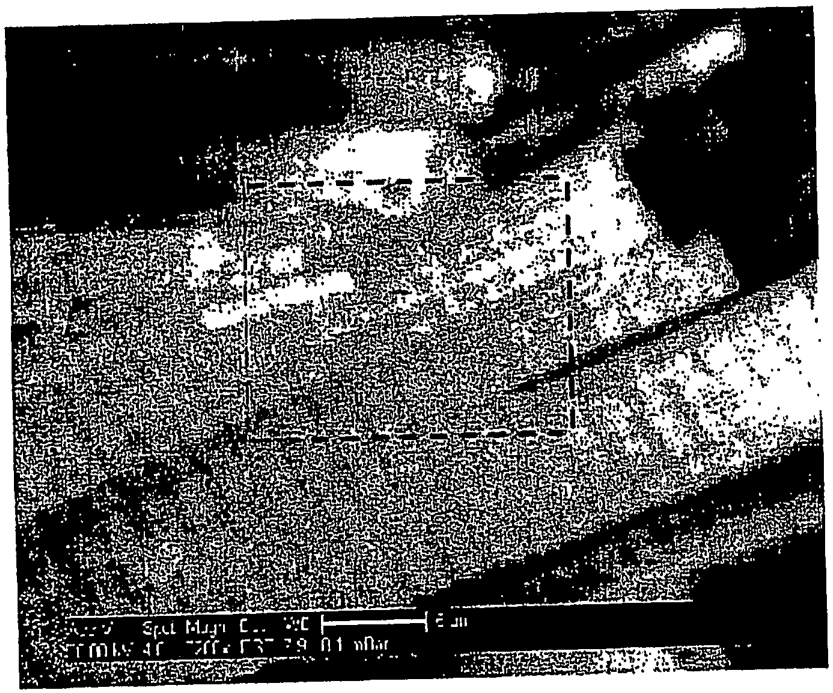

212

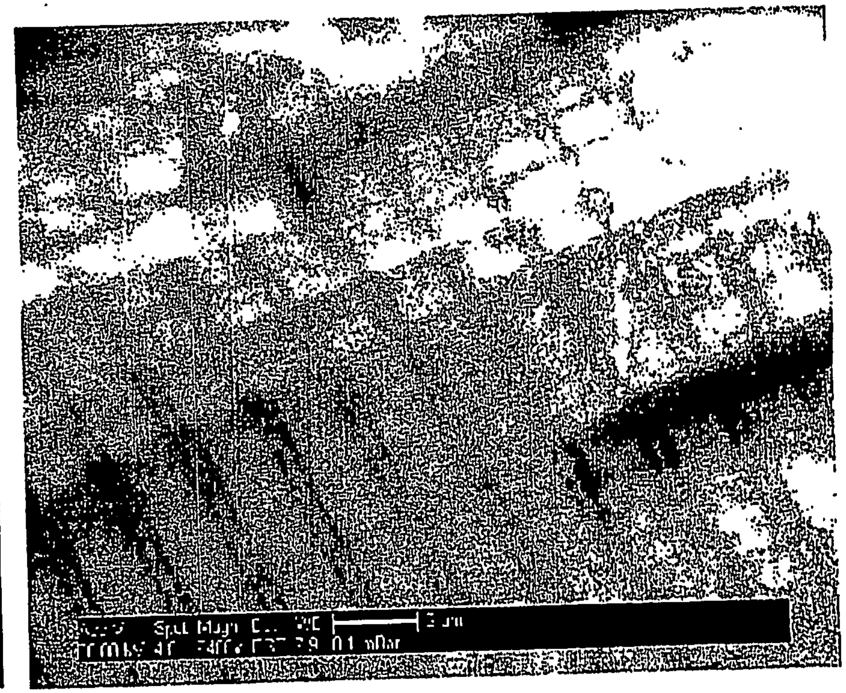

FIG. 30

221

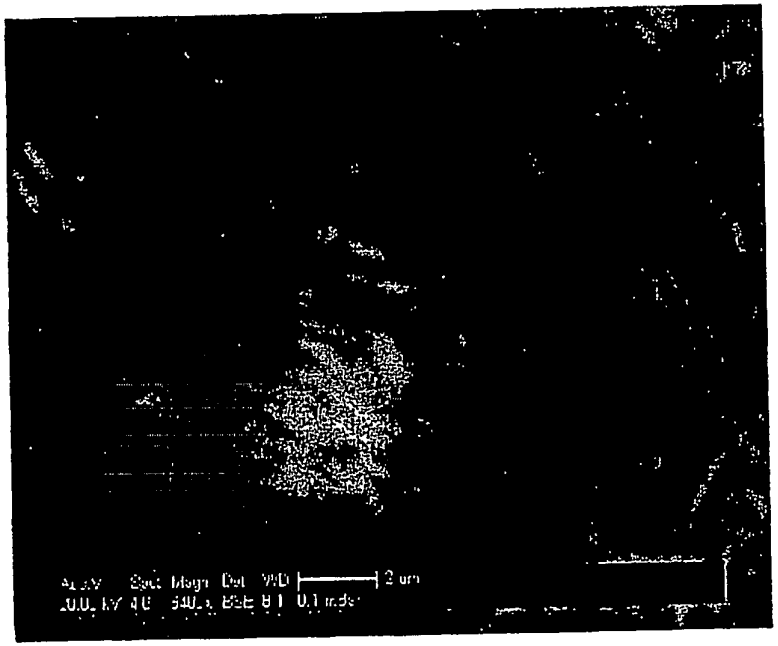

222

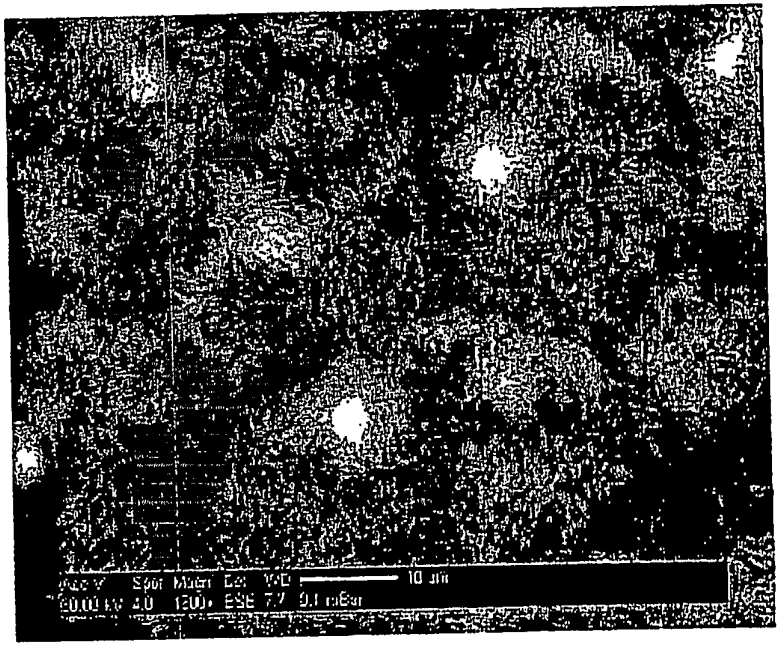

FIG. 31

231

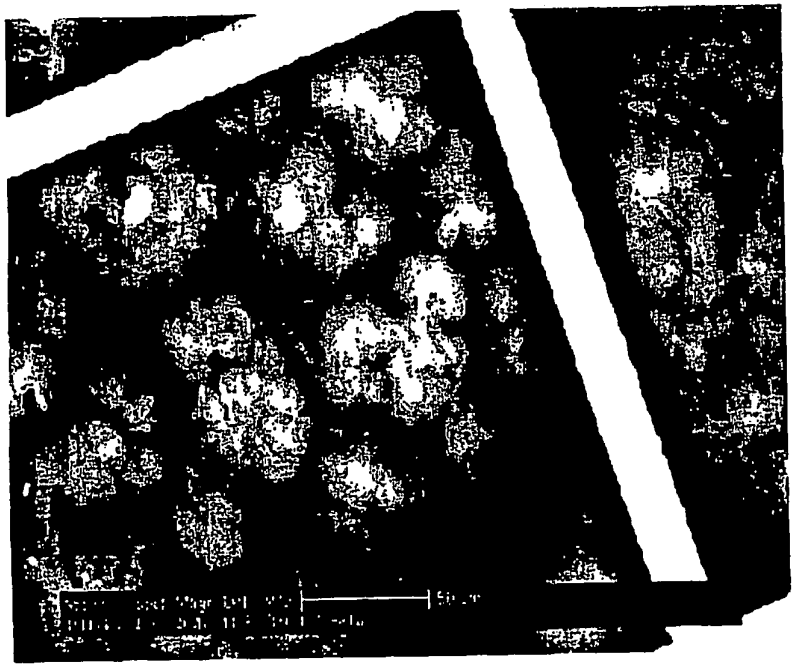

232

FIG. 32

241

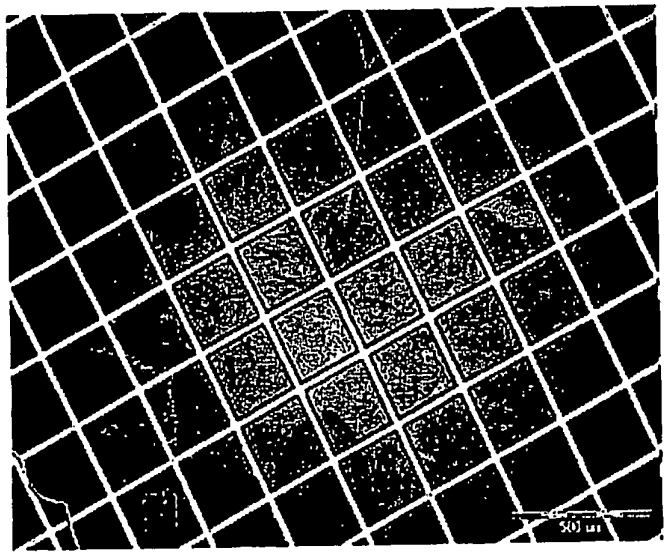

242

243

FIG. 33